AD 266 411

DISCLAIMER NOTICE

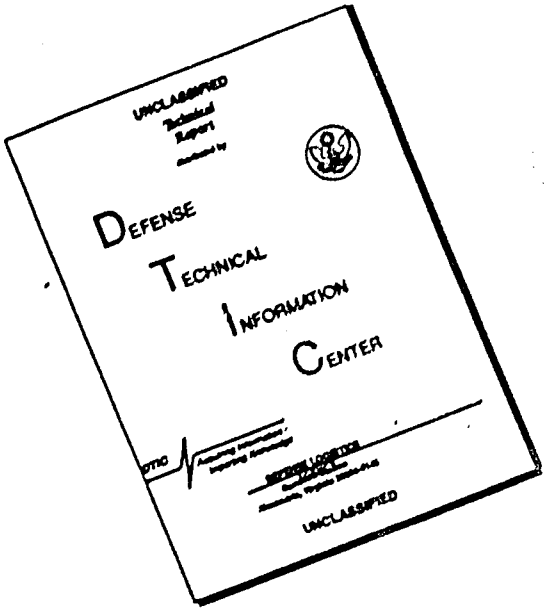

THIS DOCUMENT IS BEST QUALITY AVAILABLE. THE COPY FURNISHED TO DTIC CONTAINED A SIGNIFICANT NUMBER OF PAGES WHICH DO NOT REPRODUCE LEGIBLY.

U. S. ARMY
TRANSPORTATION RESEARCH COMMAND
FORT EUSTIS, VIRGINIA

TCREC TECHNICAL REPORT 61-119

VOLUME III

THEORETICAL INVESTIGATION OF DUCTED PROPELLER AERODYNAMICS

Task 9R38-11-009-12

Contract DA 44-177-TC-674

September 1961

prepared by :

REPUBLIC AVIATION CORPORATION
Farmingdale, Long Island, New York

DISCLAIMER NOTICE

When Government drawings, specifications, or other data are used for any purpose other than in connection with a definitely related Government procurement operation, the United States Government thereby incurs no responsibility nor any obligation whatsoever; and the fact that the Government may have formulated, furnished, or in any way supplied the said drawings, specifications, or other data is not to be regarded by implication or otherwise as in any manner licensing the holder or any other person or corporation, or conveying any rights or permission to manufacture, use, or sell any patented invention that may in any way be related thereto.

* * *

ASTIA AVAILABILITY NOTICE

Qualified requesters may obtain copies of this report from

Armed Services Technical Information Agency
Arlington Hall Station
Arlington 12, Virginia

* * *

This report has been released to the Office of Technical Services, U. S. Department of Commerce, Washington 25, D. C., for sale to the general public.

* * *

The information contained herein will not be used for advertising purposes.

* * *

The findings and recommendations contained in this report are those of the Contractor and do not necessarily reflect the views of the Chief of Transportation or the Department of the Army.

Task 9R38-11-009-12
Contract DA 44-177-TC-674
September 1961

THEORETICAL INVESTIGATION OF DUCTED PROPELLER AERODYNAMICS

Volume III

by

Dr. Th. Theodorsen & Dr. G. Nomicos

Th. Theodorsen
Director of Scientific Research

Prepared by:
Republic Aviation Corporation
Farmingdale, Long Island, New York

for

U. S. ARMY TRANSPORTATION RESEARCH COMMAND
FORT EUSTIS, VIRGINIA

HEADQUARTERS
U. S. ARMY TRANSPORTATION RESEARCH COMMAND
TRANSPORTATION CORPS
Fort Eustis, Virginia

FOREWORD

This report is one of a series presenting the results of research performed in the field of shrouded propeller aerodynamics, under contract for the U. S. Army Transportation Research Command, Fort Eustis, Virginia.

The work performed by Dr. Theodorsen and his associates at the Republic Aviation Corporation is presented in four volumes. The first two volumes were issued during August 1960, under Contract DA 44-177-TC-606. This volume presents the theoretical approach to ducted propeller flow, while Volume IV presents a discussion of vertical take-off vehicles.

The report has been reviewed by the U. S. Army Transportation Research Command and is considered to be technically sound. The report is published for the exchange of information and the stimulation of ideas.

FOR THE COMMANDER:

RAPHAEL F. GAROFALO
CWO-4 USA
Assistant Adjutant

APPROVED BY:
DEAN E. WRIGHT
Captain TC
USATRECOM Project Engineer

ACKNOWLEDGEMENT

The author wishes to extend his acknowledgement to Dr. G. Nomicos for work on the theoretical sections and to Messrs. A. Lange and J. Sinacori for the collection of experimental data. I am indebted to Prof. Dr. H. Schlichting, Director of the Institute at Braunschweig for conducting the tests on cascades and to Mr. Robert R. Piper for assistance in arranging this work. Finally, my acknowledgement to Mr. J. McHugh and his staff at TRECOM, who monitored the contract.

VOLUME III

CONTENTS

INTRODUCTION

As this investigation is limited to ducted propeller aerodynamics the following conclusions are, in general, restricted to this field with reference to other types for purposes of comparison or to emphasize differences. The present treatment is perfectly general and not intended to cover any particular design or to give elementary design data. The purpose is, on the other hand, to illuminate the fundamental knowledge required to arrive at a preliminary layout which, at a later stage, does not provide undesirable and unexpected surprises.

It is perfectly clear that such a considerable departure from the theory of conventional aircraft can be handled effectively only by engineers or scientistswell skilled in the treatment of complex airflow problems. It should be noted that the actual performance can be predicted with considerable precision since, with a few exceptions, no really unknown factors are involved. Let us take as an example the propeller or fan itself. In the first place, it is perfectly well known that the propeller efficiency reaches its maximum only with uniform circumferential and a prescribed and predictable radial load distribution. Since the propeller is or may be located in a duct, it is quite obvious that, in addition, the flow pattern of the duct itself must be known.

This particular problem has been treated in detail in Ref. A1, Chapter IV and the universal flow lines are shown in Figures I and II of this reference. These are the exact flow lines which correspond to the ideal case of uniform downflow velocity at the plane of the propeller. Great confusion has existed on this problem due to a lack of basic understanding. By inspection of the pattern of the ideal streamlines, any one of which may represent the wall of the duct inlet, it should be noticed that any smaller radius of curvature of the duct entrance results unavoidably in an increase in the inlet velocity at and near the wall. A standard type propeller operating in this inlet will thus be unloaded at the tip producing a condition quite detrimental to the efficiency of the propeller. Conversely, the inlet must be designed as shown in Ref. A1 in order to reach maximum efficiency with a normal type propeller, that is a propeller designed to operate in a circular duct.

The second step in the procedure is then to obtain the load distribution on a multiblade propeller in a circular infinitely long duct. The theory of the optimum loading of propellers has been given by Prandtl, and with more refinement by Goldstein (Ref. A2). For counter rotation propellers which are desirable for heavier loading, the general theory is given by Theodorsen (Ref. A3). However, the actual case of a propeller in a circular duct, single or counter rotating, has not been specifically treated in any of the above references, being of no significance at the time. The single rotating case has been treated in the present investigation in Section B. Both the loading functions

and the mass coefficients are expressed by appropriate formulas. Numerical results and graphs remain to be processed. With such tables and graphs available for multiblade propellers the ideal propeller can be designed with perfect accuracy.

It may be remarked that although the duct -streamlines are independent of the magnitude of the flow velocity, the propeller itself has to be designed for a prescribed velocity and thrust. As the take-off condition requires the highest power and efficiency, the propeller twist distribution must be designed to fit this case. If a variable pitch propeller is employed, the loss in efficiency is not excessive as the thrust is being reduced. However, any decrease in the angle of attack of the propeller will decrease the loading at the tip relative to that at the root section. This is particularly true if the design employs a relatively low lift coefficient.

In summary, to obtain the most efficient duct-propeller combination, the duct, whenever possible, should be designed with internal flow-lines so designed as to provide a uniform flow over the inlet area at the location of the propeller. The propeller will then be designed for the ideal load distribution. Experimental checking either on full scale or

on models is not at all required, if and when the ideal combination may be employed.

If and when deviations from the ideal case of duct design are unavoidable, it is still possible to estimate very nearly the resulting radial non-uniformity of the inflow and correct the blade angle distribution of the propeller accordingly. Only if drastic deviations from the ideal inlet are employed may it be desirable to run a final experimental check rather than to obtain the services of an organization sufficiently qualified to obtain the ideal combination by direct calculations.

As a further remark it is stated that the complimentary combination always exists: for any duct design, the complimentary propeller is a matter of proper design. This point must not be overlooked, since any deficiency reflects itself directly in the weight of the power plant and in the fuel consumption.

As we are not, in particular, referring to any specific design, we shall, nevertheless, note that there exists somewhat of a difference between the case of a propeller in a wing and the case of a free duct a-la-Doak. In the latter case the numerical calculation of the flow velocity in the inlet plane in the take-off condition is quite complex. However, it is possible to estimate, at least to the first order of magnitude, the effect of any particular radius of curvature at the duct inlet. The velocity at the propeller tip will be somewhat greater than the average and a corresponding correction must be applied to the propeller twist distribution. Experimentally, if

theoretical determination is unavailable, one need only insert the duct as an extension of a long cylindrical pipe of the same diameter as that of the duct exit, apply a suction at the other end and measure the radial velocity distribution at the plane of the location of the intended propeller. With the other data available the propeller may thus be fully specified. It should be emphasized that the duct enclosing the propeller is not necessarily beneficial. We shall discuss this matter briefly. (See also Volume IV.)

Favoring the duct arrangement are the following facts:

1. The propeller diameter is reduced. The theoretical limit of such reduction as shown in the first report (Ref. A1) is in the order of 30% based on the diameter of the free propeller, but actually, depending on the case, only about 10 to 15%.

2. The RPM of the propeller and the related shafting and gearing is (correspondingly) higher resulting in a saving of weight.

The adverse factors are as follows:

1. Skin friction of the duct walls has been added to that of the assembly. Based on the area of the duct, the solidity of the propeller and the flow velocities, it will

be found that the duct loss generally outweighs the reduction in propeller skin friction loss. Again there is a limit: If the propeller is heavily loaded a balance may result. No credit should be given to the duct as a lifting surface since the critical situation exists at take off and in transition, in which cases any potential lifting capacity is destroyed by stalling.

2. Adverse is, of course, also the effect of the weight of the duct. This must be balanced against the decrease in weight of the shafting and gearing. Adverse is also the external drag of the duct.

The effects of transition or forward speed will be discussed next. It is quite essential to be aware of these effects in the early design stage to avoid later difficulties. The most essential requirement is an understanding of the nature and magnitude of the various effects.

Pitch-up moments are the first in line to be considered. Large pitch-up moment represents an inherent deficiency of the propeller-in-wing arrangement. It has been shown in the previous investigation (Ref. A1, Chapter II) that for a propeller inserted in a surface of area A there exists an associated pitch-up moment equal to the full momentum

drag times a distance equal to one half of the "mean radius" of the area A and, as may be noted, fairly independent of the shape. It should be pointed out that this moment cannot be eliminated by baffles or any other means as has sometimes been attempted.

In the case of shrouded propeller a-la-Doak, the case is less serious. The adverse pitching moment is reduced with forward tilt of the propeller axis as has been shown in Ref. A1 (Page 106). Also the numerical value of the moment is smaller. The momentum of the inlet air-column attacks with an arm of approximately one half the radius of the bellmouth at zero tilt angle. As the tilt angle is increased the arm is reduced to offset the gradual increase in the absolute magnitude of the momentum drag with forward speed. Also, the propeller itself has a slightly favorable pitching moment. This is caused by the fact that the air enters the propeller disk with more downward velocity at the front edge and correspondingly less velocity at the rear. This contribution to cancel part of the pitch-up moment is relatively more effective in the case of the separate duct.

Finally, the pitch-up moment of a free propeller may be mentioned. From the theory of a lifting surface it can be concluded that the lift force is as always concentrated near the front quarter chord. This fact has been confirmed by tests (See Ref. A1, Page 106 and Figures 161 and 165). The magnitude of the pitch-up moment is quite considerable but with the lift force maintained constant the value of the moment does not change

appreciably with forward speed so in this hypothetical case the effect may be eliminated by choosing the proper location of the hypothetical free lift propeller with respect to the center of gravity of the aircraft.

To summarize: The propeller-in-wing type suffers from an inherent adverse pitching moment of considerable magnitude. The numerical values may be obtained with considerable accuracy by use of the methods given in the previous report (Ref. A1). The propeller-in-duct case is more favorable as the acting moment arm is smaller and is gradually decreased in transition to forward speed. The hypothetical case of a free propeller is essentially free of the defect.

Transition effects on propeller or fan efficiency is a serious matter. The problem is closely related to the problem of propeller operating life as function of vibratory stresses. A free propeller is thus out of the question, and a helicopter design is necessary. The basic intent of the duct design is, of course, to force the flow to become more realigned with the propeller axis.

As contrasted with the case of a free propeller, the opposite case is a propeller with a long entrance duct. The propeller would then, if designed according to theory, reach full efficiency and would not be exposed to vibratory stresses caused by the unsymmetric flow pattern. As the duct may be shortened, the efficiency of the lifting fan will gradually decrease as a function of the nonsymmetry of the flow

pattern. The center of lift of the fan will gradually move from the axis toward the rear and laterally into the advancing quadrant. Anyone skilled in the art can calculate with adequate precision the effect of a given travel on the efficiency of the propeller. Also, the corresponding one-per-turn vibratory stresses can be estimated with adequate accuracy.

In regard to the required length of a duct it is again clear that the case of the fan in the wing is again in the most unfavorable position. The fan-in-fuselage and the separate ducts are more favorable. Another parameter of equal importance is the ratio of forward speed to that of the fan tip velocity. A low value of the aircraft forward speed to the fan inlet velocity is, of course, beneficial. An example of such favorable combination is thus the GE high pressure fan type when installed in a fuselage.

To prevent excessive vibratory stresses and to improve the fan efficiency it is desirable to employ inlet vanes. These cannot be treated in a general case and present quite a difficult construction problem if they are to give high efficiency in the entire transition range. An example of a simple deflection grid is treated in Sections G, H, and I of the present report.

Another effect apparent in the transition to forward flight is an interference effect between the fan-in-wing and the wing itself. In Ref.A1, Chapter III is presented the classical solution of a wing with a sink on the upper surface and a line jet issuing from the lower side. These results

are exact and show that the circulation is increased by the action of the propeller in an amount given by the expression III-18 on Page 25 of reference report. The direct contribution of the propeller is given by the standard expression III-19 on Page 26. Finally, the classical expression for the moment arm of the pitch-up moment in terms of the half chord of the wing is given for the two-dimensional case by the expression III-21 on Page 27.

We shall next consider another very important interference effect. In the theoretical treatment, Ref.A1, the jet was treated as a line jet issuing from the lower surface in order to obtain the essential facts of a complex problem. However, the jet is of considerable dimensions and in the present report the displacement jet on the wing proper has been investigated. The two-dimensional pattern of the flow around a cylinder and the pressure distribution on a flat plate perpendicular to the cylinder is also known. By reference to Section E of this work it may be seen that the loss of lift on the area adjacent to the jet approaches the value $C_L = -1$ based on the area of the jet itself. This is a theoretical fact: There is a lift reduction caused by the displacement of the jet which has to be or may be recovered by a noticeable change in the angle of attack of the wing. If the wing area is ten times the jet cross section, the angle of attack of the main wing must be increased by about one degree. This gives an indication of the magnitude of this loss of lift.

A more serious effect is, however, that of the negative pressure region existing behind the jet as a result of the breakdown of the air flow around the jet. An investigation has been conducted under Section F to clarify the situation, based on the theoretical study in Section E and on a series of experiments conducted by NASA on cylinders and jets at right angles to a flat plate and with the airstream perpendicular to the cylinder or jet. Incidentally, the data confirm closely to the theoretical data for the front area ahead of the cylinder. Behind the jet exists, however, a large negative pressure region resulting in a negative lift coefficient of $C_L = -3$ and an adverse moment coefficient of about $C_M = 6$ based on the area and the radius of the jet, respectively. These values are, however, obtained for low Reynolds number below the critical value of the drag coefficient of a cylinder.

There is little doubt that the negative area behind the jet is, to a large extent, caused by the pumping action of the jet which blows the passing main airstream downward due to the mixing at the intersurface. The normal negative region observed behind a solid cylinder is thus intensified by the downward momentum imposed on the airstream by the jet. The presence of any extended surface behind the jet will, therefore, contribute to the magnitude of pitch-up moment. On the whole it must therefore be stated that the fan-in-wing design is not justified from aerodynamic reasons only.

RECOMMENDATION ON FURTHER RESEARCH

There appears to be at least two distinct problems which might advantageously be subject to further research..

The first field is the calculation of propeller load distribution for a multiblade propeller in a circular duct, based on the formulas of Section B of the present volume.

The second problem is the basic study over a wide range of Reynolds number of the obstructive effect and the "pumping action" of a jet on the flow pattern and pressure distribution on the lower surface of an airfoil or more generally on any extended plane surface parallel to the airstream. This work would be conducted and would represent an extension to the study reported in Section F and would serve as a master reference for special cases and might possibly be of such general value as to obviate investigations of individual cases as proposed above.

SECTION A

GENERAL METHODS FOR THE DESIGN OF VERTICAL TAKE-OFF AIRCRAFT

In the following is given a condensed summary of the design information that has been produced by the work of the present and the immediately preceeding investigation reported in Ref. A1. The work covers the aerodynamic aspects of the problem and is presented under separate headings indicated below. The purpose of the presentation is to provide a basis for rational design methods based on a theoretical analysis of each problem and supported by complimentary experiments in particular cases.

The following types of aircraft are under consideration or may be of interest:

1. Flying platforms or "jeeps".
2. Lifting propellers in wing or fuselage.
3. Direct jet-lift and propulsion.
4. Combination of lifting propellers and jet propulsion with means for conversion during transition.

The aerodynamic problem which is the restricted subject of the present investigation may be divided into the following subjects:

1. Propeller or fan.
2. Duct design.
3. Problems of combination of propeller and duct.
4. Baffles and inlet vanes.
5. Interaction of ducted propeller and wing or fuselage.
6. The effect of the jet on the lower surface of wing or fuselage.

It is conceivable that one or more of the four types of aircraft indicated above may arrive at a practical stage and become generally operational. In the meantime, it is essential to arrive at the basic design philosophy to the extent that all the fundamental aspects of the problems are understood. The aerodynamic considerations are covered under the above headings as other problems are of a nature common to any aircraft. We shall briefly cover the listed subjects and give reference to the appropriate treatment given in this presentation.

1. Propeller or Fan

The propeller design problem represents a rather straightforward case, except that the propeller in a duct must comply with the design instruction given by the formulas in Section B of the present report. In contrast to the case of the normal type propeller employing the Goldstein load-distribution or the contra-rotating type with the distribution given by the author, the prese t case of a propeller in a circular duct requires a radial loading which increases towards the tip. Tables for this case are not yet available. However, anyone skilled in the art of the propeller theory can obtain approximate graphs for the loading of multiblade propellers in a circular duct based on the formulas of Section B.

Design Method: Comply with the condition of ideal disk loading given in Section B. (Tables not yet available.)

2. Duct Design

Duct streamlines for an ideal duct are given in Ref. A1, Volume I, Chapter IV, and in Figures I and II, Pages 72 and 73. It may be possible to design an ideal duct in some cases. The ideal duct is defined as a duct whose inlet wall conforms to any one of the streamlines shown in these figures. Such a duct as distinguished from any other duct provides a constant axial component of the inlet velocity at the plane of the propeller. Any other duct design, for instance the bellmouth duct, causes deviations from the ideal case by producing an excess velocity at the circumference or at the tip of the propeller.

Design Method: Employ the ideal streamline shape when possible or obtain radial velocity distribution in any other case by calculation or, if necessary, by a model test.

3. Problems of Combination of Propeller and Duct

The ideal cases of propeller and duct defined above fit together perfectly. If deviations are necessary, as is usually the case in the duct design, calculate the resulting velocity distribution, which normally exhibits an increase in the velocity near the circumference. Such is the case both for short ducts and for bellmouth ducts. This work can only be done by engineers skilled in the art and has to be done as each case will be different. Experimental models or the electric analogy method may also be employed. In designing the propeller, make the twist distribution

comply exactly with the particular axial velocity distribution, but maintain the loading as in the ideal case.

Design Method: Match propeller with particular imposed axial velocity distribution of the duct proper.

4. Baffles and Inlet Vanes

As the propeller, under no circumstances, will operate efficiently with a non-uniform or skewed flow distribution, there are obviously cases in which baffles or vanes of some type should be employed. While outlet vanes may be used for control, no particular problem of efficiency is involved. In the design of inlet vanes, it is imperative to employ the existing potential theory. (See reference in present volume, Section G.) Tests performed as part of the present study confirm theory and show remarkably high efficiency. (Sections H and I.)

Design Method: Design baffles according to potential theory as indicated in Section G. In complex cases experimental work may be needed.

5. Interaction of Ducted Propeller and Wing or Fuselage

This aspect is of importance in regard to the required control forces, lift, drag, and general performance of the aircraft. The first item of concern is the pitch-up moment. Numerical values have been given in Ref. A1, Volume I, Chapter II for a sink in a rectangular plate and in Chapter III for the classical case of a two-dimensional line sink in a wing.

Design Method: To obtain pitch-up moment, employ the simple formula given in Ref. A1, Chapter II. The pitch-up moment arm is given in Chapter III under the formula III-21.

There is also a lift increase due to induced circulation on the wing which can be estimated with sufficient accuracy by formula III-18 of the same chapter.

6. The Effect of the Jet on the Lower Surface of the Wing or Fuselage

This subject is of more empirical nature and represents the only area which cannot, for the most part, be covered by theory. The only exception is the direct displacement effect of the jet on the pressure distribution for the lower surface of the wing or fuselage. This subject is treated in the present paper in Section E. Due essentially to the high velocity on the lateral sides of the jet there results a negative lift in magnitude equal to the product of the velocity head times the area of the jet cross section and a negative lift coefficient approaching the value of unity, if the adjacent flat area is large enough.

Design Method: Estimate extent of adversely affected area and employ negative lift and thrust coefficients given in Section E and shown in Figures E1 and E2.

There is, however, a much larger negative contribution both to the lift and to the adverse pitching moment. This subject has been treated

in the present volume, Section F. The deficiency in pressure recovery which is the cause of the drag of a cylinder and which exists behind the jet produces a pressure-deficiency on the lower wing surface behind the jet. Tests analyzed in Section F indicate that there exists a drastic decrease of lift and a large increase in the pitching moment. However, since the drag of a cylindrical body is reduced to a fraction of its value beyond a certain critical Reynolds number, it is probable that the effect is less serious than indicated.

Design Method: Yet inadequate. Tests of pressure distribution at higher Reynolds number ($R > 10^6$) are needed. In the meantime, employ values of one quarter of the ones indicated from small scale tests in Section F.

There exists a few cases in which the theoretical treatment is either too laborious or inadequate. In conjunction with a design of any consequence, certain complimentary experiments could be carried on to considerable advantage.

The first problem concerns the matching of the propeller to the duct. A simple experiment may be performed, the purpose of which is to establish the flow pattern of the duct-inlet at zero forward velocity. This test is most conveniently performed by attaching a cylindrical extension of some length to the model duct outlet to remove the local effect of the suction device. Measure the velocity distribution along the

radius of the duct at the proposed plane of the propeller. This is also an excellent case in which the electric analogy may be employed. The advantage is that the effect of the viscosity or Reynolds number is then completely eliminated. Thus a very small model may be employed to represent properly the condition of the actual flow at a high Reynolds number. The matching propeller can then be designed. Testing of a model propeller will not be necessary. The model duct should be of at least one-foot diameter to insure reasonable Reynolds numbers in a typical low speed wind tunnel.

The second experimental problem concerns the empirical effect of the obstruction of the jet on the flow pattern on the lower side of a wing. As has been pointed out, the deficiency in pressure recovery behind the jet causes a loss in lift and creates an additional unfavorable pitch-up moment of some magnitude. In addition, the jet exhibits a pumping action on the lower side of the wing tending to aggrevate these effects. To obtain numerical values of the loss in lift and the adverse pitching moment and to investigate means for improvements, a fan-in-wing model test should be run at a reasonable Reynolds number and the model should be equipped with means for measuring the pressure distribution on the lower surface as affected by the jet in the range of forward speeds corresponding to transition.

SECTION B

THE IDEAL LOADING OF SINGLE-ROTATION PROPELLERS IN A CIRCULAR DUCT

I. INTRODUCTION

In this problem, the flow field of a single shrouded propeller is examined. The shroud is considered as an infinite cylindrical surface, and the velocity potential function ϕ which describes the flow within the shroud is determined. Use has been made of Sydney Goldstein's method in solving the boundary problem for the ideal case of a single rotating propeller.

In this case a two-bladed propeller will be considered and the helical surface produced by the propeller is given by

$$\theta - \omega z \frac{1}{V+w} = 0 \quad \text{or} \quad \pi \tag{1}$$

where r, θ and z are the cylindrical polar coordinates with the helix axis as the reference axis. The axial displacement of the spiral is w and the expression for the slope at any radius r is

$$\tan \alpha = \frac{dz}{r d\theta} = \frac{V+w}{r\omega} \tag{2}$$

Thus, the velocity normal to the surface is

$$w \cos \alpha = \frac{\partial \phi}{\partial z} \cos \alpha - \frac{\partial \phi}{r \partial \theta} \sin \alpha \tag{3}$$

The above boundary condition is given for the helix surface only for $r < R$ where R is the radius of the helix. The boundary condition for $r = R$ is that $\partial \phi / \partial r = 0$.

Changing the variables r, θ and z into μ and ζ given by

$$\mu = \frac{r}{V+w}\omega, \qquad \zeta = \theta - z\frac{\omega}{V+w} \tag{4}$$

and taking into consideration that ζ = constant, gives a spiral line, the three-dimensional problem reduces to a two-dimensional one. From Eqs. (4), one obtains the relations

$$\frac{\partial\phi}{\partial z} = -\frac{\omega}{V+w}\frac{\partial\phi}{\partial\zeta}, \qquad \frac{\partial\phi}{\partial\theta} = \frac{\partial\phi}{\partial\zeta} \tag{5}$$

Making use of Eq. (3), we find the following for the boundary conditions in the (μ, ζ) system

$$\frac{\partial\phi}{\partial\zeta} = -\frac{\mu^2}{1+\mu^2}\frac{V+w}{\omega}w \quad \& \quad \frac{\partial\phi}{\partial\mu} = 0 \quad \text{at} \quad \mu = \mu_0 = \frac{R}{V+w}\omega \tag{6}$$

Substituting the following function for the velocity potential

$$\frac{V+w}{\omega}w\varphi = \phi \tag{7}$$

the boundary conditions become

$$\frac{\partial\varphi}{\partial\zeta} = -\frac{\mu^2}{1+\mu^2} \quad \& \quad \left.\frac{\partial\varphi}{\partial\mu}\right|_{\mu_0} = 0 \tag{8}$$

The differential equation for the potential φ in conventional cylindrical coordinates is given by

$$\nabla^2\varphi = \frac{1}{r}\frac{\partial}{\partial r}\left(r\frac{\partial\varphi}{\partial r}\right) + \frac{\partial^2\varphi}{r^2\partial\theta^2} + \frac{\partial^2\varphi}{\partial z^2} = 0 \tag{9}$$

From Eqs. (4) and (5), we obtain the following relations among the partial derivatives of the function φ in the two coordinate systems:

$$\frac{\partial}{\partial\theta} = \frac{\partial}{\partial\zeta} \qquad \frac{\partial}{\partial z} = -\frac{\omega}{V+w}\frac{\partial}{\partial\zeta}$$

$$\frac{\partial^2}{\partial\theta^2} = \frac{\partial^2}{\partial\zeta^2} \qquad \frac{\partial^2}{\partial z^2} = \left(\frac{\omega}{V+w}\right)^2\frac{\partial^2}{\partial\zeta^2}$$

$$\frac{\partial}{\partial x} = \frac{\omega}{V+w}\frac{\partial}{\partial \mu} \qquad \frac{\partial^2}{\partial x^2} = \left(\frac{\omega}{V+w}\right)^2 \frac{\partial^2}{\partial \mu^2}$$

Substituting for the above relations in Eq. (9), we find the Laplacian in the transformed (μ, ζ) coordinate system

$$\mu \frac{\partial}{\partial \mu}\left(\mu \frac{\partial}{\partial \mu}\varphi\right) + \left(1+\mu^2\right)\frac{\partial^2 \varphi}{\partial \zeta^2} = 0 \tag{10}$$

Thus, the problem of the flow field of the shrouded propeller is given by the solution of the partial differential Eq. (10) with the boundary conditions given by Eqs. (8).

II. SOLUTION OF THE POTENTIAL PROBLEM

Since it has been assumed that the shroud is a circular cylindrical surface extending to infinity, we are interested in obtaining only the flow field in the region $r \leq R$. Changing the dependent variable into

$$\varphi_1 = \frac{\mu^2}{1+\mu^2}\zeta + \varphi \tag{11}$$

the above Eq. (10) becomes

$$\left(\mu \frac{\partial}{\partial \mu}\right)^2 \varphi_1 + \left(1+\mu^2\right)\frac{\partial^2 \varphi_1}{\partial \zeta^2} = \left(\mu \frac{\partial}{\partial \mu}\right)^2 \left(\frac{\mu^2}{1+\mu^2}\right)\zeta \tag{12}$$

From Eqs. (8), the boundary conditions for the function φ_1 are given by

$$\frac{\partial \varphi_1}{\partial \zeta} = 0 \qquad \& \qquad \left.\frac{\partial \varphi_1}{\partial \mu}\right|_{\mu_0} = 0 \tag{13}$$

Expanding the independent variable ζ on the "right-hand side" of Eq. (12) in a Fourier-series for the interval $0 \leq \zeta \leq \pi$ we find

$$\zeta = \frac{\pi}{2} - \frac{4}{\pi}\sum_{m=0}^{\infty} \frac{\cos(2m+1)\zeta}{(2m+1)^2} \tag{14}$$

Assuming a solution φ_1, which is expanded in the form

$$\varphi_1 = f_0(\mu) + \sum_{m=0}^{\infty} f_m(\mu) \cos(2m+1)\zeta \tag{15}$$

and substituting both Eqs. (14) and (15) into Eq. (12), we find the following by equating the coefficients of $\cos(2m+1)\zeta$,

$$\left(\mu\frac{d}{d\mu}\right)^2 f_0(\mu) = \frac{\pi}{2}\left(\mu\frac{d}{d\mu}\right)^2\left(\frac{\mu^2}{1+\mu^2}\right) \tag{16}$$

$$\left(\mu\frac{d}{d\mu}\right)^2 f_m(\mu) - (2m+1)^2(1+\mu^2) f_m(\mu) = -\frac{4}{\pi}\frac{1}{(2m+1)^2}\left(\mu\frac{d}{d\mu}\right)^2\left(\frac{\mu^2}{1+\mu^2}\right) \tag{17}$$

Since the potential φ_1 is finite at $r = 0$, the above Eq. (16) gives

$$f_0(\mu) = \frac{\pi}{2}\frac{\mu^2}{1+\mu^2} \tag{18}$$

Using for the function $f_m(\mu)$, the expression

$$f_m(\mu) = -\frac{4}{\pi}\frac{1}{(2m+1)^2}\left\{\frac{\mu^2}{1+\mu^2} - g_m(\mu)\right\} \tag{19}$$

and substituting into Eq. (17), we find the following differential equation for $g_m(\mu)$.

$$\left(\mu\frac{d}{d\mu}\right)^2 g_m(\mu) - (2m+1)^2(1+\mu^2) g_m(\mu) = -(2m+1)^2\mu^2 \tag{20}$$

A particular solution of Eq. (20) is

$$S_{1,\nu}(iz) = \frac{\nu\pi}{2\sin\frac{1}{2}\nu\pi} I_\nu(z) + \nu e^{\frac{i}{2}\nu\pi} K_\nu(z) - t_{1,\nu}(z) \tag{21}$$

where $t_{1,\nu}(z)$ is given by the series

$$t_{1,\nu}(z) = \frac{z^2}{2^2-\nu^2} + \frac{z^4}{(2^2-\nu^2)(4^2-\nu^2)} + \cdots + \frac{z^{2m}}{(2^2-\nu^2)(4^2-\nu^2)\cdots(4m^2-\nu^2)} + \cdots \tag{22}$$

and $\nu = 2m+1$ & $z = (2m+1)\mu$.

We define a new function $T_{1,2m+1}([2m+1]\mu)$.

$$T_{1,2m+1}([2m+1]\mu) = (-1)^m (2m+1)\frac{\pi}{2} I_{2m+1}([2m+1]\mu) - t_{1,2m+1}([2m+1]\mu) \qquad (23)$$

Then the above function $T_{1,2m+1}$ is also a particular solution of Eq. (20). The general solution of Eq. (20) which remains finite on the axis, (i.e., $\mu = 0$) is thus given by

$$g_m(\mu) = T_{1,2m+1}([2m+1]\mu) + b_m I_{2m+1}([2m+1]\mu) \qquad (24)$$

Substituting into Eq. (11) for ζ from Eq. (14), for φ_1 from Eq. (15), for f_0 from Eq. (18), and for f_m from Eq. (19), we find

$$\varphi = \frac{4}{\pi}\sum_{m=0}^{\infty} \frac{1}{(2m+1)^2} g_m(\mu)\cos(2m+1)\zeta \qquad (25)$$

$$= \sum_{m=0}^{\infty}\left\{\frac{4}{\pi}\frac{T_{1,2m+1}([2m+1]\mu)}{(2m+1)^2} + a_m \frac{I_{2m+1}([2m+1]\mu)}{I_{2m+1}([2m+1]\mu_0)}\right\}\cos(2m+1)\zeta$$

Since the function φ is an odd function, it is obvious that for the interval $-\pi \leq \zeta \leq 0$, we find the same expression for φ with the opposite sign. At $\zeta = 0$ or π, the potential function φ has a discontinuity which is given by

$$[\varphi]_0 = \frac{8}{\pi}\sum_{m=0}^{\infty}\frac{T_{1,2m+1}([2m+1]\mu)}{(2m+1)^2} + 2\sum_{m=0}^{\infty} a_m \frac{I_{2m+1}([2m+1]\mu)}{I_{2m+1}([2m+1]\mu_0)} \qquad (26)$$

The unknown coefficients a_m are determined from the second of the boundary conditions given by Eq. (8). Differentiating the above Eq. (25) with respect to μ, we get

$$\frac{\partial\varphi}{\partial\mu} = \sum_{m=0}^{\infty}\left\{\frac{4}{\pi}\frac{T'_{1,2m+1}([2m+1]\mu)}{(2m+1)^2} + a_m \frac{I'_{2m+1}([2m+1]\mu)}{I_{2m+1}([2m+1]\mu_0)}\right\}(2m+1)\cos(2m+1)\zeta \qquad (27)$$

Making use of Eq. (27), the boundary condition given by the second of Eqs. (8) gives

$$a_m = -\frac{4}{\pi} \frac{T'_{1,2m+1}([2m+1]/\mu_0)}{(2m+1)^2} \frac{I_{2m+1}([2m+1]/\mu_0)}{I'_{2m+1}([2m+1]/\mu_0)} \tag{28}$$

Substituting Eq. (28) into Eq. (25), we get

$$\varphi = \frac{4}{\pi} \sum_{m=0}^{\infty} \frac{1}{(2m+1)^2} \left\{ T_{1,2m+1}([2m+1]/\mu) - \frac{T'_{1,2m+1}([2m+1]/\mu_0)}{I'_{2m+1}([2m+1]/\mu_0)} I_{2m+1}([2m+1]/\mu) \right\} \cos(2m+1)\zeta \tag{29}$$

Thus, the velocity potential ϕ from Eq. (7) becomes

$$\phi = \frac{4w(V+w)}{\pi\omega} \sum_{m=0}^{\infty} \left\{ T_{1,2m+1}([2m+1]/\mu) - \frac{T'_{1,2m+1}([2m+1]/\mu_0)}{I'_{2m+1}([2m+1]/\mu_0)} I_{2m+1}([2m+1]/\mu) \right\} \frac{\cos(2m+1)\zeta}{(2m+1)^2} \tag{30}$$

Similarly, the jump of the velocity potential at $\zeta = 0$ or π, given by Eq. (26) becomes

$$\left[\Phi\right]_0 = \frac{8w(V+w)}{\pi\omega} \sum_{m=0}^{\infty} \frac{1}{(2m+1)^2} \left\{ T_{1,2m+1}([2m+1]/\mu) - \frac{T'_{1,2m+1}([2m+1]/\mu_0)}{I'_{2m+1}([2m+1]/\mu_0)} I_{2m+1}([2m+1]/\mu) \right\} \tag{31}$$

III. VELOCITY FIELD

The velocity field within the shroud is formed by the gradient of the velocity potential, i.e., $v = \nabla\phi$. Making use of Eqs. (4) and (5), we find the following for the velocity components in the cylindrical coordinate system

$$u_r = \frac{\partial\phi}{\partial r}, \qquad u_\theta = \frac{\partial\phi}{r\partial\theta}, \qquad u_z = \frac{\partial\phi}{\partial z} \tag{32}$$

In the (μ, ζ) system, the above equations become

$$u_r = \frac{\omega}{V+w} \frac{\partial\phi}{\partial\mu}, \qquad u_\theta = \frac{\omega}{V+w} \frac{1}{\mu} \frac{\partial\phi}{\partial\zeta}, \qquad u_z = -\frac{\omega}{V+w} \frac{\partial\phi}{\partial\zeta} \tag{33}$$

From Eqs. (33), it is obvious that

$$u_\zeta = -\mu \, u_\theta$$

Differentiating Eq. (30) with respect to ζ and μ, we get respectively

$$\frac{\partial \phi}{\partial \zeta} = -\frac{4w(V+w)}{\pi\omega} \sum_{m=0}^{\infty} \left\{ T_{1,2m+1}([2m+1]\mu) - \frac{T'_{1,2m+1}([2m+1]\mu_0)}{I'_{2m+1}([2m+1]\mu_0)} I_{2m+1}([2m+1]\mu) \right\} \frac{\sin(2m+1)\zeta}{(2m+1)} \tag{34}$$

$$\frac{\partial \phi}{\partial \mu} = \frac{4w(V+w)}{\pi\omega} \sum_{m=0}^{\infty} \left\{ T'_{1,2m+1}([2m+1]\mu) - \frac{T'_{1,2m+1}([2m+1]\mu_0)}{I'_{2m+1}([2m+1]\mu_0)} I'_{2m+1}([2m+1]\mu) \right\} \frac{\cos(2m+1)\zeta}{(2m+1)} \tag{35}$$

From Eqs. (32), (34) and (35), the velocity components u_r, u_θ and u_z become

$$u_r = \frac{4w}{\pi} \sum_{m=0}^{\infty} A'_m(\mu_0,\mu) \frac{\cos(2m+1)\zeta}{2m+1} \tag{36}$$

$$u_\theta = -\frac{4w}{\pi\mu} \sum_{m=0}^{\infty} A_m(\mu_0,\mu) \frac{\sin(2m+1)\zeta}{2m+1} \tag{37}$$

$$u_\zeta = \frac{4w}{\pi} \sum_{m=0}^{\infty} A_m(\mu_0,\mu) \frac{\sin(2m+1)\zeta}{2m+1} \tag{38}$$

where:

$$A_m(\mu_0,\mu) \equiv T_{1,2m+1}([2m+1]\mu) - \frac{T'_{1,2m+1}([2m+1]\mu_0)}{I'_{2m+1}([2m+1]\mu_0)} I_{2m+1}([2m+1]\mu) \tag{39}$$

$$A'_m(\mu_0,\mu) \equiv T'_{1,2m+1}([2m+1]\mu) - \frac{T'_{1,2m+1}([2m+1]\mu_0)}{I'_{2m+1}([2m+1]\mu_0)} I'_{2m+1}([2m+1]\mu) \tag{40}$$

IV. LOADING FUNCTION

The loading function K(r) is a dimensionless quantity defined by

$$K(r) = \frac{\omega \rho \Gamma(r)}{2\pi (V+w) w} \tag{41}$$

where p is the number of blades or helix surfaces and Γ (r) is the circulation which is equal to the potential difference across the helix surface at the radius r.

From Eq. (31), the circulation Γ (r) becomes

$$\Gamma(r) = \frac{8w(V+w)}{\pi\omega} \sum_{m=0}^{\infty} \frac{1}{(2m+1)^2} \left\{ T_{1,2m+1}([2m+1]\mu) - \frac{T'_{1,2m+1}([2m+1]\mu_0)}{I'_{2m+1}([2m+1]\mu_0)} I_{2m+1}([2m+1]\mu) \right\} \tag{42}$$

Introducing the dimensionless quantity

$$\tau = \frac{r}{R} \tag{43}$$

and making use of Eq. (41), we get the following from the above Eq. (42)

$$K(\tau) = \frac{8}{\pi^2} \sum_{m=0}^{\infty} \frac{1}{(2m+1)^2} \left\{ T_{1,2m+1}([2m+1]\mu) - \frac{T'_{1,2m+1}([2m+1]\mu_0)}{I'_{2m+1}([2m+1]\mu_0)} I_{2m+1}([2m+1]\mu) \right\} \tag{44}$$

where

$$\mu = \frac{\omega}{V+w} r = \frac{\omega R}{V+w} \tau \tag{45}$$

The momentum within a volume confined between two successive vortex surfaces become

$$M = \rho \iiint_{Vol} V d\omega = \rho \oiint_{Area} \phi \, dA = \rho \iint_{A} \Gamma \, dA \tag{46}$$

where Γ is the circulation function for one blade and A is the area of the projected cross-section of one turn of the spiral, which is equal to the cross-section of the shroud. Introducing again the dimensionless quantity τ, the momentum per surface per turn becomes

$$M = \rho \pi w \frac{V+w}{\omega} \pi R^2 \frac{1}{\pi} \int_0^{2\pi} \int_0^1 K(\tau,\theta) \tau \, d\tau \, d\theta \tag{47}$$

Thus, the mass coefficient for single-rotation propellers is

$$\mu = \frac{1}{\pi} \int_0^{2\pi} \int_0^1 K(\tau,\theta) \tau \, d\tau \, d\theta = 2 \int_0^1 K(\tau) \tau \, d\tau \tag{48}$$

Substituting for $K(\tau)$ from Eq. (44) into the above equation, the mass coefficient becomes

$$\mu = \left[\frac{4}{\pi}\right]^2 \sum_{m=0}^{\infty} \frac{1}{(2m+1)^2} \int_0^1 \left\{ T_{1,2m+1}\left([2m+1]\frac{\omega R}{V+w}\tau\right) - \frac{T'_{1,2m+1}\left([2m+1]\frac{\omega R}{V+w}\right)}{I'_{2m+1}\left([2m+1]\frac{\omega R}{V+w}\right)} I_{2m+1}\left([2m+1]\frac{\omega R}{V+w}\tau\right) \right\} \tau \, d\tau \tag{49}$$

From Eqs. (44) and (49) for the loading function K and the mass coefficient μ, we find the design relations of a propeller.

V. APPENDIX

So long as μ is not too small, we might make the following approximations. The functions $T_{1,2m+1}$ given by Eq. (23) are approximated by

$$T_{1,2m+1} \simeq \frac{\mu^2}{1+\mu^2} \tag{A-1}$$

Thus, its derivative will be

$$T'_{1,(2m+1)} \simeq \frac{1}{2m+1} \frac{2\mu}{(1+\mu^2)^2} \tag{A-2}$$

From the approximate relations

$$\frac{(2m+1) I'_{2m+1}}{I_{2m+1}} - 2m \frac{K'_{2m}}{K_{2m}} \simeq \sqrt{1+\mu^2}\,(2m+1+2m) \tag{A-3}$$

$$\frac{K'_{2m}}{K_{2m}} \simeq -\sqrt{1+\mu^2}$$

we find

$$\frac{I'_{2m+1}}{I_{2m+1}} \simeq \sqrt{1+\mu^2} \tag{A-4}$$

Solving the above equations for I_{2m+1}, we find

$$I_{2m+1} \simeq e^{\frac{2m+1}{2}\left\{\mu\sqrt{1+\mu^2} + \ln\left(\mu+\sqrt{1+\mu^2}\right)\right\}} \tag{A-5}$$

and its derivative becomes

$$I'_{2m+1} \simeq \sqrt{1+\mu^2}\, e^{\frac{2m+1}{2}\left\{\mu\sqrt{1+\mu^2} + \ln\left(\mu+\sqrt{1+\mu^2}\right)\right\}} \tag{A-6}$$

Equations (A-5) and (A-6) are approximated by

$$I_{2m+1} \simeq e^{\frac{2m+1}{2}\mu\sqrt{1+\mu^2}} \tag{A-7}$$

$$I'_{2m+1} \simeq \sqrt{1+\mu^2}\; e^{\frac{2m+1}{2}\mu\sqrt{1+\mu^2}} \tag{A-8}$$

Making use of Eqs. (A-1), (A-2), (A-7) and (A-8), we find the following for the functions $A_m(\mu_0,\mu)$ and $A'_m(\mu_0,\mu)$ given by Eqs. (39) and (40).

$$A_m(\mu_0,\mu) \simeq \frac{\mu^2}{1+\mu^2} - \frac{1}{2m+1}\frac{2\mu_0}{(1+\mu_0^2)^2}\frac{e^{\frac{2m+1}{2}\mu\sqrt{1+\mu^2}}}{e^{\frac{2m+1}{2}\mu_0\sqrt{1+\mu_0^2}}} \tag{A-9}$$

$$A'_m(\mu_0,\mu) \simeq \frac{2}{2m+1}\left[\frac{\mu}{(1+\mu^2)^2} - \frac{\mu_0}{(1+\mu_0^2)^{5/2}}\frac{e^{\frac{2m+1}{2}\mu\sqrt{1+\mu^2}}}{e^{\frac{2m+1}{2}\mu_0\sqrt{1+\mu_0^2}}}\right] \tag{A-10}$$

Substituting Eqs. (A-9) and (A-10) into Eqs. (44) and (49), we find an approximate estimate for the loading function K and the mass coefficient ν of the propeller.

Similarly, Eqs. (36), (37) and (38) will give an approximation for the flow field within the shroud.

SECTION C

FLOW FIELD FOR NON-UNIFORM SINK DISTRIBUTION IN A CIRCULAR DISK

I. INTRODUCTION

In the Interim Report Number 7 of contract DA 44-177-TC-606, the flow field for uniform sink distribution in a circular disk was derived. In this paper the case of non-uniform sink distribution will be examined. For simplification, axially symmetric cases will be considered and a step-wise constant distribution over circular rings will be assumed.

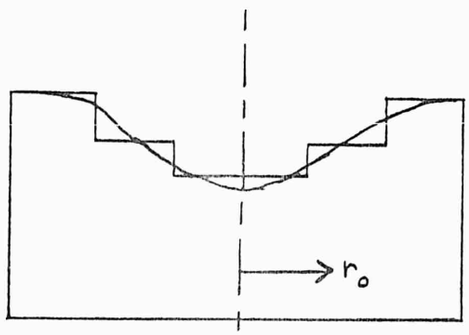

Figure C1

The case of a uniform sink distribution in an annulus is found as a special case, by considering the strength of the sinks in the central region as zero.

The flow field of a propeller in an annulus of an infinite plate is then represented by a uniform sink distribution at the annulus and a superposition of a uniform flow in the semi-infinite region of the cylindrical annulus behind the propeller.

Finally, the case of a continuous and axially symmetric sink distribution is examined which is expressed as a polynomial of even powers of the radius r_o.

II. VELOCITY POTENTIAL

For the case of only one step in the distribution of the sinks, we have the following

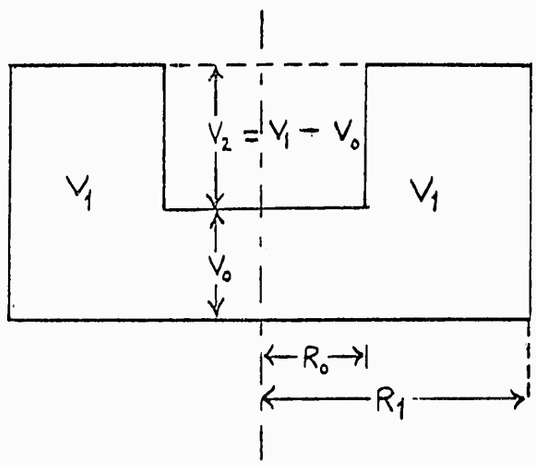

Figure C2

From the velocity potential of a point sink of strength δQ and an angle $\omega = 90^o$ at a distance r_o from the origin, we have

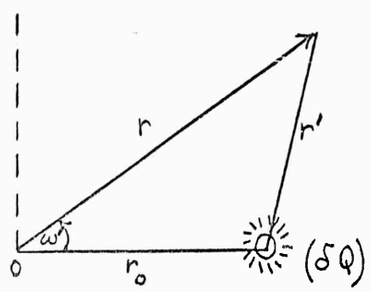

Figure C3

$$\delta\Phi(r,90^\circ) = \begin{cases} \dfrac{\delta Q}{4\pi r}\sum_{n=0}^{\infty}\left(\dfrac{r_o}{r}\right)^n P_n(0) & \text{for } \dfrac{r}{r_o} > 1 \\ \dfrac{\delta Q}{4\pi r_o}\sum_{n=0}^{\infty}\left(\dfrac{r}{r_o}\right)^n P_n(0) & \text{for } \dfrac{r}{r_o} < 1 \end{cases} \qquad (1)$$

In Figure C2 the step-wise sink distribution can be considered as the algebraic summation of two uniform sink distributions over two co-axial disks of different radius

Thus, in the above case, the velocity potential is found as follows:

Region A: $r > R_1$

For $r > R_1$, i.e., $r/r_0 > 1$, the velocity potential, for the sink distribution of strength δQ_1, along the axis of symmetry $\theta = 0$ is found by integrating Eqs. (1) from 0 to R_1, i.e.,

$$\Phi_{1\,\theta=0,\omega=90^\circ}(r,0) = \int_0^{R_1}\int_0^{2\pi} \frac{\delta Q_1}{4\pi r} \sum_{n=0}^{\infty} \left(\frac{r_0}{r}\right)^n P_n(0)\, r_0\, dr_0\, d\varphi \tag{2}$$

Integrating and substituting $\delta Q_1 \times \pi R_1^2 = Q_1$, we find

$$\Phi_1(r,0) = \frac{Q_1}{2\pi} \sum_{n=0}^{\infty} \frac{P_n(0)}{n+2} \frac{R_1^n}{r^{n+1}} \tag{3}$$

where

$$Q_1 = 2\pi R_1^2 V_1 \tag{4}$$

Similarly, for the second uniform distribution δQ_2 from 0 to R_0, we get

$$\Phi_2(r,0) = \int_0^{R_0}\int_0^{2\pi} \frac{\delta Q_2}{4\pi r} \sum_{n=0}^{\infty} \left(\frac{r_0}{r}\right)^n P_n(0)\, r_0\, dr_0\, d\varphi \tag{5}$$

Integrating and substituting $Q_2 = \delta Q_2 \times \pi R_0^2$, we find

$$\Phi_2(r,0) = \frac{Q_2}{2\pi} \sum_{n=0}^{\infty} \frac{P_n(0)}{n+2} \frac{R_0^n}{r^{n+1}} \tag{6}$$

where

$$Q_2 = 2\pi R_o^2 V_2 = 2\pi R_o^2 (V_1 - V_o) \tag{7}$$

Thus, for $r > R_1$ the velocity potential along the axis of symmetry becomes

$$\Phi_A(r,o) = \Phi_1 - \Phi_2 = \frac{1}{2\pi r} \sum_{n=0}^{\infty} \frac{P_n(o)}{n+2} \left[Q_1 \left(\frac{R_1}{r}\right)^n - Q_2 \left(\frac{R_o}{r}\right)^n \right] \tag{8}$$

Since the flow is axial symmetric, the general solution of the Laplace equation is given by

$$\Phi(r,\theta) = \sum_{n=0}^{\infty} A_n r^n P_n(\cos\theta) + \sum_{n=0}^{\infty} B_n \frac{1}{r^{n+1}} P_n(\cos\theta) \tag{9}$$

It is obvious that the velocity potential in the region $r > R_1$ for any angle θ is given by

$$\Phi_A(r,\theta) = \frac{1}{2\pi r} \sum_{n=0}^{\infty} \frac{P_n(o)}{n+2} \left[Q_1 \left(\frac{R_1}{r}\right)^n - Q_2 \left(\frac{R_o}{r}\right)^n \right] P_n(\cos\theta) \tag{10}$$

Region B: $r < R_o$

For $r < R_o$ we have that

$$\begin{aligned} r/r_o &> 1 \qquad \text{for} \quad o < r_o < r \\ r/r_o &< 1 \qquad \text{for} \quad r < r_o < R_o \end{aligned} \tag{11}$$

Thus, the velocity potential, for the sink distribution of strength δQ_1, along the axis of symmetry $\theta = 0$ is found by integrating Eqs. (1) from 0 to r and from r to R_1, respectively, i.e.,

$$\begin{aligned} \Phi_1(r,o) = &\int_o^r \int_o^{2\pi} \frac{\delta Q_1}{4\pi r} \sum_{n=0}^{\infty} \left(\frac{r_o}{r}\right)^n P_n(o)\, r_o\, dr_o\, d\varphi \\ &+ \int_r^{R_1} \int_o^{2\pi} \frac{\delta Q_1}{4\pi r_o} \sum_{n=0}^{\infty} \left(\frac{r}{r_o}\right)^n P_n(o)\, r_o\, dr_o\, d\varphi \end{aligned} \tag{12}$$

Performing the integration, we find

$$\Phi_1(r,o) = \frac{Q_1 r}{2\pi R_1^2} \sum_{n=o}^{\infty}{}^{*} \frac{P_n(o)}{n-1}\left\{\frac{2n+1}{n+2} - \left(\frac{r}{R_1}\right)^{n-1}\right\} \tag{13}$$

where

$$\sum_{n=o}^{\infty}{}^{*} \equiv \sum_{\substack{n=o \\ n\neq 1}}^{\infty}$$

Similarly, for the second sink distribution of strength δQ_2, we get

$$\Phi_2(r,o) = \frac{Q_2 r}{2\pi R_o^2} \sum_{n=o}^{\infty}{}^{*} \frac{P_n(o)}{n-1}\left[\frac{2n+1}{n+2} - \left(\frac{r}{R_o}\right)^{n-1}\right] \tag{14}$$

Thus, for $r < R_o$ the velocity potential along the axis of symmetry becomes

$$\Phi_B(r,o) = \Phi_1 - \Phi_2 = \frac{1}{2\pi} \sum_{n=o}^{\infty}{}^{*} \frac{P_n(o)}{n-1}\left\{\frac{Q_1 r}{R_1^2}\left[\frac{2n+1}{n+2} - \left(\frac{r}{R_1}\right)^{n-1}\right] - \right. \tag{15}$$

$$\left. - \frac{Q_2 r}{R_o^2}\left[\frac{2n+1}{n+2} - \left(\frac{r}{R_o}\right)^{n-1}\right]\right\}$$

or

$$\Phi_B(r,o) = \frac{r}{2\pi} \sum_{n=o}^{\infty}{}^{*} \frac{P_n(o)}{n-1}\left\{\frac{2n+1}{n+2}\left[\frac{Q_1}{R_1^2} - \frac{Q_2}{R_o^2}\right] + \left[\frac{Q_2}{R_o^2}\left(\frac{r}{R_o}\right)^{n-1} - \frac{Q_1}{R_1^2}\left(\frac{r}{R_1}\right)^{n-1}\right]\right\} \tag{16}$$

where

$$\frac{Q_1}{R_1^2} - \frac{Q_2}{R_o^2} = \frac{2\pi R_1^2}{R_1^2} V_1 - \frac{2\pi R_o^2 (V_1 - V_o)}{R_o^2} = 2\pi V_o \tag{17}$$

Making use of Eq. (9), since the flow field is axially symmetric, we get

$$A_1 = \frac{1}{2\pi}\left(\frac{Q_1}{R_1^2} - \frac{Q_2}{R_o^2}\right) \sum_{K=o}^{\infty}{}^{*} \frac{P_K(o)}{K-1} \frac{2K+1}{K+2}$$

$$A_n = -\frac{1}{2\pi} \frac{P_n(o)}{n-1}\left(\frac{Q_1}{R_1^{n+1}} - \frac{Q_2}{R_o^{n+1}}\right) \tag{18}$$

$$B_n \equiv 0$$

From the sum (see Interim Report No. 7)

$$\sum_{K=0}^{\infty}{}^{*}\,\frac{P_K(0)}{K-1}\,\frac{2K+1}{K+2} = -1 \tag{19}$$

and from Eqs. (9) and (18) we have that the velocity potential in the region $r < R_0$ for any angle θ is given by

$$\Phi_B(r,\theta) = -\frac{1}{2\pi}\left(\frac{Q_1}{R_1^2} - \frac{Q_2}{R_0^2}\right) r P_1(\cos\theta) - \sum_{n=0}^{\infty}{}^{*}\,\frac{1}{2\pi}\,\frac{P_n(0)}{(n-1)}$$

$$\left[\frac{Q_1}{R_1}\left(\frac{r}{R_1}\right)^n - \frac{Q_2}{R_0}\left(\frac{r}{R_0}\right)^n\right] P_n(\cos\theta) \tag{20}$$

Region C: $R_0 < r < R_1$

For $R_0 < r < R_1$ we have that

$$r/r_0 > 1 \quad \text{for} \quad R_0 < r_0 < r$$

$$r/r_0 < 1 \quad \text{for} \quad r < r_0 < R_1$$

Thus, the velocity potential, for the sink distribution δQ_1, along the axis of symmetry $\theta = 0$, is found by integrating Eqs. (1) from 0 to r and from r to R_1, i.e.,

$$\Phi_1(r,0) = \int_0^r \int_0^{2\pi} \frac{\delta Q_1}{4\pi r} \sum_{n=0}^{\infty} \left(\frac{r_0}{r}\right)^n P_n(0)\, r_0\, dr_0\, d\varphi$$

$$+ \int_r^{R_1} \int_0^{2\pi} \frac{\delta Q_1}{4\pi r_0} \sum_{n=0}^{\infty} \left(\frac{r}{r_0}\right)^n P_n(0)\, r_0\, dr_0\, d\varphi \tag{21}$$

Performing the integration, we get

$$\Phi_1(r,0) = \frac{Q_1}{2\pi}\,\frac{r}{R_1^2} \sum_{n=0}^{\infty}{}^{*}\,\frac{P_n(0)}{(n-1)}\left[\frac{2n+1}{n+2} - \left(\frac{r}{R_1}\right)^{n-1}\right] \tag{22}$$

Similarly, for the second sink distribution δQ_2, we have

$$\Phi_2(r,0) = \int_0^{R_0} \int_0^{2\pi} \frac{\delta Q_2}{4\pi r} \sum_{n=0}^{\infty} \left(\frac{r_0}{r}\right)^n P_n(0)\, r_0\, dr_0\, d\varphi \tag{23}$$

or

$$\Phi_2(r,0) = \frac{Q_2}{2\pi} \sum_{n=0}^{\infty} \frac{P_n(0)}{n+2} \frac{R_0^n}{r^{n+1}} \tag{24}$$

Thus, for $R_0 < r < R_1$ the velocity potential along the axis of symmetry becomes

$$\Phi_C(r,0) = \Phi_1 - \Phi_2 = \frac{Q_1}{2\pi} \frac{r}{R_1^2} \sum_{n=0}^{\infty}{}^{*} \frac{P_n(0)}{n-1} \left[\frac{2n+1}{n+2} - \left(\frac{r}{R_1}\right)^{n-1}\right] + \\ - \frac{Q_2}{2\pi} \sum_{n=0}^{\infty} \frac{P_n(0)}{n+2} \frac{R_0^n}{r^{n+1}} \tag{25}$$

or

$$\Phi_C(r,0) = \frac{Q_1}{2\pi R_1} \left(\frac{r}{R_1}\right) \sum_{n=0}^{\infty}{}^{*} \frac{P_n(0)}{n-1} \frac{2n+1}{n+2} + \\ - \frac{Q_1}{2\pi R_1} \sum_{n=0}^{\infty}{}^{*} \frac{P_n(0)}{n-1} \left(\frac{r}{R_1}\right)^n \\ - \frac{Q_2}{2\pi R_0} \sum_{n=0}^{\infty} \frac{P_n(0)}{n+2} \left(\frac{R_0}{r}\right)^{n+1} \tag{26}$$

Making use of Eq. (19), the above equation becomes

$$\Phi_C(r,0) = -\frac{Q_1}{2\pi R_1} \left(\frac{r}{R_1}\right) \\ - \frac{Q_1}{2\pi R_1} \sum_{n=0}^{\infty}{}^{*} \frac{P_n(0)}{n-1} \left(\frac{r}{R_1}\right)^n \\ - \frac{Q_2}{2\pi R_0} \sum_{n=0}^{\infty} \frac{P_n(0)}{n+2} \left(\frac{R_0}{r}\right)^{n+1} \tag{27}$$

Thus, the velocity potential in the region $R_0 < r < R_1$ and any angle θ becomes

$$\Phi_C(r,\theta) = -\frac{Q_1}{2\pi_1 R_1}\left(\frac{r}{R_1}\right)P_1(\cos\theta) +$$

$$-\left[\frac{Q_1}{2\pi R_1}\sum_{n=0}^{\infty}{}^{*}\frac{P_n(0)}{n-1}\left(\frac{r}{R_1}\right)^n + \frac{Q_2}{2\pi R_0}\sum_{n=0}^{\infty}\frac{P_n(0)}{n+2}\left(\frac{R_0}{r}\right)^{n+1}\right]P_n(\cos\theta) \tag{28}$$

III. VELOCITIES

The velocity components for the three regions, A, B and C, are given from the derivatives

$$u_r = \frac{\partial\Phi}{\partial r} \quad \& \quad u_\theta = \frac{\partial\Phi}{r\partial\theta} \tag{29}$$

Region A: $r > R_1$

From Eos. (10) and (29) we find

$$u_r = -\frac{1}{2\pi r^2}\sum_{n=0}^{\infty}\frac{n+1}{n+2}P_n(0)\left[Q_1\left(\frac{R_1}{r}\right)^n - Q_2\left(\frac{R_0}{r}\right)^n\right]P_n(\cos\theta)$$

$$u_\theta = -\frac{1}{2\pi r^2}\sin\theta\sum_{n=0}^{\infty}\frac{P_n(0)}{n+2}\left[Q_1\left(\frac{R_1}{r}\right)^n - Q_2\left(\frac{R_0}{r}\right)^n\right]\frac{dP_n(\mu)}{d\mu} \tag{30}$$

Region B: $r < R_0$

From Eqs. (20) and (29), we find

$$u_r = -\frac{1}{2\pi}\left(\frac{Q_1}{R_1^2} - \frac{Q_2}{R_0^2}\right)P_1(\cos\theta) - \frac{1}{2\pi}\sum_{n=0}^{\infty}{}^{*}\frac{nP_n(0)}{n-1}\left[\frac{Q_1}{R_1^2}\left(\frac{r}{R_1}\right)^{n-1} - \frac{Q_2}{R_0^2}\left(\frac{r}{R_0}\right)^{n-1}\right]P_n(\cos\theta)$$

$$u_\theta = \frac{\sin\theta}{2\pi}\left\{\left(\frac{Q_1}{R_1^2} - \frac{Q_2}{R_0^2}\right) + \sum_{n=0}^{\infty}{}^{*}\frac{P_n(0)}{n-1}\left[\frac{Q_1}{R_1^2}\left(\frac{r}{R_1}\right)^{n-1} - \frac{Q_2}{R_0^2}\left(\frac{r}{R_0}\right)^{n-1}\right]\frac{dP_n(\mu)}{d\mu}\right\} \tag{31}$$

Region C: $R_0 < r < R_1$

From Eqs. (28) and (29), we find

$$u_r = -\frac{Q_1}{2\pi R_1^2}\cos\theta - \left[\frac{Q_1}{2\pi R_1^2}\sum_{n=0}^{\infty}{}^{*}\frac{nP_n(0)}{n-1}\left(\frac{r}{R_1}\right)^{n-1} - \frac{Q_2}{2\pi R_0^2}\sum_{n=0}^{\infty}\frac{n+1}{n+2}P_n(0)\left(\frac{R_0}{r}\right)^{n+2}\right]P_n(\cos\theta) \tag{32}$$

$$u_\theta = \frac{\sin\theta}{2\pi}\left\{\frac{Q_1}{R_1^2} + \left[\frac{Q_1}{R_1^2}\sum_{n=0}^{\infty}{}^{*}\frac{P_n(0)}{n-1}\left(\frac{r}{R_1}\right)^{n-1} + \frac{Q_2}{R_0^2}\sum_{n=0}^{\infty}\frac{P_n(0)}{n+2}\left(\frac{R_0}{r}\right)^{n+2}\right]\frac{dP_n(\mu)}{d\mu}\right\}$$

where

$$\begin{aligned} Q_1 &= 2\pi R_1^2 V_1 \\ Q_2 &= 2\pi R_0^2 (V_1 - V_0) \\ \frac{Q_1}{R_1^2} - \frac{Q_2}{R_0^2} &= 2\pi V_0 \end{aligned} \tag{33}$$

IV. STREAMFUNCTION

From the continuity equation in spherical coordinates, i.e.,

$$\frac{1}{r^2}\frac{\partial}{\partial r}(r^2 u_r) + \frac{1}{r\sin\theta}\frac{\partial}{\partial\theta}(u_\theta \sin\theta) = 0 \tag{34}$$

the streamfunction is defined as follows

$$\begin{aligned} \frac{\partial\Psi}{\partial r} &= -2\pi r\, u_\theta \sin\theta \\ \frac{\partial\Psi}{\partial\theta} &= 2\pi r^2 u_r \sin\theta \end{aligned} \tag{35}$$

So that the flux is given by

$$d\Psi = \frac{\partial\Psi}{\partial r}dr + \frac{\partial\Psi}{\partial\theta}d\theta \tag{36}$$

Region A: $r > R_1$

From Eqs. (35) and (30) we have

$$\frac{\partial \Psi}{\partial r} = -2\pi r u_\theta \sin\theta =$$

$$= \frac{1}{r}\sin^2\theta \sum_{n=0}^{\infty} \frac{P_n(0)}{n+2}\left[Q_1\left(\frac{R_1}{r}\right)^n - Q_2\left(\frac{R_0}{r}\right)^n\right]\frac{dP_n}{d\mu} \tag{37}$$

Integrating we get

$$\Psi_A = -\sin^2\theta \sum_{n=1}^{\infty} \frac{P_n(0)}{n(n+2)}\left[Q_1\left(\frac{R_1}{r}\right)^n - Q_2\left(\frac{R_0}{r}\right)^n\right]\frac{dP_n}{d\mu} + f(\theta) \tag{38}$$

Differentiating the above equation with respect to θ, we find

$$\frac{\partial \Psi}{\partial \theta} = -\sum_{n=1}^{\infty} \frac{P_n(0)}{n(n+2)}\left[Q_1\left(\frac{R_1}{r}\right)^n - Q_2\left(\frac{R_0}{r}\right)^n\right]\left\{2\sin\theta\cos\theta\frac{dP_n}{d\mu} - \sin^3\theta\frac{d^2P_n}{d\mu^2}\right\} + f'(\theta) \tag{39}$$

or

$$\frac{\partial \Psi}{\partial \theta} = \sin\theta \sum_{n=1}^{\infty} \frac{P_n(0)}{n(n+2)}\left[Q_1\left(\frac{R_1}{r}\right)^n - Q_2\left(\frac{R_0}{r}\right)^n\right]\left\{(1-\mu^2)\frac{d^2P_n}{d\mu^2} - 2\mu\frac{dP_n}{d\mu}\right\} + f'(\theta) \tag{40}$$

From the second of Eqs. (35) and from the first of Eqs. (30), we have that

$$\frac{\partial \Psi}{\partial \theta} = 2\pi r^2 u_r \sin\theta$$

$$= -\sin\theta \sum_{n=0}^{\infty} \frac{n+1}{n+2} P_n(0)\left[Q_1\left(\frac{R_1}{r}\right)^n - Q_2\left(\frac{R_0}{r}\right)^n\right]P_n(\mu) \tag{41}$$

Comparing Eqs. (40) and (41) and rearranging terms, we get

$$\sin\theta \sum_{n=1}^{\infty} \frac{P_n(0)}{n(n+2)}\left[Q\left(\frac{R_1}{r}\right)^n - Q_2\left(\frac{R_0}{r}\right)^n\right]\left\{(1-\mu^2)\frac{d^2P_n}{d\mu^2} - 2\mu\frac{dP_n}{d\mu} + n(n+1)P_n\right\} =$$

$$= -f'(\theta) - \sin\theta\,\frac{1}{2}(Q_1 - Q_2) \tag{42}$$

Since the differential equation in the brackets is equal to 0 the above equation becomes

$$f'(\theta) = -\frac{Q_1 - Q_2}{2}\sin\theta \tag{43}$$

Integrating, we get

$$f(\theta) = \frac{Q_1 - Q_2}{2}(\cos\theta + C_1) \tag{44}$$

where the constant C_1 is evaluated from the condition $\psi(0) = 0$ for $\theta = 0$. Consequently,

$$C_1 = -1 \tag{45}$$

And Eq. (38) for the streamfunction in the region $r > R_1$ becomes

$$\psi_A(r,\theta) = \frac{Q_1 - Q_2}{2}(\cos\theta - 1) - \sin^2\theta \sum_{n=1}^{\infty} \frac{P_n(0)}{n(n+2)}\left[Q_1\left(\frac{R_1}{r}\right)^n - Q_2\left(\frac{R_0}{r}\right)^n\right]\frac{dP_n(\mu)}{d\mu} \tag{46}$$

Region B: $r < R_0$

We follow the same procedure as that for the Region A.

From Eqs. (35) and (31), we have

$$\begin{aligned}\frac{\partial\psi}{\partial r} &= -2\pi r u_\theta \sin\theta \\ &= -r\sin^2\theta\left\{\left(\frac{Q_1}{R_1^2} - \frac{Q_2}{R_0^2}\right) + \sum_{n=0}^{\infty}{}^{*}\frac{P_n(0)}{n-1}\left[\frac{Q_1}{R_1^2}\left(\frac{r}{R_1}\right)^{n-1} - \frac{Q_2}{R_0^2}\left(\frac{r}{R_0}\right)^{n-1}\right]\frac{dP_n(\mu)}{d\mu}\right\}\end{aligned} \tag{47}$$

Integrating, we find

$$\psi_B = -r^2\sin^2\theta\left\{\frac{1}{2}\left(\frac{Q_1}{R_1^2} - \frac{Q_2}{R_0^2}\right) + \sum_{n=0}^{\infty}{}^{*}\frac{P_n(0)}{(n-1)(n+1)}\left[\frac{Q_1}{R_1^2}\left(\frac{r}{R_1}\right)^{n-1} - \frac{Q_2}{R_0^2}\left(\frac{r}{R_0}\right)^{n-1}\right]\frac{dP_n(\mu)}{d\mu}\right\} + g(\theta) \tag{48}$$

Differentiating the above equation with respect to θ we get

$$\begin{aligned}\frac{\partial\psi}{\partial\theta} &= -r^2\left\{\frac{1}{2}\left(\frac{Q_1}{R_1^2} - \frac{Q_2}{R_0^2}\right) + \sum_{n=0}^{\infty}{}^{*}\frac{P_n(0)}{(n-1)(n+1)}\left[\frac{Q_1}{R_1^2}\left(\frac{r}{R_1}\right)^{n-1} - \frac{Q_2}{R_0^2}\left(\frac{r}{R_0}\right)^{n-1}\right]\frac{dP_n}{d\mu}\right\} 2\sin\theta\cos\theta \\ &+ r^2\sin^3\theta \sum_{n=0}^{\infty}{}^{*}\frac{P_n(0)}{(n-1)(n+1)}\left[\frac{Q_1}{R_1^2}\left(\frac{r}{R_1}\right)^{n-1} - \frac{Q_2}{R_0^2}\left(\frac{r}{R_0}\right)^{n-1}\right]\frac{d^2P_n}{d\mu^2} + g'(\theta)\end{aligned} \tag{49}$$

From the second of Eqs. (35) and from the first of Eqs. (31), we have that

$$\frac{\partial \Psi}{\partial \theta} = -r^2 \sin\theta \left\{ \left(\frac{Q_1}{R_1^2} - \frac{Q_2}{R_0^2} \right) \cos\theta + \sum_{n=0}^{\infty *} \frac{n P_n(0)}{n-1} \left[\frac{Q_1}{R_1^2} \left(\frac{r}{R_1} \right)^{n-1} - \frac{Q_2}{R_0^2} \left(\frac{r}{R_0} \right)^{n-1} \right] P_n(\mu) \right\} \tag{50}$$

Comparing Eqs. (49) and (50) and rearranging terms, we find

$$r^2 \sin\theta \sum_{n=0}^{\infty *} \frac{P_n(0)}{(n-1)(n+1)} \left[\frac{Q_1}{R_1^2} \left(\frac{r}{R_1} \right)^{n-1} - \frac{Q_2}{R_0^2} \left(\frac{r}{R_0} \right)^{n-1} \right] \left\{ (1-\mu^2) \frac{d^2 P_n}{d\mu^2} - 2\mu \frac{dP_n}{d\mu} + \right.$$

$$\left. + n(n+1) P_n(\mu) \right\} = -g'(\theta) \tag{51}$$

Since the differential equation in the brackets is equal to 0, the above equation becomes

$$g'(\theta) = 0 \tag{52}$$

Integrating, we get

$$g(\theta) = C_2 \tag{53}$$

where the constant C_2, is evaluated from the condition $\Psi(0) = 0$ for $\theta = 0$. Consequently,

$$g(\theta) = C_2 \equiv 0 \tag{54}$$

And Eq. (40) for the streamfunction in the region $r < R_0$ becomes

$$\Psi_B(r,\theta) = -r^2 \sin^2\theta \left\{ \frac{1}{2} \left(\frac{Q_1}{R_1^2} - \frac{Q_2}{R_0^2} \right) + \sum_{n=0}^{\infty *} \frac{P_n(0)}{(n-1)(n+1)} \left[\frac{Q_1}{R_1^2} \left(\frac{r}{R_1} \right)^{n-1} - \frac{Q_2}{R_0^2} \left(\frac{r}{R_0} \right)^{n-1} \right] \frac{dP_n}{d\mu} \right\} \tag{55}$$

Region C: $R_0 < r < R_1$

From Eqs. (35) and (32) we have

$$\frac{\partial \Psi}{\partial r} = -2\pi r u_\theta \sin\theta$$

$$= -r \sin^2\theta \left\{ \frac{Q_1}{R_1^2} + \left[\frac{Q_1}{R_1^2} \sum_{n=0}^{\infty *} \frac{P_n(0)}{n-1} \left(\frac{r}{R_1} \right)^{n-1} + \frac{Q_2}{R_0^2} \sum_{n=0}^{\infty} \frac{P_n(0)}{n+2} \left(\frac{R_0}{r} \right)^{n+2} \right] \frac{dP_n}{d\mu} \right\} \tag{56}$$

Integrating, we get

$$\psi_c = -r^2 \sin^2\theta \left\{ \frac{Q_1}{2R_1^2} + \left[\frac{Q_1}{R_1^2} \sum_{n=0}^{\infty}{}^{*} \frac{P_n(0)}{(n+1)(n-1)} \left(\frac{r}{R_1}\right)^{n-1} - \frac{Q_2}{R_0^2} \sum_{n=0}^{\infty} \frac{P_n(0)}{n(n+2)} \left(\frac{R_0}{r}\right)^{n+2} \right] \frac{dP_n}{d\mu} \right\} + j(\theta) \tag{57}$$

Differentiating the above equation with respect to θ we find

$$\frac{\partial \psi}{\partial \theta} = -r^2 \left\{ \frac{Q_1}{2R_1^2} + \left[\frac{Q_1}{R_1^2} \sum_{n=0}^{\infty}{}^{*} \frac{P_n(0)}{(n+1)(n-1)} \left(\frac{r}{R_1}\right)^{n-1} - \frac{Q_2}{R_0^2} \sum_{n=0}^{\infty} \frac{P_n(0)}{n(n+2)} \left(\frac{R_0}{r}\right)^{n+2} \right] \frac{dP_n}{d\mu} \right\} 2\sin\theta\cos\theta +$$

$$+ r^2 \sin^3\theta \left[\frac{Q_1}{R_1^2} \sum_{n=0}^{\infty}{}^{*} \frac{P_n(0)}{(n+1)(n-1)} \left(\frac{r}{R_1}\right)^{n-1} - \frac{Q_2}{R_0^2} \sum_{n=0}^{\infty} \frac{P_n(0)}{n(n+2)} \left(\frac{R_0}{r}\right)^{n+2} \right] \frac{d^2P_n}{d\mu^2} + j''(\theta) \tag{58}$$

or

$$\frac{\partial \psi}{\partial \theta} = r^2 \sin\theta \left\{ \frac{Q_1}{R_1^2} \sum_{n=0}^{\infty}{}^{*} \frac{P_n(0)}{(n+1)(n-1)} \left(\frac{r}{R_1}\right)^{n-1} - \frac{Q_2}{R_0^2} \sum_{n=0}^{\infty} \frac{P_n(0)}{n(n+2)} \left(\frac{R_0}{r}\right)^{n+2} \right\} \cdot$$

$$\cdot \left\{ (1-\mu^2) \frac{d^2P_n}{d\mu^2} - 2\mu \frac{dP_n}{d\mu} \right\} - r^2 \frac{Q_1}{R_1^2} \sin\theta\cos\theta + j'(\theta) \tag{59}$$

From the second of Eos. (35) and from the first of Eqs. (32), we have that

$$\frac{\partial \psi}{\partial \theta} = 2\pi r^2 u_r \sin\theta \tag{60}$$

$$= -r^2 \sin\theta \left\{ \frac{Q_1}{R_1^2} \cos\theta + \left[\frac{Q_1}{R_1^2} \sum_{n=0}^{\infty}{}^{*} \frac{n P_n(0)}{n-1} \left(\frac{r}{R_1}\right)^{n-1} - \frac{Q_2}{R_0^2} \sum_{n=0}^{\infty} \frac{n+1}{n+2} P_n(0) \left(\frac{R_0}{r}\right)^{n+2} \right] P_n(\mu) \right\}$$

Comparing Eqs. (59) and (60) and rearranging terms, we get

$$r^2 \sin\theta \left\{ \frac{Q_1}{R_1^2} \sum_{n=0}^{\infty}{}^{*} \frac{P_n(0)}{(n+1)(n-1)} \left(\frac{r}{R_1}\right)^{n-1} - \frac{Q_2}{R_0^2} \sum_{n=0}^{\infty} \frac{P_n(0)}{n(n+2)} \left(\frac{R_0}{r}\right)^{n+2} \right\}$$

$$\left\{ (1-\mu^2) \frac{d^2 P_n}{d\mu^2} - 2\mu \frac{dP_n}{d\mu} + n(n+1) P_n \right\} + j'(\theta) = 0 \tag{61}$$

Since the differential equation in the brackets is equal to 0 the above equation becomes

$$j'(\theta) = 0 \tag{62}$$

Integrating with respect to θ we get

$$j(\theta) = C_3 \tag{63}$$

where the constant C_3 is evaluated from the condition $\Psi(0)$ for $\theta = 0$. Consequently,

$$j(0) = C_3 = 0 \tag{64}$$

And Eq. (57) for the streamfunction in the region $R_0 < r < R_1$ becomes

$$\Psi_c(r,\theta) = -r^2 \sin^2\theta \left\{ \left[\frac{Q_1}{R_1^2} \sum_{n=0}^{\infty}{}^{*} \frac{P_n(0)}{(n+1)(n-1)} \left(\frac{r}{R_1}\right)^{n-1} - \frac{Q_2}{R_0^2} \sum_{n=0}^{\infty} \frac{P_n(0)}{n(n+2)} \left(\frac{R_0}{r}\right)^{n+2} \right] \frac{dP_n}{d\mu} + \frac{Q_1}{R_1^2} \right\} \tag{65}$$

V. SINK DISTRIBUTION IN AN ANNULUS

For a uniform sink distribution in an annulus with internal radius R_0 and external radius R_1 the flow field is derived by putting $V_0 = 0$ in Figure C2.

Thus, from Eqs. (33), we have that

$$\frac{Q_1}{2\pi R_1^2} = \frac{Q_2}{2\pi R_o^2} = V_1 \equiv V \tag{66}$$

Substituting for Q_1 and Q_2 from Eq. (66) into Eqs. (30), (31) and (32), we find the following for the velocity field in the regions A, B and C.

Region A: $r > R_1$

$$u_r = -V \sum_{n=0}^{\infty} \frac{n+1}{n+2} P_n(0) \left[\left(\frac{R_1}{r}\right)^{n+2} - \left(\frac{R_o}{r}\right)^{n+2}\right] P_n(\cos\theta)$$

$$u_\theta = -V \sin\theta \sum_{n=0}^{\infty} \frac{P_n(0)}{n+2} \left[\left(\frac{R_1}{r}\right)^{n+2} - \left(\frac{R_o}{r}\right)^{n+2}\right] \frac{dP_n(\mu)}{d\mu} \tag{67}$$

Region B: $r < R_o$

$$u_r = -V \sum_{n=0}^{\infty}{}^{*} \frac{nP_n(0)}{n-1} \left[\left(\frac{r}{R_1}\right)^{n-1} - \left(\frac{r}{R_o}\right)^{n-1}\right] P_n(\cos\theta)$$

$$u_\theta = V \sin\theta \sum_{n=0}^{\infty}{}^{*} \frac{P_n(0)}{n-1} \left[\left(\frac{r}{R_1}\right)^{n-1} - \left(\frac{r}{R_o}\right)^{n-1}\right] \frac{dP_n(\mu)}{d\mu} \tag{68}$$

Region C: $R_o < r < R_1$

$$u_r = -V \left\{\cos\theta + \left[\sum_{n=0}^{\infty}{}^{*} \frac{nP_n(0)}{n-1} \left(\frac{r}{R_1}\right)^{n-1} - \sum_{n=0}^{\infty}{}^{*} \frac{n+1}{n+2} P_n(0) \left(\frac{R_o}{r}\right)^{n+2}\right] P_n(\cos\theta)\right\}$$

$$u_\theta = V \sin\theta \left\{1 + \left[\sum_{n=0}^{\infty}{}^{*} \frac{P_n(0)}{n-1} \left(\frac{r}{R_1}\right)^{n-1} + \sum_{n=0}^{\infty} \frac{P_n(0)}{n+2} \left(\frac{R_o}{r}\right)^{n+2}\right] \frac{dP_n}{d\mu}\right\} \tag{69}$$

Similarly, substituting for Q_1 and Q_2 from Eqs. (66) into Eqs. (46), (55) and (65), the streamfunction in the Regions A, B and C becomes:

Region A: $r > R_1$

$$\psi_A(r,\theta) = 2\pi V\left\{\frac{(R_1^2-R_0^2)}{2}(\cos\theta-1) - \sin^2\theta \sum_{n=1}^{\infty} \frac{P_n(0)}{n(n+2)} \cdot \left[R_1^2\left(\frac{R_1}{r}\right)^n - R_0^2\left(\frac{R_0}{r}\right)^n\right]\frac{dP_n(\mu)}{d\mu}\right\} \tag{70}$$

Region B: $r < R_0$

$$\psi_B(r,\theta) = -2\pi V r^2 \sin^2\theta \sum_{n=0}^{\infty}{}^{*} \frac{P_n(0)}{(n-1)(n+1)}\left[\left(\frac{r}{R_1}\right)^{n-1} - \left(\frac{r}{R_0}\right)^{n-1}\right]\frac{dP_n(\mu)}{d\mu} \tag{71}$$

Region C: $R_0 < r < R_1$

$$\psi_C(r,\theta) = -2\pi V r^2 \sin^2\theta\left\{\left[\sum_{n=0}^{\infty}{}^{*} \frac{P_n(0)}{(n+1)(n-1)}\left(\frac{r}{R_1}\right)^{n-1} - \sum_{n=0}^{\infty} \frac{P_n(0)}{n(n+2)}\left(\frac{R_0}{r}\right)^{n+2}\right]\frac{dP_n(\mu)}{d\mu} + 1\right\} \tag{72}$$

VI. PROPELLER IN AN ANNULUS

The flow field of a propeller in an annulus of an infinite plate might be represented by a uniform sink distribution at the annulus with strength equal to twice the normal velocity at the propeller plane.

At the sink plane there are symmetric radial flow velocities and a uniform axial velocity.

Thus, the flow field in the region above the propeller is represented by the Eqs. (67), (68), (69) and (70), (71) and (72).

In the region under the sink plane, an annular jet emerges with an increased total energy due to the energy added by the loading of the propeller.

For this region, a solution to the potential flow field might be found by adding a uniform flow of double the axial velocity, in the cylindrical annular region with cross-sectional area equal to that of the annular sink.

Thus, superimposing the annular sink flow field to the uniform velocity field, we get a flow field which has an annular jet with a contraction ratio equal to two.

At infinity, the mass flow from the annulus of the plate is equal to the mass inflow from the cylindrical surface due to the sinks. A sketch of the flow field is given in the following Fig. C4.

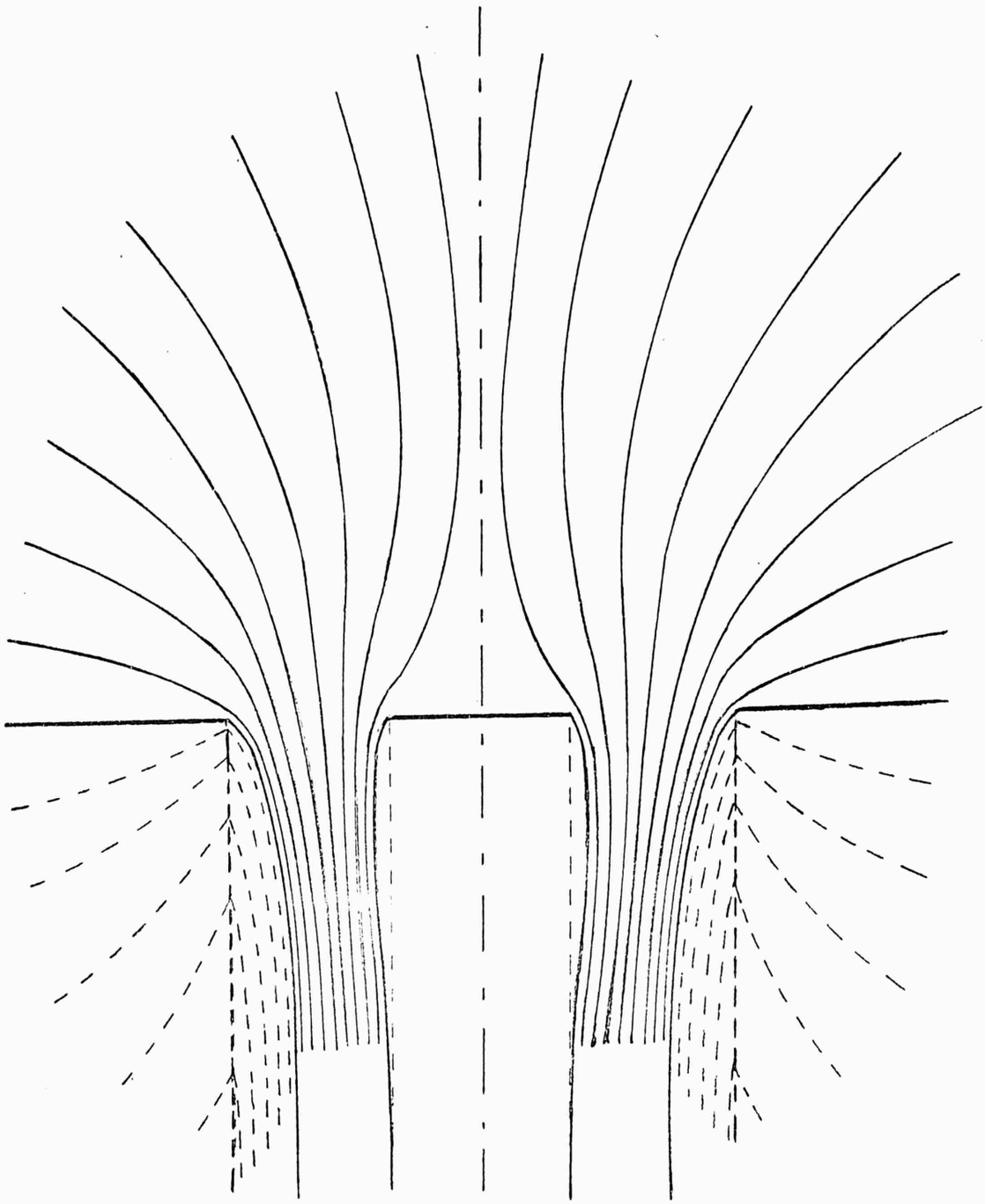

Figure C4

Streamlines of a propeller in an
annular opening of an infinite plate.

VII. CONTINUOUS NON-UNIFORM SINK DISTRIBUTION

For axial symmetric non-uniform sink distribution we have that the strength of the sinks is given as a function of the radius r_o. i.e.,

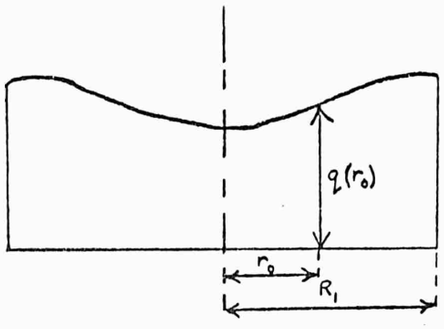

Figure C5

1. Velocity Potential

The velocity potential is found as follows:

Region (A) : $r > R_1$

For $r > R_1$, i.e., $r/r_o > 1$ the velocity potential for the sink distribution of strength $q(r_o)$ along the axis of symmetry $\theta = 0$ is found by integrating Eos. (1) from 0 to R_1, i.e.,

$$\Phi_{\theta=0,\ \omega=90^\circ}(r,0) = \int_0^{R_1}\int_0^{2\pi} \frac{q(r_o)}{4\pi r} \sum_{n=0}^{\infty} \left(\frac{r_o}{r}\right)^n P_n(0)\, r_o\, dr_o\, d\varphi \tag{73}$$

Integrating with respect to φ we find

$$\Phi(r,0) = \frac{1}{2}\int_0^{R_1} \frac{q(r_o)}{r} \sum_{n=0}^{\infty} \left(\frac{r_o}{r}\right)^n P_n(0)\, r_o\, dr_o \tag{74}$$

Expressing $q(r_o)$ as a polynomial in r_o we have

$$q(r_o) = \sum_{K=0}^{N} a_K\, r_o^K \tag{75}$$

Substituting Eq. (75) into Eq. (74) we get

$$\Phi(r,0) = \frac{1}{2}\int_0^{R_1} \sum_{K=0}^{N} a_K r_0^K \sum_{n=0}^{\infty} \left(\frac{r_0}{r}\right)^n \left(\frac{r_0}{r}\right) P_n(0)\, dr_0 \tag{76}$$

or

$$\Phi(r,0) = \frac{1}{2}\int_0^{R_1} \sum_{K=0}^{N} b_K \left(\frac{r_0}{r}\right)^K \sum_{n=0}^{\infty} \left(\frac{r_0}{r}\right)^{n+1} P_n(0)\, dr_0 \tag{77}$$

where

$$a_K r^K = b_K \tag{78}$$

Performing the integration, we find

$$\Phi(r,0) = \frac{1}{2} \sum_{n=0}^{\infty} P_n(0) \sum_{K=0}^{N} \frac{b_K}{n+K+2} \frac{R_1^{n+K+2}}{r^{n+K+1}} \tag{79}$$

or

$$\Phi(r,0) = \frac{A_1}{2\pi} \sum_{n=0}^{\infty} P_n(0) \sum_{K=0}^{N} \frac{b_K}{n+K+2} \frac{R_1^{n+K}}{r^{n+K+1}} \tag{80}$$

where

$$A_1 = \pi R_1^2 \tag{81}$$

Making use of Eq. (9) for the general solution of the Laplace equation, we have that the velocity potential in the region $r > R_1$ for any angle θ is given by

$$\Phi_{\text{(A)}}(r,\theta) = \frac{A_1}{2\pi} \sum_{n=0}^{\infty} P_n(0) \sum_{K=0}^{N} \frac{b_K}{n+K+2} \frac{R_1^{n+K}}{r^{n+K+1}} P_{n+K}(\cos\theta) \tag{82}$$

Region (B) : $r < R_1$

For $r < R_1$ we have that

$$\frac{r}{r_o} > 1 \qquad \text{for } o < r_o < r$$
$$\frac{r}{r_o} < 1 \qquad \text{for } r < r_o < R_1 \tag{83}$$

Thus, the velocity potential, for the sink distribution of strength $q(r_o)$, along the axis of symmetry $\theta = 0$ is found by integrating Eqs. (1) from 0 to r and from r to R_1, respectively, i.e.,

$$\Phi(r,0) = \int_o^r \int_o^{2\pi} \frac{q(r_o)}{4\pi r} \sum_{n=0}^{\infty} \left(\frac{r_o}{r}\right)^n P_n(0)\, r_o\, dr_o\, d\varphi$$
$$+ \int_r^{R_1} \int_o^{2\pi} \frac{q(r_o)}{4\pi r_o} \sum_{n=0}^{\infty} \left(\frac{r}{r_o}\right)^n P_n(0)\, r_o\, dr_o\, d\varphi \tag{84}$$

Substituting for $q(r_o)$ from Eq. (75) and integrating with respect to φ, we get

$$\Phi(r,0) = \frac{1}{2}\int_o^r \sum_{K=0}^{N} a_K\, r_o^K \sum_{n=0}^{\infty} \left(\frac{r_o}{r}\right)^{n+1} P_n(0)\, dr_o$$
$$- \frac{1}{2}\int_r^{R_1} \sum_{K=0}^{N} a_K\, r_o^K \sum_{n=0}^{\infty} \left(\frac{r}{r_o}\right)^n P_n(0)\, dr_o \tag{85}$$

Making use of Eq. (78), we find

$$\Phi(r,0) = \frac{1}{2}\int_o^r \sum_{K=0}^{N} b_K \left(\frac{r_o}{r}\right)^K \sum_{n=0}^{\infty} \left(\frac{r_o}{r}\right)^{n+1} P_n(0)\, dr_o$$
$$+ \frac{1}{2}\int_r^{R_1} \sum_{K=0}^{N} b_K \left(\frac{r_o}{r}\right)^K \sum_{n=0}^{\infty} \left(\frac{r}{r_o}\right)^n P_n(0)\, dr_o \tag{86}$$

Interchanging summation and integration, we get

$$\Phi(r,0)=\frac{1}{2}\sum_{n=0}^{\infty}P_n(0)\sum_{K=0}^{N}b_K\, r\int_0^{\frac{r}{r}}\left(\frac{r_0}{r}\right)^{n+K+1}d\left(\frac{r_0}{r}\right)$$

$$+\frac{1}{2}\sum_{n=0}^{\infty}P_n(0)\sum_{K=0}^{N}b_K\int_r^{R_1}\left(\frac{r}{r_0}\right)^{n-K}dr_0 \tag{87}$$

Performing the integration, we find

$$\Phi(r,0)=\frac{r}{2}\sum_{n=0}^{\infty}P_n(0)\sum_{K=0}^{N}\frac{b_K}{n+K+2}$$

$$+\frac{r}{2}\sum_{n=0}^{\infty}{}^{**}P_n(0)\sum_{K=0}^{N}b_K\,\frac{1}{n-K-1}\left[1-\left(\frac{r}{R_1}\right)^{n-K-1}\right]+$$

$$+\frac{r}{2}\sum_{K=0}^{N}P_{K+1}(0)\,b_K\,(\ln R_1-\ln r) \tag{88}$$

where

$$\sum_{n=0}^{\infty}{}^{**}=\sum_{\substack{n=0\\ n\neq K+1}}^{\infty} \tag{89}$$

For k = even, i.e., ($k^* = 2k$), we have an even polynomial for $q(r_0)$ and

$$P_{K^*+1}(0)=P_{2K+1}(0)=0 \tag{90}$$

Thus, Eq. (88) becomes

$$\Phi(r,0)=\frac{r}{2}\left\{\sum_{n=0}^{\infty}P_n(0)\sum_{K=0}^{\frac{N}{2}}\frac{b_{2K}}{n+2K+2}+\sum_{n=0}^{\infty}{}^{**}P_n(0)\sum_{K=0}^{\frac{N}{2}}\frac{b_{2K}}{n-2K-1}\left[1-\left(\frac{r}{R_1}\right)^{n-2k-1}\right]\right\} \tag{91}$$

And the velocity potential in the region $r < R_1$ for any angle θ is given by

$$\Phi_{\textcircled{B}}(r,\theta)=\frac{A_1}{2\pi R_1}\left[\sum_{n=0}^{\infty}P_n(0)\sum_{K=0}^{\frac{N}{2}}\frac{b_{2K}}{n+2K+2}+\sum_{n=0}^{\infty}{}^{**}P_n(0)\sum_{K=0}^{\frac{N}{2}}\frac{b_{2K}}{n-2K-1}\right]\left(\frac{r}{R_1}\right)P_1(\cos\theta)$$

$$-\frac{A_1}{2\pi R_1}\sum_{n=0}^{\infty}{}^{**}P_n(0)\sum_{K=0}^{\frac{N}{2}}\frac{b_{2K}}{n-2k-1}\left(\frac{r}{R_1}\right)^{n-2K}P_{n-2K}(\cos\theta) \tag{92}$$

where

$$P_{-(n+1)} = P_n \tag{93}$$

The velocity components for the two regions are given from Eqs. (29) and Eqs. (82) and (92) respectively, i.e.,

Region (A) : $r > R_1$

$$u_r = -\frac{A_1}{2\pi r^2}\sum_{n=0}^{\infty} P_n(0)\sum_{K=0}^{\frac{N}{2}} \frac{n+2K+1}{n+2K+2}\, b_{2K}\left(\frac{R_1}{r}\right)^{n+2K} P_{n+2K}(\cos\theta)$$

$$u_\theta = -\frac{A_1}{2\pi r^2}\sin\theta\sum_{n=0}^{\infty} P_n(0)\sum_{K=0}^{\frac{N}{2}} \frac{b_{2K}}{n+2K+2}\left(\frac{R_1}{r}\right)^{n+2K}\frac{dP_{n+2K}(\mu)}{d\mu} \tag{94}$$

Region (B) : $r < R_1$

$$u_r = \frac{A_1}{2\pi R_1^2}\left\{\sum_{n=0}^{\infty} P_n(0)\sum_{K=0}^{\frac{N}{2}} \frac{b_{2K}}{n+2K+2} + \sum_{n=0}^{\infty}{}^{**} P_n(0)\sum_{K=0}^{\frac{N}{2}} \frac{b_{2K}}{n-2K-1}\right\} P_1(\cos\theta)$$

$$-\frac{A_1}{2\pi R_1^2}\sum_{n=0}^{\infty}{}^{**} P_n(0)\sum_{K=0}^{\frac{N}{2}} \frac{b_{2K}(n-2K)}{n-2K-1}\left(\frac{r}{R_1}\right)^{n-2K-1} P_{n-2K}(\cos\theta)$$

$$u_\theta = -\frac{A_1\sin\theta}{2\pi R}\left[\sum_{n=0}^{\infty} P_n(0)\sum_{K=0}^{\frac{N}{2}} \frac{b_{2K}}{n+2K+2} + \sum_{n=0}^{\infty}{}^{**} P_n(0)\sum_{K=0}^{\frac{N}{2}} \frac{b_{2K}}{n-2K-1}\right] \tag{95}$$

$$+\frac{A_1}{2\pi R_1^2}\sin\theta\sum_{n=0}^{\infty}{}^{**} P_n(0)\sum_{K=0}^{\frac{N}{2}} \frac{b_{2K}}{n-2K-1}\left(\frac{r}{R_1}\right)^{n-2K-1}\frac{dP_{n-2K}(\mu)}{d\mu}$$

2. Streamfunction

The streamfunction for the two regions is found from Eqs. (35) and Eqs. (94).

Region Ⓐ : $r > R_1$

From Eqs. (35) and (94), we have

$$\frac{\partial \Psi}{\partial r} = -2\pi r\, u_\theta \sin\theta = \tag{96}$$

$$= \frac{A_1 \sin^2\theta}{r} \sum_{n=0}^{\infty} P_n(0) \sum_{K=0}^{\frac{N}{2}} \frac{b_{2K}}{n+2K+2} \left(\frac{R_1}{r}\right)^{n+2K} \frac{dP_{n+2K}(\mu)}{d\mu}$$

Integrating we get

$$\Psi = -A_1 \sin^2\theta \sum_{n=0}^{\infty *} P_n(0) \sum_{K=0}^{\frac{N}{2}} \frac{b_{2K}}{(n+2K)(n+2K+2)} \left(\frac{R_1}{r}\right)^{n+2K} \frac{dP_{n+2K}(\mu)}{d\mu} + f_1(\theta) \tag{97}$$

where

$$\sum_{n=0}^{\infty *} = \sum_{\substack{n=0 \\ n+2K \neq 0}}^{\infty} \tag{98}$$

Differentiating Eq. (97) with respect to θ, we find

$$\frac{\partial \Psi}{\partial \theta} = A_1 \sin\theta \sum_{n=0}^{\infty *} P_n(0) \sum_{K=0}^{\frac{N}{2}} \frac{b_{2K}}{(n+2K)(n+2K+2)} \left(\frac{R_1}{r}\right)^{n+2K} \left\{ (1-\mu^2) \frac{d^2 P_{n+2K}}{d\mu^2} - 2\mu \frac{dP_{n+2K}}{d\mu} \right\} + f_1'(\theta) \tag{99}$$

From the second of Eqs. (35) and the first of Eqs. (94), we have that

$$\frac{\partial \Psi}{\partial \theta} = 2\pi r^2 u_r \sin\theta = \tag{100}$$

$$= -A_1 \sin\theta \sum_{n=0}^{\infty} P_n(0) \sum_{K=0}^{\frac{N}{2}} \frac{n+2K+1}{n+2K+2}\, b_{2K} \left(\frac{R_1}{r}\right)^{n+2K} P_{n+2K}(\cos\theta)$$

Comparing Eqs. (99) and (100) and rearranging terms, we get

$$A_1 \sin\theta \sum_{n=0}^{\infty *} P_n(0) \sum_{K=0}^{\frac{N}{2}} \frac{b_{2K}}{(n+2K)(n+2K+2)} \left(\frac{R_1}{r}\right)^{n+2K} \left\{ (1-\mu^2) \frac{d^2 P_{n+2K}}{d\mu^2} - 2\mu \frac{dP_{n+2K}}{d\mu} + \right. \tag{101}$$

$$\left. + (n+2K)(n+2K+1) P_{n+2K} \right\} = -f_1'(\theta) - \frac{1}{2} A_1 b_0 \sin\theta$$

Since the differential equation in the brackets is equal to zero, the above equation becomes

$$f_1'(\theta) = -\frac{1}{2} A_1 b_0 \sin\theta \tag{102}$$

Integrating, we get

$$f_1(\theta) = \frac{1}{2} A_1 b_0 (\cos\theta + C_4) \tag{103}$$

where the constant C_4 is evaluated from the condition $\Psi(0) = 0$ for $\theta = 0$. Consequently

$$C_4 = -1 \tag{104}$$

And Eq. (97) for the streamfunction in the region $r > R_1$ becomes

$$\Psi_{(A)}(r,\theta) = \frac{1}{2} A_1 b_0 (\cos\theta - 1) - A_1 \sin^2\theta \sum_{n=0}^{\infty *} P_n(0) \sum_{K=0}^{\frac{N}{2}} \frac{b_{2K}}{(n+2K)(n+2K+2)} \left(\frac{R_1}{r}\right)^{n+2K} \frac{dP_{n+2K}}{d\mu} \tag{105}$$

Region (B) : $r < R_1$

From Eqs. (35) and (95), we have

$$\frac{\partial\Psi}{\partial r} = -2\pi r u_\theta \sin\theta$$

$$= r \frac{A_1}{R_1^2} \sin^2\theta \left[\sum_{n=0}^{\infty} P_n(0) \sum_{K=0}^{\frac{N}{2}} \frac{b_{2K}}{n+2K+2} + \sum_{n=0}^{\infty **} P_n(0) \sum_{K=0}^{\frac{N}{2}} \frac{b_{2K}}{n-2K-1} \right]$$

$$- r \frac{A_1}{R_1^2} \sin^2\theta \sum_{n=0}^{\infty **} P_n(0) \sum_{K=0}^{\frac{N}{2}} \frac{b_{2K}}{n-2K-1} \left(\frac{r}{R_1}\right)^{n-2K-1} \frac{dP_{n-2K}}{d\mu} \tag{106}$$

Integrating, we get

$$\Psi = \frac{r^2}{2} \frac{A_1}{R_1^2} \sin^2\theta \left[\sum_{n=0}^{\infty} P_n(0) \sum_{K=0}^{\frac{N}{2}} \frac{b_{2K}}{n+2K+2} + \sum_{n=0}^{\infty **} P_n(0) \sum_{K=0}^{\frac{N}{2}} \frac{b_{2K}}{n-2K-1} \right]$$

$$- r^2 \frac{A_1}{R_1^2} \sin^2\theta \sum_{n=0}^{\infty **} P_n(0) \sum_{K=0}^{\frac{N}{2}} \frac{b_{2K}}{(n-2K+1)(n-2K-1)} \left(\frac{r}{R_1}\right)^{n-2K-1} \frac{dP_{n-2K}}{d\mu} + g_1(\theta) \tag{107}$$

Differentiating the above equation with respect to θ, and substituting $\sin^2\theta = 1 - \cos^2\theta = 1 - \mu^2$, we find

$$\frac{\partial \Psi}{\partial \theta} = \frac{r^2}{2}\frac{A_1}{R_1^2}\sin\theta\left[\sum_{n=0}^{\infty} P_n(0)\sum_{K=0}^{\frac{N}{2}}\frac{b_{2K}}{n+2K+2} + \sum_{n=0}^{\infty}{}^{**} P_n(0)\sum_{K=0}^{\frac{N}{2}}\frac{b_{2K}}{n-2K-1}\right]2\cos\theta$$

$$-r^2\frac{A_1}{R_1^2}\sin\theta\sum_{n=0}^{\infty}{}^{**} P_n(0)\sum_{K=0}^{\frac{N}{2}}\frac{b_{2K}}{(n-2K+1)(n-2K-1)}\left(\frac{r}{R_1}\right)^{n-2K-1}\cdot \tag{108}$$

$$\cdot\left\{2\mu\frac{dP_{n-2K}}{d\mu} - (1-\mu^2)\frac{d^2P_{n-2K}}{d\mu^2}\right\} + g_1'(\theta)$$

From the second of Eqs. (35) and from the first of Eqs. (95), we have that

$$\frac{\partial \Psi}{\partial \theta} = 2\pi r^2 u_r \sin\theta$$

$$= r^2\frac{A_1}{R_1^2}\sin\theta\left\{\sum_{n=0}^{\infty} P_n(0)\sum_{K=0}^{\frac{N}{2}}\frac{b_{2K}}{n+2K+2} + \sum_{n=0}^{\infty}{}^{**} P_n(0)\sum_{K=0}^{\frac{N}{2}}\frac{b_{2K}}{n-2K-1}\right\}P_1(\cos\theta) \tag{109}$$

$$-r^2\frac{A_1}{R_1^2}\sin\theta\sum_{n=0}^{\infty}{}^{**} P_n(0)\sum_{K=0}^{\frac{N}{2}}\frac{n-2K}{n-2K-1}\left(\frac{r}{R_1}\right)^{n-2K-1} b_{2K}\,P_{n-2K}(\cos\theta)$$

Comparing Eqs. (108) and (109) and rearranging terms we get

$$r^2\frac{A_1}{R_1^2}\sin\theta\sum_{n=0}^{\infty}{}^{**} P_n(0)\sum_{K=0}^{\frac{N}{2}}\frac{b_{2K}}{(n-2K+1)(n-2K-1)}\left(\frac{r}{R_1}\right)^{n-2K-1}$$

$$\left\{(1-\mu^2)\frac{d^2P_{n-2K}}{d\mu^2} - 2\mu\frac{dP_{n-2K}}{d\mu} + (n-2K)(n-2K+1)P_{n-2K}(\mu)\right\} + g_1'(\theta) = 0 \tag{110}$$

Since the differential equation in the brackets is equal to 0, the above equation becomes

$$g_1'(\theta) = 0 \tag{111}$$

Integrating, we get

$$g_1(\theta) = C_5 \tag{112}$$

where the constant C_5 is evaluated from the condition $\Psi(0) = 0$ for $\theta = 0$. Consequently

$$g_1(\theta) = C_5 = 0 \tag{113}$$

And Eq. (107) for the streamfunction in the region $r < R_1$ becomes

$$\Psi_{\textcircled{B}} = r^2 \frac{A_1}{2R_1^2} \sin^2\theta \left[\sum_{n=0}^{\infty} P_n(0) \sum_{K=0}^{\frac{N}{2}} \frac{b_{2K}}{n+2K+2} + \sum_{n=0}^{\infty}{}^{**} P_n(0) \sum_{K=0}^{\frac{N}{2}} \frac{b_{2K}}{n-2K-1} \right]$$

$$- r^2 \frac{A_1}{R_1^2} \sin^2\theta \sum_{n=0}^{\infty}{}^{**} P_n(0) \sum_{K=0}^{\frac{N}{2}} \frac{b_{2K}}{(n-2K+1)(n-2K-1)} \left(\frac{r}{R_1}\right)^{n-2K-1} \frac{dP_{n-2K}(\mu)}{d\mu} \tag{114}$$

VIII. SUMMARY OF EQUATIONS

1. One Step in the Distribution of Sinks

$$\bar{\Phi}_A(r,\theta)=\frac{1}{2\pi r}\sum_{n=0}^{\infty}\frac{P_n(0)}{n+2}\left[Q_1\left(\frac{R_1}{r}\right)^n-Q_2\left(\frac{R_0}{r}\right)^n\right]P_n(\mu) \tag{10}$$

$$\bar{\Phi}_B(r,\theta)=-\frac{1}{2\pi}\left(\frac{Q_1}{R_1^2}-\frac{Q_2}{R_0^2}\right)rP_1(\mu)-\sum_{n=0}^{\infty}{}^{*}\frac{1}{2\pi}\frac{P_n(0)}{(n-1)}\left[\frac{Q_1}{R_1}\left(\frac{r}{R_1}\right)^n-\frac{Q_2}{R_0}\left(\frac{r}{R_0}\right)^n\right]P_n(\mu) \tag{20}$$

$$\bar{\Phi}_C(r,\theta)=-\frac{Q_1}{2\pi R_1}\frac{r}{R_1}P_1(\mu)-\left[\frac{Q_1}{2\pi R_1}\sum_{n=0}^{\infty}{}^{*}\frac{P_n(0)}{n-1}\frac{r}{R_1}+\frac{Q_2}{2\pi R_0}\sum_{n=0}^{\infty}\frac{P_n(0)}{n+2}\left(\frac{R_0}{r}\right)^{n+1}\right]P_n(\mu) \tag{28}$$

$$\Psi_A(r,\theta)=\frac{Q_1-Q_2}{2}(\cos\theta-1)-\sin^2\theta\sum_{n=1}^{\infty}\frac{P_n(0)}{n(n+2)}\left[Q_1\left(\frac{R_1}{r}\right)^n-Q_2\left(\frac{R_0}{r}\right)^n\right]\frac{dP_n(\mu)}{d\mu} \tag{46}$$

$$\Psi_B(r,\theta)=-r^2\sin^2\theta\left\{\frac{1}{2}\left(\frac{Q_1}{R_1^2}-\frac{Q_2}{R_0^2}\right)+\sum_{n=0}^{\infty}{}^{*}\frac{P_n(0)}{(n-1)(n+1)}\left[\frac{Q_1}{R_1^2}\left(\frac{r}{R_1}\right)^{n-1}-\frac{Q_2}{R_0^2}\left(\frac{r}{R_0}\right)^{n-1}\right]\frac{dP_n}{d\mu}\right\} \tag{55}$$

$$\Psi_C(r,\theta)=-r^2\sin^2\theta\left\{\left[\frac{Q_1}{R_1^2}\sum_{n=0}^{\infty}\frac{P_n(0)}{(n+1)(n-1)}\left(\frac{r}{R_1}\right)^{n-1}-\frac{Q_2}{R_0^2}\sum_{n=0}^{\infty}\frac{P_n(0)}{n(n+2)}\left(\frac{R_0}{r}\right)^{n+2}\right]\frac{dP_n}{d\mu}+\frac{Q_1}{R_1^2}\right\} \tag{65}$$

2. Sink Distribution in an Annulus

$$\Psi_A(r,\theta)=2\pi V\left\{\frac{(R_1^2-R_0^2)}{2}(\cos\theta-1)-\sin^2\theta\sum_{n=1}^{\infty}\frac{P_n(0)}{n(n+2)}\cdot\left[R_1^2\left(\frac{R_1}{r}\right)^n-R_0^2\left(\frac{R_0}{r}\right)^n\right]\frac{dP_n(\mu)}{d\mu}\right\} \tag{70}$$

$$\Psi_B(r,\theta)=-2\pi Vr^2\sin^2\theta\sum_{n=0}^{\infty}{}^{*}\frac{P_n(0)}{(n-1)(n+1)}\left[\left(\frac{r}{R_1}\right)^{n-1}-\left(\frac{r}{R_0}\right)^{n-1}\right]\frac{dP_n(\mu)}{d\mu} \tag{71}$$

$$\Psi_c(r,\theta) = -2\pi V r^2 \sin^2\theta \left\{ \left[\sum_{n=0}^{\infty *} \frac{P_n(0)}{(n+1)(n-1)} \left(\frac{r}{R_1}\right)^{n-1} - \sum_{n=0}^{\infty} \frac{P_n(0)}{n(n+2)} \left(\frac{R_0}{r}\right)^{n+2} \right] \frac{dP_n(\mu)}{d\mu} + 1 \right\} \qquad (72)$$

3. Continuous Non-uniform Sink Distribution

$$\Phi_{(A)}(r,\theta) = \frac{A_1}{2\pi} \sum_{n=0}^{\infty} P_n(0) \sum_{K=0}^{\frac{N}{2}} \frac{b_{2K}}{n+2K+2} \frac{R_1^{n+2K}}{r^{n+2K+1}} P_{n+2K}(\mu) \qquad (82)$$

$$\Phi_{(B)}(r,\theta) = \frac{A_1}{2\pi R_1} \left[\sum_{n=0}^{\infty} P_n(0) \sum_{K=0}^{\frac{N}{2}} \frac{b_{2K}}{n+2K+2} + \sum_{n=0}^{\infty **} P_n(0) \sum_{K=0}^{\frac{N}{2}} \frac{b_{2K}}{n-2K-1} \right] \left(\frac{r}{R_1}\right) P_1(\mu)$$

$$- \frac{A_1}{2\pi R} \sum_{n=0}^{\infty **} P_n(0) \sum_{K=0}^{\frac{N}{2}} \frac{b_{2K}}{n-2K-1} \left(\frac{r}{R_1}\right)^{n-2K} P_{n-2K}(\mu) \qquad (92)$$

$$\Psi_{(A)}(r,\theta) = \frac{1}{2} A_1 b_0 (\cos\theta - 1) - A_1 \sin^2\theta \sum_{n=0}^{\infty *} P_n(0) \sum_{K=0}^{\frac{N}{2}} \frac{b_{2K}}{(n+2K)(n+2K+2)} \left(\frac{R_1}{r}\right)^{n+2K} \frac{dP_{n+2K}}{d\mu} \qquad (105)$$

$$\Psi_{(B)} = r^2 \frac{A_1}{2R_1^2} \sin^2\theta \left[\sum_{n=0}^{\infty} P_n(0) \sum_{K=0}^{\frac{N}{2}} \frac{b_{2K}}{n+2K+2} + \sum_{n=0}^{\infty **} P_n(0) \sum_{K=0}^{\frac{N}{2}} \frac{b_{2K}}{n-2K-1} \right]$$

$$- r^2 \frac{A_1}{R_1^2} \sin^2\theta \sum_{n=0}^{\infty **} P_n(0) \sum_{K=0}^{\frac{N}{2}} \frac{b_{2K}}{(n-2K+1)(n-2K-1)} \left(\frac{r}{R_1}\right)^{n-2K-1} \frac{dP_{n-2K}(\mu)}{d\mu} \qquad (114)$$

SECTION D

FLOW FIELD FOR CYLINDRICAL NON-UNIFORM VORTEX SHEET

SUMMARY

In this report the flow field of a shrouded propeller has been investigated by considering a vorticity distribution on a cylindrical surface.

For high speed shrouds the vorticity distribution has been assumed on a cylinder with constant radius ρ_o which corresponds to the exit radius of the shroud.

The vorticity distribution on the semi-infinite cylinder behind the shroud is considered constant and on the cylindrical surface of the shroud is approximated by a linear distribution and an expansion in Birnbaum series.

The strength of the constant vorticity downstream from the shrouds is calculated from the difference of the exit velocity and forward velocity of the shrouded propeller. The strength of the vorticity distribution along the shroud is calculated from the condition that the shroud is a streamline, by solving a system of equations for the unknown coefficients of the terms of the Birnbaum series.

For an approximate evaluation of the flow field we might consider only the first three terms of the series and solve a system of three equations for the three unknown coefficients.

Since the high speed shroud is always a smooth curve, three flow conditions at the leading edge, at the middle line and at the trailing edge, might be enough for a good approximation of the flow field by the first three terms of the Birnbaum series.

The flow field, the pressure distribution and the forces along the shroud are determined from the calculated vorticity distribution.

I. INTRODUCTION

In this report the flow field of a high speed shrouded propeller is investigated by the method of singularity distributions. Since the high speed shroud is a cylindrical surface with approximately constant radius, the vorticity distribution is considered on a cylinder with radius $\rho = \rho_0 =$ constant.

Making use of non-dimensional variables, we consider the shroud extending from $x = -1$ to $x = 1$. Fig. D1.

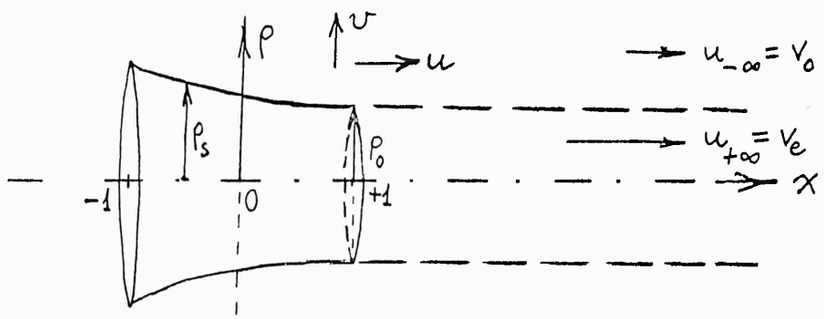

Figure D1

The vorticity distribution $\gamma(x)$ on the cylinder $\rho = \rho_0$ from $x = -1$ to $x = \infty$ is not known and it will be determined from the boundary conditions and the flow at $x = \pm\infty$.

From the strength of the vorticity distribution, we determine the flow field, the pressure distribution and the forces along the shroud.

The evaluation of the vortex distribution is facilitated by an approximation for the representation of the flow due to the propeller by a semi-infinite

vortex sheet of constant strength $\gamma = \gamma_0$ from $x = +1$ to $x = +\infty$ and a linear distribution $\gamma = \frac{\gamma_0}{2}(1+x)$ in the interval $x = -1$ to $x = +1$.

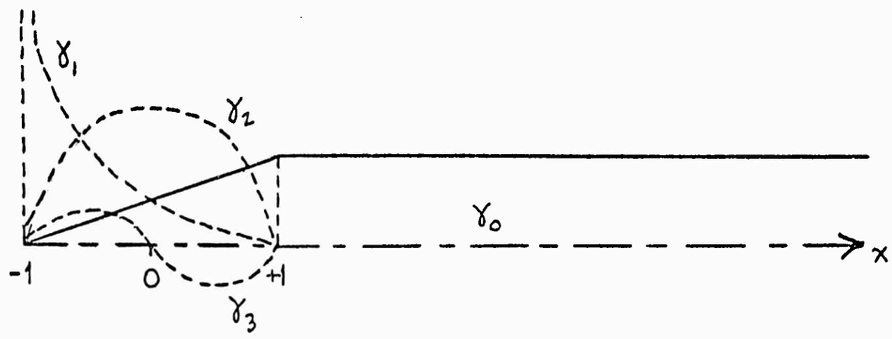

Figure D2

In addition to the above vortex sheet, the effect of the shroud is represented by expanding the vorticity distribution in Birnbaum series of normal functions in the interval $-1 \leq x \leq +1$.

Thus

$$\gamma^*(x) = \sum_{n=1}^{\infty} \gamma_n(x) \tag{1}$$

where

$$\gamma_1(x) = C_1 \sqrt{\frac{1-x}{1+x}}$$

$$\gamma_2(x) = C_2 \sqrt{1-x^2}$$

$$\gamma_3(x) = C_3\, x \sqrt{1-x^2} \tag{2}$$

$$- - - - - - - -$$

$$- - - - - - - -$$

For an approximate evaluation of the flow field we might consider only the first three terms of the above series, and the vorticity distribution becomes

$$\gamma(x) = \frac{\gamma_0}{2}(1+x) + C_1\sqrt{\frac{1-x}{1+x}} + C_2\sqrt{1-x^2} + C_3 x\sqrt{1-x^2} \qquad \text{for } -1 \le x \le +1$$

$$\gamma(x) = \gamma_0 \qquad \text{for } 1 \le x \le \infty \tag{3}$$

II. FLOW FIELD OF A VORTEX RING

The velocity for the flow of a vortex filament of strength $\gamma d\vec{s}$ is given by

$$d\vec{V} = \frac{\gamma}{4\pi}\frac{d\vec{s}\times\vec{R}}{R^3} \tag{4}$$

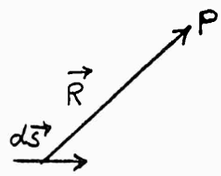

where $\vec{R}$ is the polar vector from the vortex filament to the point P.

For a vortex ring with radius ρ_0 at the plane normal to the x-axis at the origin, we have

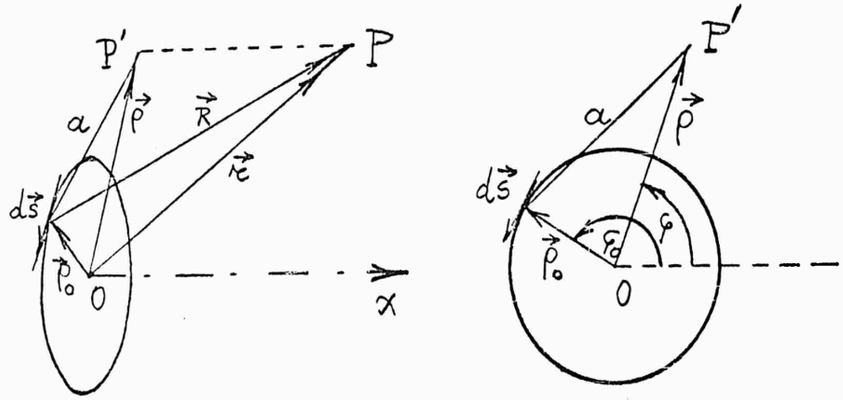

Figure D3

$$\vec{V} = \int_0^{2\pi} \frac{\gamma}{4\pi}\frac{d\vec{s}\times\vec{R}}{R^3} \tag{5}$$

where

$$d\vec{s} = \rho_0\, d\varphi_0\, \vec{e}_{\varphi_0}$$

Thus, the velocity becomes

$$\vec{V} = \frac{\rho_0 \gamma}{4\pi} \int_0^{2\pi} \frac{\vec{e}_{\varphi_0} \times \vec{R}}{R^3} \, d\varphi_0 \tag{6}$$

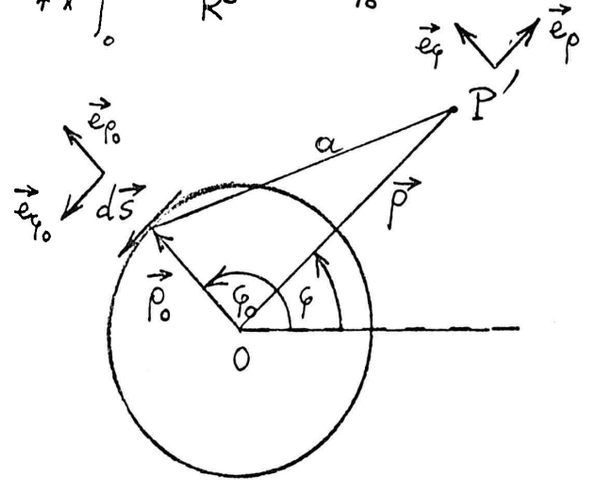

Figure D4

From Figs. D3 and D4 we have,

$$\vec{R} = \vec{r} - \vec{\rho}_0, \qquad \vec{r} = \vec{\rho} + \vec{x}$$

$$\vec{R} = \vec{x} + \vec{\rho} - \vec{\rho}_0 \tag{7}$$

$$R^2 = x^2 + a^2 = x^2 + \rho^2 + \rho_0^2 - 2\rho\,\rho_0 \cos(\varphi_0 - \varphi)$$

Thus, the cross-product in Eq. (6) becomes

$$\vec{e}_{\varphi_0} \times \vec{R} = \vec{e}_{\varphi_0} \times \left[\vec{x} + \vec{\rho} - \vec{\rho}_0\right] = \vec{e}_{\varphi_0} \times \vec{x} + \vec{e}_{\varphi_0} \times \vec{\rho} - \vec{e}_{\varphi_0} \times \vec{\rho}_0$$

or

$$\vec{e}_{\varphi_0} \times \vec{R} = x\,\vec{e}_{\rho_0} - \rho \cos(\varphi_0 - \varphi)\,\vec{e}_x + \rho_0 \vec{e}_x = -x\,\vec{e}_{\rho_0} + \left[\rho_0 - \rho\cos(\varphi_0 - \varphi)\right]\vec{e}_x \tag{8}$$

where $\vec{e}_\rho$, $\vec{e}_\varphi$, $\vec{e}_x$ are the cylindrical unit vectors and

$$\vec{e}_\rho \times \vec{e}_\varphi = \vec{e}_x, \qquad \vec{e} \times \vec{e}_x = \vec{e}_\rho \quad \& \quad \vec{e}_x \times \vec{e}_\rho = \vec{e}_\varphi$$

Substituting Eq. (8) into Eq. (6), we get

$$\vec{V} = \frac{\rho_0 \gamma}{4\pi} \int_0^{2\pi} \frac{x\,\vec{e}_{\rho_0} + [\rho_0 - \rho\cos(\varphi_0 - \varphi)]\vec{e}_x}{\left[x^2 + \rho^2 + \rho_0^2 - 2\rho\rho_0\cos(\varphi_0 - \varphi)\right]^{3/2}} d\varphi_0 \tag{9}$$

Since

$$\vec{e}_{\rho_0} \cdot \vec{e}_{\rho} = \cos(\varphi_0 - \varphi)$$

and

$$\vec{V}(\rho, \varphi, x) = u\,\vec{e}_x + v\,\vec{e}_\rho$$

we have that

$$\vec{V} \cdot \vec{e}_x = u \qquad \& \qquad \vec{V} \cdot \vec{e}_\rho = v$$

And the velocity components in the x and ρ direction are

$$u = \frac{\rho_0 \gamma}{4\pi} \int_0^{2\pi} \frac{[\rho_0 - \rho\cos(\varphi_0 - \varphi)]}{\left[x^2 + \rho^2 + \rho_0^2 - 2\rho\rho_0\cos(\varphi_0 - \varphi)\right]^{3/2}} d\varphi_0 \tag{10}$$

$$v = \frac{\rho_0 \gamma}{4\pi} \int_0^{2\pi} \frac{x\cos(\varphi_0 - \varphi)}{\left[x^2 + \rho^2 + \rho_0^2 - 2\rho\rho_0\cos(\varphi_0 - \varphi)\right]^{3/2}} d\varphi_0 \tag{11}$$

From the identities of Bessel functions (Appendix), we have

$$\int_0^\infty e^{-s|x|} J_0(s\rho) J_1(s\rho_0)\, s\,ds \equiv$$

$$\equiv \frac{1}{2\pi} \int_0^{2\pi} \frac{\rho_0 - \rho\cos\theta'}{\left[\rho^2 + \rho_0^2 + x^2 - 2\rho\rho_0\cos\theta'\right]^{3/2}} d\theta' \tag{12}$$

and

$$\pm \int_0^\infty e^{-s|x|} J_1(s\rho) J_1(s\rho_0)\, s\,ds \equiv \qquad \begin{matrix} (\text{"}+\text{"} \text{ for } x > 0) \\ (\text{"}-\text{"} \text{ for } x < 0) \end{matrix}$$

$$\equiv \frac{1}{2\pi} \int_0^{2\pi} \frac{x\cos\theta'}{\left[\rho^2 + \rho_0^2 + x^2 - 2\rho\rho_0\cos\theta\right]^{3/2}} d\theta' \tag{13}$$

Making use of Eqs. (12) and (13), the Eqs. (10) and (11) for the velocity components due to a vortex ring of constant strength γ and radius ρ_0 at $x = 0$, become

$$u(\rho,x) = \frac{\rho_0 \gamma}{2} \int_0^\infty e^{-s|x|} J_0(s\rho)\, J_1(s\rho_0)\, s\,ds \tag{14}$$

$$v(\rho,x) = \pm \frac{\rho_0 \gamma}{2} \int_0^\infty e^{-s|x|} J_1(s\rho)\, J_1(s\rho_0)\, s\,ds \tag{15}$$

III. SEMI-INFINITE VORTEX SHEET $\{\gamma = \gamma_0\}$

For a semi-infinite cylindrical vortex sheet of constant radius ρ_0 and vorticity strength $\gamma(x) = \gamma_0$ in the interval $1 \leq x \leq \infty$, the flow field is found by integrating Eqs. (14) and (15) for u and v from 1 to ∞ with respect to x.

Thus,

$$u(\rho,x) = \int_1^\infty \frac{\rho_0 \gamma_0}{2} \int_0^\infty e^{-s|x-x'|} J_0(s\rho)\, J_1(s\rho_0)\, s\,ds\,dx' \tag{16}$$

$$v(\rho,x) = \int_1^\infty \pm \frac{\rho_0 \gamma_0}{2} \int_0^\infty e^{-s|x-x'|} J_1(s\rho)\, J_1(s\rho_0)\, s\,ds\,dx' \tag{17}$$

("+" for $(x-x') > 0$, "-" for $(x-x') < 0$)

From the evaluation of the integral with respect to x' we have (Ref. D1).

$$\int_1^\infty e^{-s|x-x'|}\,dx' = \begin{cases} \frac{1}{s} e^{-s(x-1)} & \text{for } x \leq 1 \\ -\frac{1}{s}\left(e^{-s(x-1)} - [1 \pm 1]\right) & \begin{matrix}\text{"+" for } (u) \\ \text{"-" for } (v)\end{matrix} \quad \text{for } 1 \leq x \end{cases} \tag{18}$$

Substituting into Eqs. (16) and (17), we find

$$u(\rho,x) = \frac{\rho_0\gamma_0}{2}\int_0^\infty e^{s(x-1)} J_0(s\rho)\, J_1(s\rho_0)\, ds \qquad \text{for } x \le 1$$

$$u(\rho,x) = -\frac{\rho_0\gamma_0}{2}\int_0^\infty \left[e^{-s(x-1)} - 2\right] J_0(s\rho)\, J_1(s\rho_0)\, ds \qquad \text{for } x \ge 1 \tag{19}$$

And

$$v(\rho,x) = -\frac{\rho_0\gamma_0}{2}\int_0^\infty e^{s(x-1)} J_1(s\rho)\, J_1(s\rho_0)\, ds \qquad \text{for } x \le 1$$

$$v(\rho,x) = -\frac{\rho_0\gamma_0}{2}\int_0^\infty e^{-s(x-1)} J_1(s\rho)\, J_1(s\rho_0)\, ds \qquad \text{for } x \ge 1 \tag{20}$$

From the above Eqs. (19) and (20), we see that for $x \to \pm\infty$ the velocity becomes

$$u_{-\infty} = \frac{\rho_0\gamma_0}{2}\int_0^\infty e^{-\infty} J_0(s\rho)\, J_1(s\rho)\, ds = 0$$

$$u_{+\infty} = -\frac{\rho_0\gamma_0}{2}\int_0^\infty e^{-\infty} J_0(s\rho)\, J_1(s\rho_0)\, ds + \rho_0\gamma_0\int_0^\infty J_0(s\rho)\, J_1(s\rho_0)\, ds \tag{21}$$

or

$$u_{+\infty} = u_{-\infty} + \rho_0\gamma_0 \begin{cases} \frac{1}{\rho_0} & \text{for } \rho < \rho_0 \\ \frac{1}{2\rho_0} & \text{for } \rho = \rho_0 \\ 0 & \text{for } \rho > \rho_0 \end{cases} \tag{22}$$

IV. FINITE TRIANGULAR VORTEX SHEET $\left\{\gamma = \frac{\gamma_0}{2}(1+x)\right\}$

For a finite vortex sheet of constant radius ρ_0 and strength $\gamma(x) = \frac{\gamma_0}{2}(1+x)$ in the interval $-1 \le x \le 1$, the flow field is found by integrating Eqs. (14)

and (15) for u and v from -1 to +1 with respect to x.

Thus,

$$u(\rho,x)=\int_{-1}^{+1}\frac{\rho_0\gamma_0}{4}\int_0^\infty(1+x')\,e^{-s|x-x'|}\,J_0(s\rho)\,J_1(s\rho_0)\,s\alpha\,s\alpha\,x' \tag{23}$$

$$v(\rho,x)=\int_{-1}^{+1}\pm\frac{\rho_0\gamma_0}{4}\int_0^\infty(1+x')\,e^{-s|x-x'|}\,J_1(s\rho)\,J_1(s\rho_0)\,s\alpha\,s\alpha\,x' \tag{24}$$

("+" for $x-x'>0$, "-" for $x-x'<0$)

From the evaluation of the integrals with respect to x' we have (Ref. D1)

$$\int_{-1}^{+1}e^{-s|x-x'|}\,dx'=\begin{cases}\left\{2\,\dfrac{e^{sx}}{s}\sinh s\right\} & \text{for } x\le -1\\ \left\{\dfrac{2}{s}e^{-s}\sinh sx\right\}\rightarrow(u)\\ \left\{\dfrac{2}{s}\left[1-e^{-s}\cosh sx\right]\right\}\rightarrow(v) & \text{for } -1\le x\le +1\\ \left\{2\,\dfrac{e^{-sx}}{s}\sinh s\right\} & \text{for } 1\le x\end{cases} \tag{25}$$

And

$$\int_{-1}^{+1}x'e^{-s|x-x'|}\,dx'=\begin{cases}\left\{2\,\dfrac{e^{sx}}{s}\left[\dfrac{1}{s}\sinh s-\cosh s\right]\right\} & \text{for } x\le -1\\ \left\{\dfrac{2}{s}\left[x-e^{-s}\left(1+\dfrac{1}{s}\right)\sinh sx\right]\right\}\rightarrow(u)\\ \left\{\dfrac{2}{s}\left[-\dfrac{1}{s}+e^{-s}\left(1+\dfrac{1}{s}\right)\cosh sx\right]\right\}\rightarrow(v) & \text{for } -1\le x\le 1\\ \left\{2\,\dfrac{e^{-sx}}{s}\left[\cosh s-\dfrac{1}{s}\sinh s\right]\right\} & \text{for } 1\le x\end{cases} \tag{26}$$

Substituting into Eqs. (23) and (24) for u and v we find

$$u = \frac{\rho_0 \gamma_0}{2} \int_0^\infty e^{sx} \left[\left(1 + \frac{1}{s}\right) \sinh s - \cosh s \right] J_0(s\rho) J_1(s\rho_0)\, ds \qquad \text{for } x \le -1$$

$$u = \frac{\rho_0 \gamma_0}{2} \int_0^\infty \left\{ x + 1 - e^{-s} \left[\left(1 + \frac{1}{s}\right) \sinh sx + \cosh sx \right] \right\} J_0(s\rho) J_1(s\rho_0)\, ds \qquad (27)$$

$$\text{for } -1 \le x \le +1$$

$$u = \frac{\rho_0 \gamma_0}{2} \int_0^\infty e^{-sx} \left[\left(1 - \frac{1}{s}\right) \sinh s + \cosh s \right] J_0(s\rho) J_1(s\rho_0)\, ds \qquad \text{for } 1 \le x$$

And

$$v = -\frac{\rho_0 \gamma_0}{2} \int_0^\infty e^{sx} \left[\left(1 + \frac{1}{s}\right) \sinh s - \cosh s \right] J_1(s\rho) J_1(s\rho_0)\, ds \qquad \text{for } x \le -1$$

$$v = \frac{\rho_0 \gamma_0}{2} \int_0^\infty \left\{ e^{-s} \left[\left(1 + \frac{1}{s}\right) \cosh sx + \sinh sx \right] - \frac{1}{s} \right\} J_1(s\rho) J_1(s\rho_0)\, ds \qquad (28)$$

$$\text{for } -1 < x < +1$$

$$v = \frac{\rho_0 \gamma_0}{2} \int_0^\infty e^{-sx} \left[\left(1 - \frac{1}{s}\right) \sinh s + \cosh s \right] J_1(s\rho) J_1(s\rho_0)\, ds \qquad \text{for } 1 \le x$$

V. FINITE VORTEX SHEET $\left\{ \gamma(x) = c_1 \sqrt{\frac{1-x}{1+x}} \right\}$

For a finite vortex sheet of constant radius ρ_0 and strength $\gamma(x) = c_1 \sqrt{\frac{1-x}{1+x}}$ in the interval $-1 \le x \le +1$ the flow field is found by integrating Eqs. (14) and (15) for u and v from -1 to +1 with respect to x.

Thus,

$$u = \int_{-1}^{+1} \frac{\rho_0 c_1}{2} \int_0^\infty \sqrt{\frac{1-x'}{1+x'}}\, e^{-s|x-x'|} J_0(s\rho) J_1(s\rho_0)\, s\, ds\, dx' \qquad (29)$$

$$v = \int_{-1}^{+1} \pm \frac{\rho_0 c_1}{2} \int_0^\infty \sqrt{\frac{1-x'}{1+x'}}\, e^{-s|x-x'|} J_1(s\rho)\, J_1(s\rho_0)\, s\, ds\, dx' \tag{30}$$

("+" for $x - x' > 0$, "-" for $(x - x') < 0$)

From the evaluation of the integral with respect to x' we have, (Ref.D1)

$$\int_{-1}^{+1} \sqrt{\frac{1-x'}{1+x'}}\, e^{-s|x-x'|}\, dx' = \begin{cases} \dfrac{\pi}{2} e^{sx} F_0(-s) & \text{for } x \le -1 \\ e^{-sx}\left[\xi \sum_{n=1}^{\infty} F_n(s)(1+\xi^2)^{-n} + F_0(s)\left(\dfrac{\pi}{2} - \tan^{-1}\xi\right)\right] & \text{for } -1 \le x \le 1 \\ \pm e^{sx}\left[\xi \sum_{n=1}^{\infty} F_n(-s)(1+\xi^2)^{-n} + F_0(-s)\tan^{-1}\xi\right] & \begin{cases} \text{"+" for } (u) \\ \text{"-" for } (v) \end{cases} \\ \dfrac{\pi}{2} e^{-sx} F_0(s) & \text{for } 1 \le x \end{cases} \tag{31}$$

where

$$\xi = \sqrt{\frac{1-x}{1+x}} \qquad B_{rn} = \prod_{K=0}^{r-n} \frac{2(n+K)+1}{2(n+K)}$$

$$F_r(a) = 4e^{-a}\left[1 + \sum_{r=1}^{\infty} K_r(a) A_r\right] \qquad A_r = \prod_{K=0}^{r-1} \frac{2(r-K)-1}{2(r-K)} \tag{32}$$

$$F_n(a) = 4e^{-a} \sum_{r=\lambda}^{\infty} \frac{K_r(a) B_{rn}}{2r+1} \qquad K_r(a) = \frac{(2a)^r}{\lfloor r} \left[1 - \frac{r}{2a}\right]$$

Substituting into Eqs. (29) and (30) for v and v the velocity field becomes

$$u = \frac{\rho_0 c_1}{4} \int_0^\infty e^{sx} \pi F_0(-s)\, J_0(s\rho)\, J_1(s\rho_0)\, s\, ds \qquad \text{for } x \le -1$$

$$u = \frac{\rho_0 c_1}{2}\int_0^\infty \left\{ e^{-sx}\left[F_0(s)\left(\frac{\pi}{2} - \tan^{-1}\xi\right) + \xi \sum_{n=1}^{\infty} F_n(s)(1+\xi^2)^{-n}\right] + e^{sx}\left[F_0(-s)\tan^{-1}\xi + \xi \sum_{n=1}^{\infty} F_n(-s)(1+\xi^2)^{-n}\right]\right\} \cdot J_0(s\rho)\, J_1(s\rho_0)\, s\,ds \qquad \text{for } -1 \le x \le +1 \quad (33)$$

$$u = \frac{\rho_0 c_1}{4}\int_0^\infty e^{-sx}\,\pi\, F_0(s)\, J_0(s\rho)\, J_1(s\rho_0)\, s\,ds \qquad \text{for } 1 \le x$$

And

$$v = -\frac{\rho_0 c_1}{4}\int_0^\infty e^{sx}\,\pi\, F_0(-s)\, J_1(s\rho)\, J_1(s\rho_0)\, s\,ds \qquad \text{for } x \le -1$$

$$v = \frac{\rho_0 c_1}{2}\int_0^\infty \left\{ e^{-sx}\left[F_0(s)\left(\frac{\pi}{2} - \tan^{-1}\xi\right) - \xi \sum_{n=1}^{\infty} F_n(s)(1+\xi^2)^{-n}\right] - e^{sx}\left[F_0(-s)\tan^{-1}\xi + \xi \sum_{n=1}^{\infty} F_n(-s)(1+\xi^2)^{-n}\right]\right\} \cdot J_1(s\rho)\, J_1(s\rho_0)\, s\,ds \qquad \text{for } -1 \le x \le 1 \quad (34)$$

$$v = \frac{\rho_0 c_1}{4}\int_0^\infty e^{-sx}\,\pi\, F_0(s)\, J_1(s\rho)\, J_0(s\rho_0)\, s\,ds \qquad \text{for } 1 \le x$$

VI. FINITE VORTEX SHEET $\left\{\gamma(x) = c_2\sqrt{1-x^2}\right\}$

For a finite vortex sheet of constant radius ρ_0 and strength $\gamma(x) = c_2\sqrt{1-x^2}$ in the interval $-1 \le x \le +1$, the flow field is found by integrating Eqs. (14) and (15) for u and v from -1 to +1 with respect to x.

Thus,

$$u = \int_{-1}^{+1} \frac{\rho_0 c_2}{2} \int_0^\infty \sqrt{1-x'^2}\, e^{-s|x-x'|} J_0(s\rho) J_1(s\rho_0)\, s\,ds\,ds\,dx' \tag{35}$$

$$v = \int_{-1}^{+1} \pm \frac{\rho_0 c_2}{2} \int_0^\infty \sqrt{1-x'^2}\, e^{-s|x-x'|} J_1(s\rho) J_1(s\rho_0)\, s\,ds\,ds\,dx' \tag{36}$$

("+" for $x - x' > 0$, "-" for $x - x' < 0$)

From the evaluation of the integral with respect to x' we have (Ref. D1)

$$\int_{-1}^{+1} \sqrt{1-x'^2}\, e^{-s|x-x'|}\, dx' = \begin{cases} \pi A(-s)\, e^{sx} & \text{for } x \le -1 \\ e^{-sx}\left\{A(s)\left(\frac{\pi}{2} + \sin^{-1}x + x\sqrt{1-x^2}\right) - (1-x^2)^{3/2}\sum_{n=0}^{\infty} B_n(s)\, x^n\right\} & \\ \pm e^{sx}\left\{A(-s)\left(\frac{\pi}{2} - \sin^{-1}x - x\sqrt{1-x^2}\right) + (1-x^2)^{3/2}\sum_{n=0}^{\infty} B_n(-s)\, x^n\right\} & \text{for } -1 \le x \le 1 \\ \pi A(s)\, e^{-sx} & \text{for } 1 \le x \end{cases} \tag{37}$$

("+" for $x - x' > 0$, "-" for $x - x' < 0$)

where

$$A(a) = \frac{1}{2}\left[1 + \frac{1}{2}\sum_{m=1}^{\infty} \frac{a^{2m}}{\lfloor 2m} \frac{B_{mm}}{m+1}\right]$$

$$B_n(a) = \sum_{K=1}^{\infty} \frac{a^{n-1+2K}}{(n-1+2K)!} \frac{1}{n+2K+1} B_{\frac{n-1}{2}+K,K} \quad (n = \text{odd})$$

$$B_n(a) = \sum_{K=0}^{\infty} \frac{a^{n+2K+1}}{(n+2K+1)!} \frac{1}{n+2K+3} A_{\frac{n}{2}+K,K} \quad (n = \text{even}) \tag{38}$$

$$B_{m,K} = \prod_{r=1}^{K-1} \frac{2(m-r)+1}{2(m-r+1)} \qquad \text{for } K>1 \qquad B_{m,1} = 1$$

$$A_{m,K} = \prod_{r=1}^{K} \frac{2(m-r+1)}{2(m-r)+3} \qquad \text{for } K>0 \qquad A_{m,0} = 1$$

Substituting into Eqs. (35) and (36) for u and v the velocity field becomes

$$u = \frac{\rho_0 c_2}{2} \int_0^\infty e^{sx}\, \pi A(-s)\, J_0(s\rho)\, J_1(s\rho_0)\, s\,ds \qquad \text{for } x \le -1$$

$$u = \frac{\rho_0 c_2}{2} \int_0^\infty \left\{ e^{-sx}\left[A(s)\left(\frac{\pi}{2} + \sin^{-1}x + x\sqrt{1-x^2}\right) - (1-x^2)^{3/2} \sum_{n=0}^{\infty} B_n(s)\, x^n\right]\right.$$
$$\left. + e^{sx}\left[A(-s)\left(\frac{\pi}{2} - \sin^{-1}x - x\sqrt{1-x^2}\right) + (1-x^2)^{3/2} \sum_{n=0}^{\infty} B_n(-s)\, x^n\right]\right\} \cdot \qquad (39)$$
$$\cdot J_0(s\rho)\, J_1(s\rho_0)\, s\,ds \qquad \text{for } -1 \le x \le +1$$

$$u = \frac{\rho_0 c_2}{2} \int_0^\infty e^{-sx}\, \pi A(s)\; J_0(s\rho)\, J_1(s\rho_0)\, s\,ds \qquad \text{for } 1 \le x$$

And

$$v = -\frac{\rho_0 c_2}{2} \int_0^\infty e^{sx}\, \pi A(-s)\, J_1(s\rho)\, J_0(s\rho_0)\, s\,ds \qquad \text{for } x \le -1$$

$$v = \frac{\rho_0 c_2}{2} \int_0^\infty \left\{ e^{-sx}\left[A(s)\left(\frac{\pi}{2} + \sin^{-1}x + x\sqrt{1-x^2}\right) - (1-x^2)^{3/2} \sum_{n=0}^{\infty} B_n(s)\, x^n\right]\right.$$
$$\left. - e^{sx}\left[A(-s)\left(\frac{\pi}{2} - \sin^{-1}x - x\sqrt{1-x^2}\right) + (1-x^2)^{3/2} \sum_{n=0}^{\infty} B_n(-s)\, x^n\right]\right\} \cdot$$
$$\cdot J_1(s\rho)\, J_1(s\rho_0)\, s\,ds \qquad \text{for } -1 \le x \le +1 \qquad (40)$$

$$v = \frac{\rho_0 c_2}{2} \int_0^\infty e^{-sx}\, \pi A(s)\; J_1(s\rho)\, J_1(s\rho_0)\, s\,ds \qquad \text{for } 1 \le x$$

VII. FINITE VORTEX SHEET $\left\{\gamma(x) = C_3\, x\sqrt{1-x^2}\right\}$

For a finite vortex sheet of constant radius ρ_0 and strength $\gamma(x) = C_3 x\sqrt{1-x^2}$ in the interval $-1 \le x \le +1$, the flow field is found by integrating Eqs. (14) and (15) for u and v from -1 to +1 with respect to x.

Thus,

$$u = \int_{-1}^{+1} \frac{\rho_0 C_3}{2} \int_0^\infty x'\sqrt{1-x'^2}\, e^{-s|x-x'|} J_0(s\rho) J_1(s\rho_0)\, s\,ds\,dx' \tag{41}$$

$$v = \int_{-1}^{+1} \pm \frac{\rho_0 C_3}{2} \int_0^\infty x'\sqrt{1-x'^2}\, e^{-s|x-x'|} J_1(s\rho) J_1(s\rho_0)\, s\,ds\,dx' \tag{42}$$

("+" for $x - x' > 0$, "-" for $x - x' < 0$)

From the evaluation of the integral with respect to X' we have (Ref. D1).

$$\int_{-1}^{+1} x'\sqrt{1-x'^2}\, e^{-s|x-x'|}\, dx' = \begin{cases} \pi P(-s) e^{sx} & \text{for } x \le -1 \\ e^{-sx}\left\{P(s)\left(\frac{\pi}{2} + \sin^{-1}x + x\sqrt{1-x^2}\right) - (1-x^2)^{3/2}\sum_{n=0}^{\infty} Q_n(s)\, x^n\right\} & \\ \pm e^{sx}\left\{P(-s)\left(\frac{\pi}{2} - \sin^{-1}x - x\sqrt{1-x^2}\right) + (1-x^2)^{3/2}\sum_{n=0}^{\infty} Q_n(-s)\, x^n\right\} & \text{for } -1 \le x \le 1 \\ \pi P(s) e^{-sx} & \text{for } 1 \le x \end{cases} \tag{43}$$

("+" for $x - x' > 0$, "-" for $x - x' < 0$)

where

$$P(a) = \frac{1}{4} \sum_{K=1}^{\infty} \frac{a^{2K-1}}{(2K-1)!} \frac{B_{KK}}{K+1}$$

$$Q_n(a) = \sum_{K=0}^{\infty} \frac{a^{n+2K}}{(n+2K)!\,(n+2K+3)} A_{\frac{n}{2}+K,K} \qquad (44)$$

$$Q_n(a) = \sum_{K=1}^{\infty} \frac{a^{n+2K-2}}{(n+2K-2)!\,(n+2K+1)} B_{\frac{n-1}{2}+K,K}$$

And $B_{m,k}$ $A_{m,k}$ are given by Eqs. (38).

Substituting into Eqs. (41) and (42) for u and v the velocity field becomes

$$u = \frac{\rho_0 c_3}{2} \int_0^{\infty} e^{sx}\, \pi P(-s)\, J_0(s\rho)\, J_1(s\rho_0)\, s\,ds \qquad \text{for } x \le -1$$

$$u = \frac{\rho_0 c_3}{2} \int_0^{\infty} \left\{ e^{-sx} \left[P(s)\left(\frac{\pi}{2} + \sin^{-1}x + x\sqrt{1-x^2}\right) - (1-x^2)^{3/2} \sum_{n=0}^{\infty} Q_n(s)\, x^n \right] \right.$$

$$\left. + e^{sx} \left[P(-s)\left(\frac{\pi}{2} - \sin^{-1}x - x\sqrt{1-x^2}\right) + (1-x^2)^{3/2} \sum_{n=0}^{\infty} Q_n(-s)\, x^n \right] \right\} \cdot \qquad (45)$$

$$\cdot J_0(s\rho)\, J_1(s\rho_0)\, s\,ds \qquad \text{for } -1 \le x < +1$$

$$u = \frac{\rho_0 c_3}{2} \int_0^{\infty} e^{-sx}\, \pi\, P(s)\, J_0(s\rho)\, J_1(s\rho_0)\, s\,ds \qquad \text{for } 1 \le x$$

And

$$v = -\frac{\rho_0 c_3}{2}\int_0^\infty e^{sx}\,\pi\, P(-s)\, J_1(s\rho)\, J_1(s\rho_0)\, s\,ds \qquad \text{for } x \le -1$$

$$v = \frac{\rho_0 c_3}{2}\int_0^\infty \Big\{ e^{-sx}\Big[P(s)\Big(\frac{\pi}{2} + \sin^{-1}x + x\sqrt{1-x^2}\Big) - (1-x^2)^{3/2}\sum_{n=0}^{\infty} Q_n(s)x^n\Big] - e^{sx}\Big[P(-s)\Big(\frac{\pi}{2} - \sin^{-1}x - x\sqrt{1-x^2}\Big) + (1-x^2)^{3/2}\sum_{n=0}^{\infty} Q_n(-s)x^n\Big]\Big\} \cdot J_1(s\rho)\, J_1(s\rho_0)\, s\,ds \qquad \text{for } -1 \le x \le 1 \qquad (46)$$

$$v = \frac{\rho_0 c_3}{2}\int_0^\infty e^{-sx}\,\pi\, P(s)\, J_1(s\rho)\, J_1(s\rho_0)\, s\,ds \qquad \text{for } x \le 1$$

VIII. NON-UNIFORM VORTEX SHEET

For the representation of the flow field of a shrouded propeller by singularity distributions we determine the strength of the vortices from the fact that the shroud should be a streamline of the flow.

Since only high speed shrouds are considered in this paper, the vorticity distribution has been assumed on a cylindrical surface of constant radius ρ_0 which corresponds to the exit cylindrical radius of the flow.

The strength of the semi-infinite vortex sheet γ_0 is evaluated from the forward and exit velocity u_0 and u_e, i.e.,

$$\gamma_0 = u_e - u_0 = u_{+\infty} - u_{-\infty} = v_e - v_0$$

The coefficients c_1, c_2, and c_3 are evaluated from the satisfaction of the boundary conditions on the shroud. Thus, for a number n of coefficients, we need a system of n boundary conditions.

In our special case with $n = 3$ we need three boundary conditions.

It might be recommended to take the conditions at $\left[x=-1,\ \rho=\rho_s(-1)\right]$, $\left[x=0,\ \rho=\rho_s(0)\right]$, and $\left[x=1,\ \rho=\rho_s(1)\right]$ with the corresponding slopes.

$$\frac{d\rho(x,\rho)}{dx} = \frac{v(x,\rho)}{u(x,\rho_s)} \tag{47}$$

where the velocities $v(x,\rho)$ and $u(x,\rho)$ are given by

$$\begin{aligned} u(x,\rho) &= u_1(x,\rho) + u_2(x,\rho) + u_3(x,\rho) + u_\alpha(x,\rho) + u_\beta(x,\rho) + u_0 \\ v(x,\rho) &= v_1(x,\rho) + v_2(x,\rho) + v_3(x,\rho) + v_\alpha(x,\rho) + v_\beta(x,\rho) \end{aligned} \tag{48}$$

Thus, we have

$$\begin{aligned} &\frac{v}{u} = -\alpha_{-1} \quad \text{at} \quad x=-1 \quad \& \quad \rho=\rho_s(-1) \\ &\frac{v}{u} = -\alpha_0 \quad \text{at} \quad x=0 \quad \& \quad \rho=\rho_s(0) \\ &\frac{v}{u} = -\alpha_{+1} \equiv 0 \quad \text{at} \quad x=+1 \quad \& \quad \rho=\rho_s(+1) \end{aligned} \tag{49}$$

Making use of Eqs. (48) and (49), Eq. (47) becomes

$$\left\{ \frac{(v_\alpha+v_\beta) + c_1 v_1 + c_2 v_2 + c_3 v_3}{(u_0+u_\alpha+u_\beta) + c_1 u_1 + c_2 u_2 + c_3 u_3} \right\}_{x=-1,\ \rho=\rho_s(-1)} = -\alpha_{-1}$$

$$\left\{ \frac{(v_\alpha+v_\beta) + c_1 v_1 + c_2 v_2 + c_3 v_3}{(u_0+u_\alpha+u_\beta) + c_1 u_1 + c_2 u_2 + c_3 u_3} \right\}_{x=0,\ \rho=\rho_s(0)} = -\alpha_0 \tag{50}$$

$$\left\{ \frac{(v_\alpha+v_\beta) + c_1 v_1 + c_2 v_2 + c_3 v_3}{(u_0+u_\alpha+u_\beta) + c_1 u_1 + c_2 u_2 + c_3 u_3} \right\}_{x=+1,\ \rho=\rho_s(+1)} = -\alpha_{+1} \equiv 0$$

Solving the system of Eqs. (50), we find the values of c_1, c_2 and c_3 which determine approximately the flow field of the high speed shrouded propeller.

IX. APPENDIX

IDENTITIES OF BESSEL FUNCTIONS

From the identity of the Bessel functions we have

$$\frac{1}{\sqrt{a^2+b^2}} = \int_0^\infty e^{-sa} J_0(sb)\, ds \qquad a > 0 \tag{51}$$

Differentiating with respect to a, we find

$$\frac{\partial}{\partial a}\frac{1}{\sqrt{a^2+b^2}} \equiv -\frac{a}{(a^2+b^2)^{3/2}} = -\int_0^\infty e^{-sa} J_0(sb)\, sds \tag{52}$$

Substituting a by x and b by r, we have

$$\frac{x}{\left[r^2+x^2\right]^{3/2}} = \pm\int_0^\infty e^{-s|x|} J_0(sr)\, sds \tag{53}$$

where the "+" sign is for $x > 0$ and the "-" sign for $x < 0$

and

$$r^2 = \rho^2 + \rho_0^2 - 2\rho\,\rho_0 \cos\theta' \tag{54}$$

Multiplying Eq. (53) by cos θ' and integrating from 0 to 2π with respect to θ' we get

$$\int_0^{2\pi} \frac{x\cos\theta'}{\left[r^2+x^2\right]^{3/2}}\, d\theta' = \pm\int_0^{2\pi}\int_0^\infty e^{-s|x|} J_0(sr)\, sds\left[\cos\theta'\right] d\theta' \tag{55}$$

Making use of the following identity for the Bessel functions

$$J_0(sr) = J_0(s\rho)\, J_0(s\rho_0) + 2\sum_{n=1}^{\infty} J_n(s\rho)\, J_n(s\rho_0)\cos n\theta' \tag{56}$$

and of the orthogonality property of the trigonometric functions, we perform the integration with respect to θ' and we find

$$\frac{1}{2\pi}\int_0^{2\pi} \frac{x\cos\theta'}{\left[r^2+x^2\right]^{3/2}}\, d\theta' \equiv \pm\int_0^\infty e^{-s|x|} J_1(s\rho)\, J_1(s\rho_0)\, sds \tag{57}$$

Similarly, substituting a by $|x|$ and b by r in Eq. (51), we have

$$\frac{1}{\sqrt{x^2+r^2}} = \int_0^\infty e^{-s|x|} J_0(sr)\, ds \tag{58}$$

Differentiating Eq. (58) with respect to ρ_0, we find

$$\frac{\partial}{\partial \rho_0} \frac{1}{\sqrt{x^2+r^2}} \equiv -\frac{1}{2} \frac{2(\rho_0 - \rho\cos\theta')}{(x^2+r^2)^{3/2}} = \int_0^\infty e^{-s|x|} \frac{d}{d\rho_0} \left[J_0(sr)\right] ds \tag{59}$$

Integrating from 0 to 2π with respect to θ' we get

$$-\int_0^{2\pi} \frac{\rho_0 - \rho\cos\theta'}{\left[x^2+r^2\right]^{3/2}}\, d\theta' = \int_0^{2\pi}\int_0^\infty e^{-s|x|} \frac{d}{d\rho_0} \left[J_0(sr)\right] ds \tag{60}$$

Substituting Eq. (56) and interchanging the integration and differentiation in the right member of the above equation, we perform the integration with respect to θ' and making use of the orthogonality property of the trigonometric functions, we find

$$-\int_0^{2\pi} \frac{\rho_0 - \rho\cos\theta' d\theta'}{\left[x^2+r^2\right]^{3/2}} = 2\pi \int_0^\infty e^{-s|x|} \frac{d}{d\rho_0} \left[J_0(s\rho) J_0(s\rho_0)\right] ds \tag{61}$$

Performing the differentiation with respect to ρ_0, we get

$$\frac{d}{d\rho_0} J_0(s\rho_0) = -s J_1(s\rho_0) \tag{62}$$

Substituting Eq. (62) into Eq. (61), we find

$$\frac{1}{2\pi} \int_0^{2\pi} \frac{\rho_0 - \rho\cos\theta}{\left[x^2+r^2\right]^{3/2}}\, d\theta' \equiv \int_0^\infty e^{-s|x|} J_0(s\rho) J_1(s\rho_0)\, s\, ds \tag{63}$$

SECTION E

VELOCITY FIELD AND FORCES ON A FLAT PLATE DUE TO A CYLINDRICAL JET

I. Elliptical Cylinder With Major Axis Parallel to the Flow

In this section the pressure is found on a plate parallel to the flow and normal to a cylindrical jet with elliptical cross section.

Since the velocity of the jet is very high in comparison to that of the flow field around it, we consider that the jet is a rigid cylindrical body.

The potential flow field around a cylinder with an elliptical cross section is calculated from the theory of conformal mapping, making use of the complex potential for the flow field.

For an ellipse in the z (x, y) plane with major semi-axis a and minor semi-axis b the transformation

$$\zeta = \zeta + \frac{d^2}{\zeta} \tag{1}$$

where

$$d^2 = \frac{1}{4}(a^2 - b^2) = \frac{c^2}{4} \tag{2}$$

maps the ellipse into a circle with radius $R = \frac{1}{2}(a+b)$

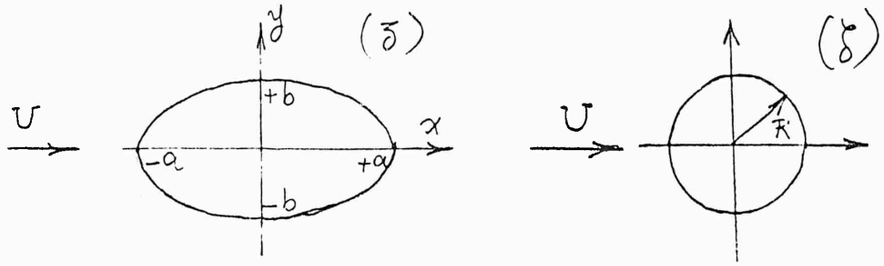

The complex potential for the flow velocity in the ζ-plane is given by

$$F(\zeta) = U\left(\zeta + \frac{R^2}{\zeta}\right) \tag{3}$$

where ζ is given by Equation (1).

Solving Equation (1) for ζ we find

$$\zeta = \frac{z + \sqrt{z^2 - c^2}}{2} \tag{4}$$

where

$$c^2 = a^2 - b^2 \tag{5}$$

Substituting from Equations (4) and (5) into Equation (3) we find

$$F(z) = \frac{U}{2}\left\{z + \sqrt{z^2 - c^2} + \frac{(a+b)^2}{z + \sqrt{z^2 - c^2}}\right\} \tag{6}$$

Making use of the elliptical transformation

$$z = x + iy = c\cosh(\xi + i\eta) \tag{7}$$

we get

$$x = c\cosh\xi\cos\eta, \qquad y = c\sinh\xi\sin\eta \tag{8}$$

Substituting Equation (7) into Equation (6) the complex potential for the flow velocity becomes

$$F(z) = \frac{U}{2}\left\{c\cosh(\xi + i\eta) + \sqrt{c^2\cosh^2(\xi + i\eta) - c^2}\right. \tag{9}$$

$$\left. + \frac{(a+b)^2}{c\cosh(\xi + i\eta) + \sqrt{c^2\cosh^2(\xi + i\eta) - c^2}}\right\}$$

Performing the algebraic manipulations and making use of the identities of the hyperbolic functions, the above Equation (9) becomes

$$F(\zeta) = \frac{U_c}{2}\left\{ e^{\xi+i\eta} + \frac{(a+b)^2}{a^2-b^2} e^{-\xi-i\eta} \right\} \tag{10}$$

Separating the real and imaginary part of the complex potential we find

$$\begin{aligned} F(\zeta) = {} & \frac{U_c}{2}\left\{ e^{\xi} + \frac{(a+b)^2}{a^2-b^2} e^{-\xi} \right\} \cos\eta \\ & + i\,\frac{U_c}{2}\left\{ e^{\xi} - \frac{(a+b)^2}{a^2-b^2} e^{-\xi} \right\} \sin\eta \end{aligned} \tag{11}$$

Thus, the velocity potential and the stream function in elliptical coordinates are given respectively by

$$\Phi(\xi,\eta) = \frac{U_c}{2}\left\{ e^{\xi} + \frac{(a+b)^2}{a^2-b^2} e^{-\xi} \right\} \cos\eta \tag{12}$$

$$\Psi(\xi,\eta) = \frac{U_c}{2}\left\{ e^{\xi} - \frac{(a+b)^2}{a^2-b^2} e^{-\xi} \right\} \sin\eta \tag{13}$$

The velocity components become

$$u_\xi = \frac{\partial\Phi}{h_\xi \partial\xi} = \frac{\partial\Psi}{h_\eta \partial\eta} = \frac{U_c}{2h}\left\{ e^{\xi} - \frac{(a+b)^2}{c^2} e^{-\xi} \right\} \cos\eta \tag{14}$$

$$u_\eta = \frac{\partial\Phi}{h_\eta \partial\eta} = -\frac{\partial\Psi}{h_\xi \partial\xi} = -\frac{U_c}{2h}\left\{ e^{\xi} + \frac{(a+b)^2}{c^2} e^{-\xi} \right\} \sin\eta \tag{15}$$

where

$$h^2 = c^2\left[\cosh^2\xi - \cos^2\eta\right] = c^2\left[\sinh^2\xi + \sin^2\eta\right] \tag{16}$$

Since the flow is isoenergetic, the Bernoulli's equation gives

$$p + \rho\frac{v^2}{2} = p_\infty + \rho\frac{U^2}{2} = \text{constant} \tag{17}$$

where

$$v^2 = u_\xi^2 + u_\eta^2 \tag{18}$$

The pressure field on the plane normal to the elliptical cylinder is given by

$$\Delta p = p - p_\infty = \frac{\rho}{2}\left(U^2 - v^2\right) \tag{19}$$

Making use of Equations (14), (15), and (18) the above Equation (19) becomes

$$\Delta p = \frac{\rho}{2}\left\{U^2 - \frac{U^2c^2}{4h^2}\left[e^{2\xi} + \frac{(a+b)^4}{c^4}e^{-2\xi} + 2\frac{(a+b)^2}{c^2}\left(\sin^2\eta - \cos^2\eta\right)\right]\right\} \tag{20}$$

The force on the plate is found by integrating the pressure field given by the above equation all over the plate outside the ellipse.

For an elliptical plate with the semi-foci distance c as that of the jet and with major semi-axis A and minor semi-axis B the force is given by

$$L = \iint \Delta p\, ds_1 ds_2 = \int_{\xi_0}^{\xi_1}\int_0^{2\pi} \Delta p\, h^2\, d\xi\, d\eta \tag{21}$$

Substituting for Δp from Equation (20) we get

$$L = \frac{\rho}{2} U^2 \int_{\xi_0}^{\xi_1} \int_0^{2\pi} \left\{ A^2 - \frac{c^2}{4} \left[e^{2\xi} + \frac{(a+b)^4}{c^4} e^{-2\xi} + 2 \frac{(a+b)^2}{c^2} (\sin^2\eta - \cos^2\eta) \right] \right\} d\xi\, d\eta \tag{22}$$

Performing the integration with respect to η we find

$$L = \frac{\rho}{2} U^2 \pi \int_{\xi_0}^{\xi_1} \left\{ 2c^2 \sinh^2\xi + c^2 - 2\frac{c^2}{4} \left[e^{2\xi} + \frac{(a+b)^4}{c^4} e^{-2\xi} \right] \right\} d\xi \tag{23}$$

Expanding the integrand in Equation (23) and making use of the identity

$$2\sinh^2\xi + 1 - \frac{1}{2} e^{2\xi} = \frac{1}{2} e^{-2\xi} \tag{24}$$

Equation (23) becomes:

$$L = -\frac{\rho}{2} U^2 \pi c^2 \frac{1}{2} \int_{\xi_0}^{\xi_1} \left[\frac{(a+b)^4}{c^4} - 1 \right] e^{-2\xi} d\xi \tag{25}$$

Integrating with respect to ξ we find

$$L = -\frac{\rho}{2} U^2 \pi \frac{c^2}{4} \left[\frac{(a+b)^4}{c^4} - 1 \right] \left\{ e^{-2\xi_0} - e^{-2\xi_1} \right\} \tag{26}$$

Since we have that:

$$e^{-2\xi_0} = \frac{a-b}{a+b} \quad , \qquad e^{-2\xi_1} = \frac{A-B}{A+B}$$

$$\frac{c^2}{4}\left[\frac{(a+b)^4}{c^4} - 1\right]\frac{a-b}{a+b} = ab \tag{27}$$

the above Equation (26) yields

$$L = -\frac{\rho}{2} U^2 \pi ab \left\{1 - \left(\frac{A-B}{a-b}\right)^2\right\} \tag{28}$$

And the lift coefficient becomes

$$C_L = \frac{L}{\frac{\rho}{2} U^2 S} = -\frac{ab}{AB-ab}\left\{1 - \left(\frac{A-B}{a-b}\right)^2\right\} \tag{29}$$

where S is the reference wing area

$$S = \pi(AB - ab)$$

Taking as reference area S^* the area of the elliptical cylinder, the lift coefficient C_L^* becomes

$$C_L^* = \frac{L}{\frac{\rho}{2} U^2 S^*} = -\left\{1 - \left(\frac{A-B}{a-b}\right)^2\right\} \tag{30}$$

where S^* is given by

$$S^* = \pi ab$$

II. Elliptical Cylinder With Major Axis Normal to the Flow

For an ellipse in the z (x, y) plate with major semi-axis a and minor semi-axis b, the transformation given by Equation (1) maps the ellipse into a circle with radius $R = \frac{1}{2}(a+b)$

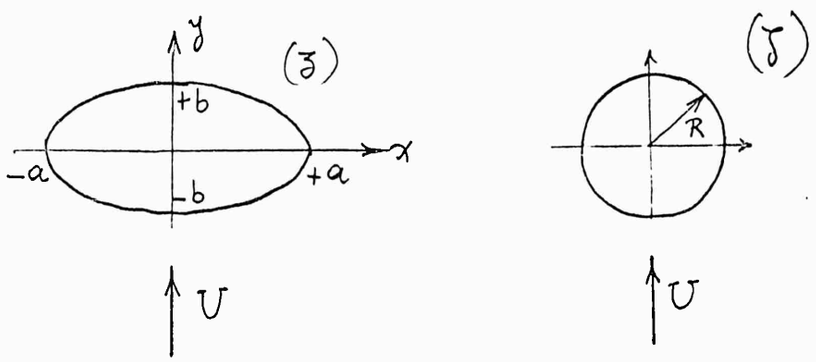

Making one more transformation given by Equation (31)

$$\zeta^* = \zeta e^{-i\frac{\pi}{2}} = -i\zeta \tag{31}$$

we find that the velocity U is turned by 90°

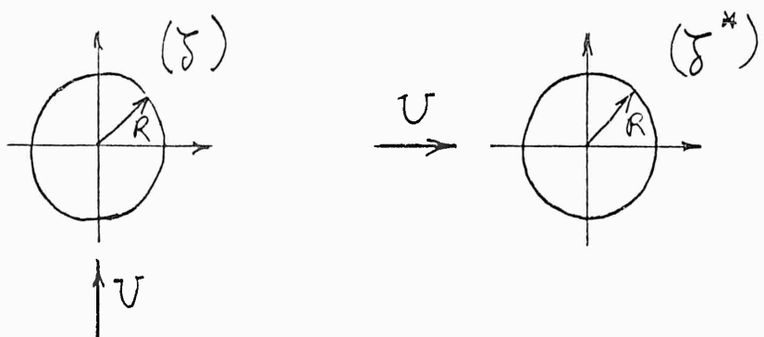

The complex potential for the flow velocity in the ζ^* -plane is given by

$$F(\zeta^*) = U\left(\zeta^* + \frac{R^2}{\zeta^*}\right) = -iU\left(\zeta - \frac{R^2}{\zeta}\right) \tag{32}$$

where ζ and ζ^* are given by Equations (1) and (31).

Substituting from Equations (4), into Equation (32) we find

$$F(\zeta) = -i\frac{U}{2}\left\{\zeta + \sqrt{\zeta^2 - c^2} - \frac{(a+b)^2}{\zeta + \sqrt{\zeta^2 - c^2}}\right\} \tag{33}$$

Making use of the elliptical transformation given by Equation (7) and performing the algebraic manipulations, the above Equation (33) becomes

$$F(\zeta) = -i\frac{U_c}{2}\left\{e^{\xi + i\eta} - \frac{(a+b)^2}{a^2 - b^2}e^{-\xi - i\eta}\right\} \tag{34}$$

Separating the real and imaginary part of the complex potential we find the velocity potential and the stream function in elliptical coordinates

$$\Phi(\xi,\eta) = \frac{U_c}{2}\left\{e^{\xi} + \frac{(a+b)^2}{a^2 - b^2}e^{-\xi}\right\}\sin\eta \tag{35}$$

$$\Psi(\xi,\eta) = -\frac{U_c}{2}\left\{e^{\xi} - \frac{(a+b)^2}{a^2 - b^2}e^{-\xi}\right\}\cos\eta \tag{36}$$

The velocity components become

$$u_\xi = \frac{\partial\Phi}{h_\xi \partial\xi} = \frac{\partial\Psi}{h_\eta \partial\eta} = \frac{U_c}{2h}\left\{e^{\xi} - \frac{(a+b)^2}{c^2}e^{-\xi}\right\}\sin\eta \tag{37}$$

$$u_\eta = \frac{\partial\Phi}{h_\eta \partial\eta} = -\frac{\partial\Psi}{h_\xi \partial\xi} = \frac{U_c}{2h}\left\{e^{\xi} + \frac{(a+b)^2}{c^2}e^{-\xi}\right\}\cos\eta \tag{38}$$

Making use of Equations (37), (38), and (18), Equation (19) becomes

$$\Delta p = \frac{\rho}{2}\left\{U^2 - \frac{U^2 c^2}{4R^2}\left[e^{2\xi} + \frac{(a+b)^4}{c^4}e^{-2\xi} - 2\frac{(a+b)^2}{c^2}\left(\sin^2\eta - \cos^2\eta\right)\right]\right\} \tag{39}$$

Substituting for Δp from Equation (39) into Equation (21) we get

$$L = \frac{\rho}{2}U^2\pi\int_{\xi_0}^{\xi_1}\int_{0}^{2\pi}\left\{R^2 - \frac{c^2}{4}\left[e^{2\xi} + \frac{(a+b)^4}{c^4}e^{-2\xi} - 2\frac{(a+b)^2}{c^2}\left(\sin^2\eta - \cos^2\eta\right)\right]\right\}d\xi\,d\eta \tag{40}$$

Performing the integrations we find Equation (26).

Thus, the force on the elliptical plate and the lift coefficient are given by the same Equations (28) and (29) as in Section EI.

For major semi-axis b and minor semi-axis a Equations (28), (29), and (30) become respectively:

$$L = -\frac{\rho}{2}U^2\pi ab\left\{1 - \left(\frac{B-A}{b-a}\right)^2\right\} \tag{41}$$

$$C_L = -\frac{ab}{AB-ab}\left\{1 - \left(\frac{B-A}{b-a}\right)^2\right\} \tag{42}$$

$$C_L^* = -\left\{1 - \left(\frac{B-A}{b-a}\right)^2\right\} \tag{43}$$

III. Circular Cylinder

In the case of a circular cylinder, the complex potential for the flow velocity is given by

$$F(\zeta) = \Phi + i\Psi = U\left(\zeta + \frac{R_0^2}{\zeta}\right) = U\cos\theta\left(r + \frac{R_0^2}{r}\right) + iU\sin\theta\left(r - \frac{R_0^2}{r}\right) \tag{44}$$

Thus, the velocity components become

$$u_r = \frac{\partial\Phi}{\partial r} = \frac{\partial\Psi}{r\partial\theta} = U\cos\theta\left(1 - \frac{R_0^2}{r^2}\right)$$
$$u_\theta = \frac{\partial\Phi}{r\partial\theta} = -\frac{\partial\Psi}{\partial r} = -U\sin\theta\left(1 + \frac{R_0^2}{r^2}\right) \tag{45}$$

Making use of Equations (45), the pressure field on the plate normal to the cylinder given by Equation (19) becomes

$$\Delta p = -\frac{\rho}{2}U^2\frac{R_0^2}{r^2}\left\{\frac{R_0^2}{r^2} - 2\cos 2\theta\right\} \tag{46}$$

The force on the plate is found by integrating the pressure field outside the circular jet. Thus we get,

$$L = \int_{R_0}^{R_1}\int_0^{2\pi} \Delta p\, r\, dr\, d\theta \tag{47}$$
$$= \int_{R_0}^{R_1}\int_0^{2\pi} -\frac{\rho}{2}U^2\frac{R_0^2}{r^2}\left[\frac{R_0^2}{r^2} - 2\cos 2\theta\right] r\, dr\, d\theta$$

Performing the integration we find

$$L = -2\pi \frac{\rho}{2} U^2 R_0^4 \left[\frac{-1}{2r^2} \right]_{R_0}^{R_1} = -\frac{\rho}{2} U^2 \pi R_0^2 \left(1 - \frac{R_0^2}{R_1^2} \right) \quad (48)$$

and the lift coefficients become

$$C_L = \frac{L}{\rho \frac{U^2}{2} S} = \frac{L}{\rho \frac{U^2}{2} \pi (R_1^2 - R_0^2)} = -\left(\frac{R_0}{R_1} \right)^2 \quad (49)$$

and

$$C_L^* = \frac{L}{\frac{\rho}{2} U^2 S^*} = \frac{L}{\rho \frac{U^2}{2} \pi R_0^2} = -\left\{ 1 - \left(\frac{R_0}{R_1} \right)^2 \right\} \quad (50)$$

Lift coefficients C_L and C_L^* for cylinders with elliptical cross-sections are shown in Figures E1 and E2.

PREPARED _____ _____

CHECKED _____ _____

REVISED _____ _____

PAGE _____

REPORT NO. _____

MODEL _____

FIG. E1

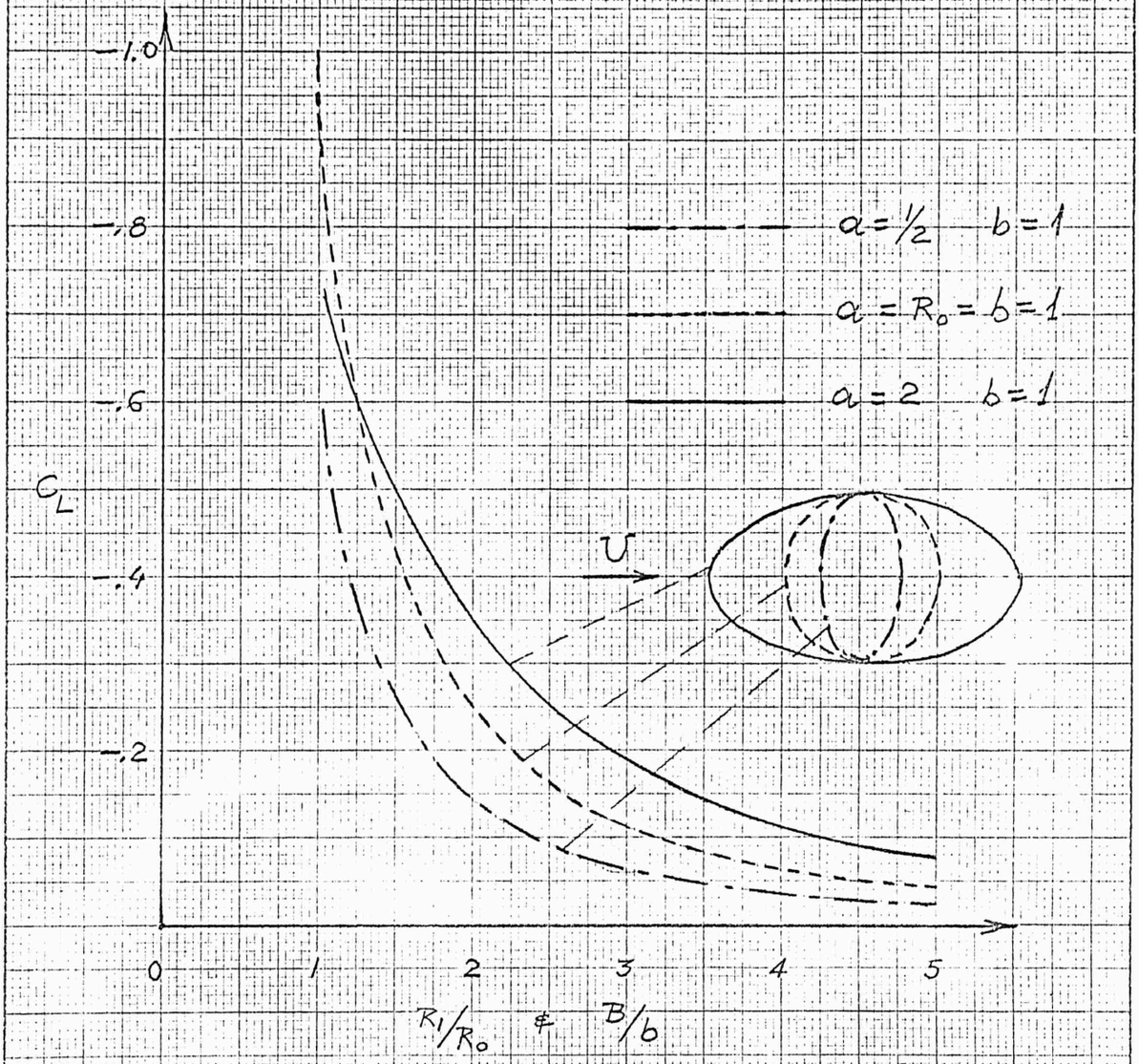

LIFT COEFFICIENT C_L

FOR $b = 1$ & $a = 1/2, 1, 2.$

E-1-10A
REV. 2/49

PREPARED _____ _____

CHECKED _____ _____

REVISED _____ _____

PAGE _____

REPORT NO. _____

MODEL _____

FIG. E2

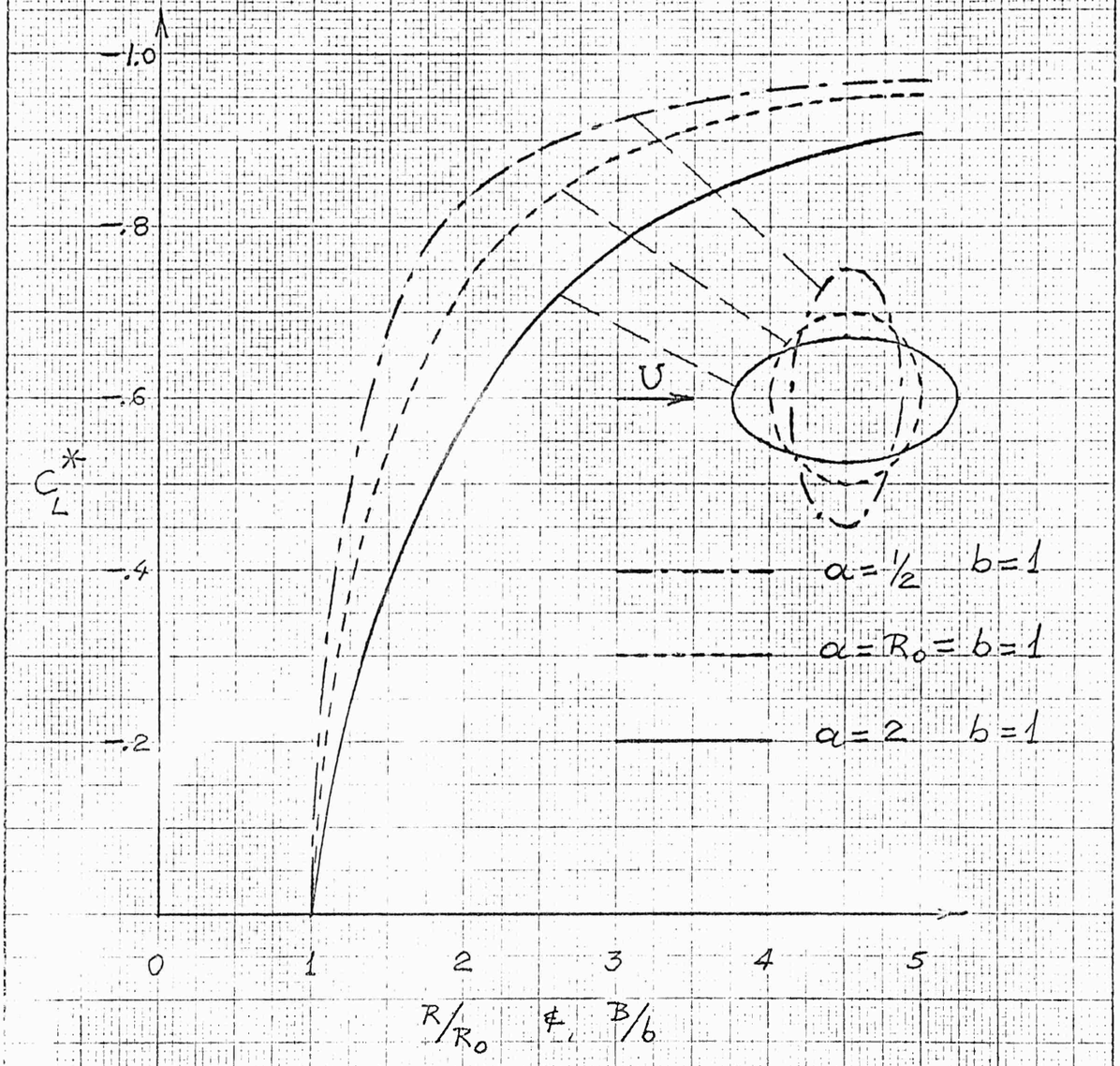

LIFT COEFFICIENT C_L^*

FOR $b = 1$ & $a = 1/2, 1, 2.$

E-1-10A
REV. 2/49

SECTION F

EXPERIMENTAL DATA ON JET INTERFERENCE EFFECTS ON VTOL AIRCRAFT

The jet issuing from a VTOL aircraft such as the fan-in-wing type, induces pressures on the lower surfaces of the aircraft which in most cases cause a loss in lift and a nose-up pitching moment during transition. Simple experiments designed to study the effect of a jet emerging normal to a flat plate placed parallel to an air stream, and similar tests on a solid circular cylinder normal to the plate were carried out at the 7' x 10' tunnel at Langley Field. These data have not been published and were obtained through a visit by Republic personnel. The pressure distributions found on the plate are shown in Figures F1 and F2 for the jet and the cylinders, respectively.

Positive pressures are produced ahead of the cylinder with rather high negative pressures to the side and rear. Similar results may be seen for the jet with the exception that the negative pressures are higher and extend to a greater distance from the center of the jet. The result is a predominance of negative pressure to the rear of the jet which in the case of a VTOL aircraft in transition would produce a loss in lift and an increase in nose-up pitching moment. Quantitative results for the two pressure distributions are given in Table H in coefficient form for the front and rear halves of the plate area.

In the case of the cylinder the lift on the front half of the plate (L_1) is negative $(C_{L_1} = -0.61)$ and acts at a point 1.18 radii downstream from the cylinder center. This checks reasonably with potential flow theory which indicates a lift coefficient of somewhat below -1. The lift on the rear half of the plate (L_2) is much more negative $(C_{L_2} = -5.59)$ and the center of pressure of this lift is at a point about two radii behind the center. The total result is a negative lift of $C_L = -3.1$ acting at a point two radii behind the center, thus producing a nose-up pitching moment.

The case of the jet is similar with the exception that higher values of the negative pressure peaks at the sides of the jet predominate to the extent that the pitching moment of the front half of the area (M_1) in this case becomes negative. Also, the total negative lift is about twice that of the cylinder and the total force acts at a point about 1 2/3 radii behind the center, producing also a larger nose-up pitching moment.

The higher negative pressures induced by the jet as compared to the case of the solid cylinder is attributed to a downward "pumping" action in the mixing region of the jet. Measurements taken at static condition indicate a total thrust loss on the plate of only one percent of the jet thrust. The pumping action of the jet increases with forward speed due to the mixing action which is also responsible for the drag on the jet. The coefficients C_L and C_M are obviously related to the drag coefficient C_D of the jet as they are all produced by a negative region behind the jet. The effect of

Reynolds number may be inferred from Figure F3 where the pressure distribution on the plate near the cylinder is compared with that on a cylinder taken from Reference F1. The drag coefficients ($C_D \approx 1.3$ based on cylinder length and diameter) obtained are characteristic of a laminar flow separation. This is to be expected since the Reynolds number is below the critical value of about 3.6×10^5 (based on forward velocity and cylinder diameter). For most VTOL applications, the Reynolds number will be above this value and consequently a turbulent separation will produce a smaller area of negative pressure behind the cylinder. If this reasoning is applied to the case of the jet, smaller lift losses and reduced nose-up pitching moments are to be expected with larger forward speeds.

In conclusion, the values of lift and moment coefficients determined from integration of the pressure distributions shown in this report and the lift and moment coefficients from the momentum theory outlined in Reference F2 have been computed and the results are presented in Figures F4 and F5. Also, some experimental values from Reference F3 are shown. The losses in lift and the increase in nose-up pitching moment caused by the jet interference are sizeable and could easily explain the actual effects observed.

The conclusions concerning jet interference which may be drawn from this study are:

1. The jet issuing from a VTOL may be regarded as a solid cylinder with a downward pumping action in the mixing region.

2. The flow on the front half of a plate normal to a cylinder resembles a two-dimensional potential flow about a cylinder.

3. The losses in lift and increase in nose-up pitching moment caused by the interference of a jet are large and do explain the deviations from momentum theory observed in experiments.

TABLE F1

CIRCULAR CYLINDER - R = $\frac{1}{2}$" q_o = 174 $^{lb}/_{ft^2}$ RN = 2×10^5				
	FRONT HALF	REAR HALF		TOTAL
$C_{L_{1,2}} = \frac{L_{1,2}}{q_o \pi \frac{R^2}{2}}$	-0.61	-5.59	$C_L = \frac{L}{q_o \pi R^2}$	-3.10
$C_{M_{1,2}} = \frac{M_{1,2}}{q_o \pi \frac{R^3}{2}}$	0.72	11.68	$C_M = \frac{M}{q_o \pi R^3}$	6.20
$\frac{M}{L}$	-1.18R	-2.09R	$\frac{M}{L}$	-2.0R

JET - v_o/v_e = 0.3 q_o = 27.2 $^{lb}/_{ft^2}$				
	FRONT HALF	REAR HALF		TOTAL
$C_{L_{1,2}} = \frac{L_{1,2}}{q_o \pi \frac{R^2}{2}}$	-2.34	-11.66	$C_L = \frac{L}{q_o \pi R^2}$	-7.0
$C_{M_{1,2}} = \frac{M_{1,2}}{q_o \pi \frac{R^3}{2}}$	-0.68	22.68	$C_M = \frac{M}{q_o \pi R^3}$	11.6
$\frac{M}{L}$	0.29R	-1.95R	$\frac{M}{L}$	-1.67R

MODEL AND NOMENCLATURE

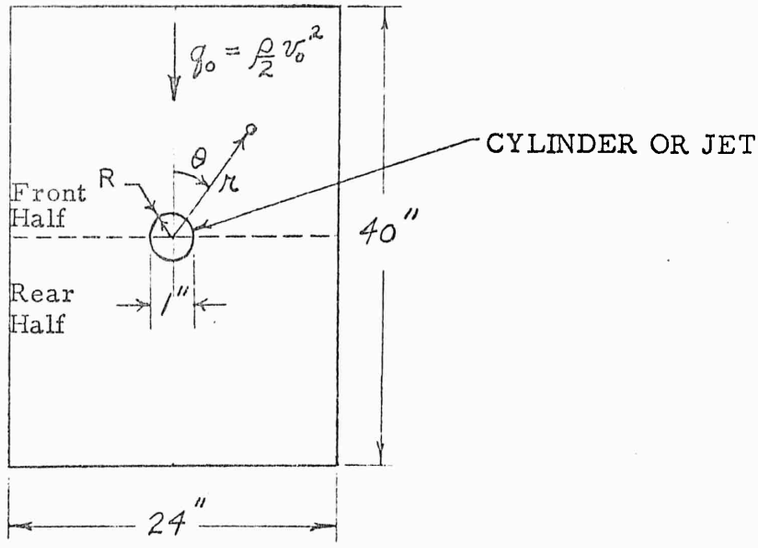

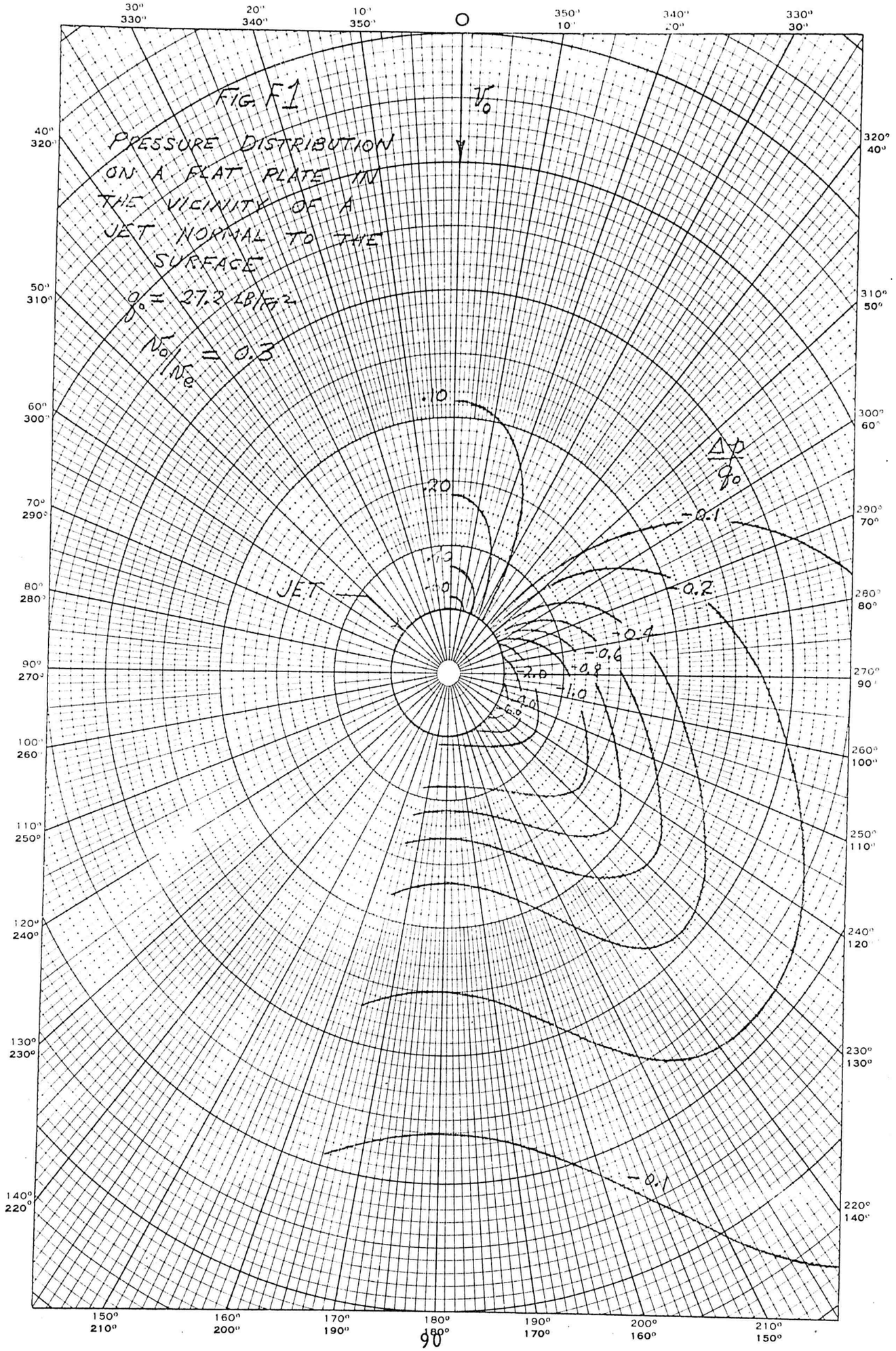

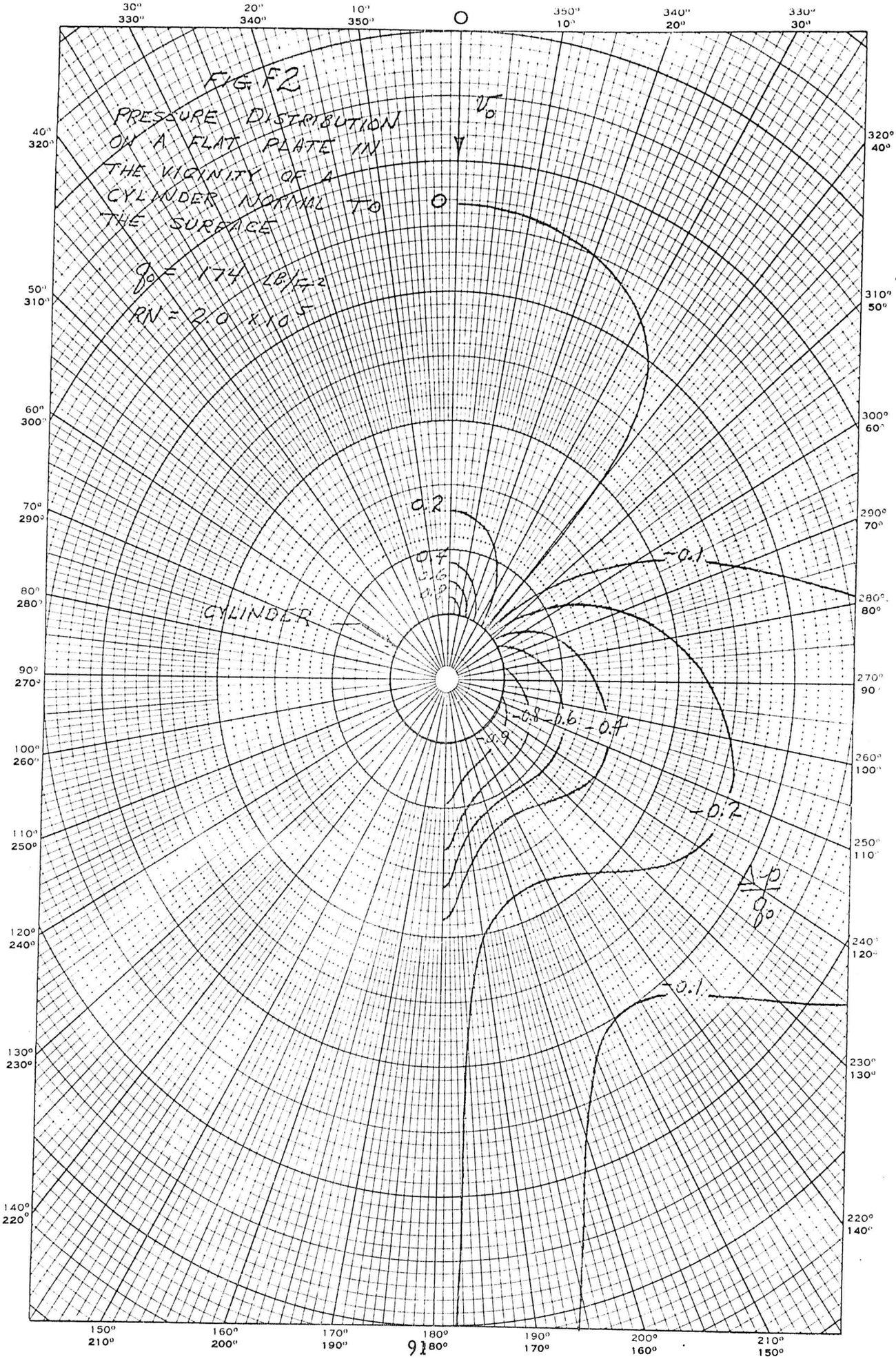

PREPARED JBS 7-20-61 | PAGE

CHECKED | REPORT NO

REVISED | MODEL

REPUBLIC AVIATION

FIG. F3

PRESSURE DISTRIBUTION ON A MODEL OF A CIRCULAR CYLINDER WHOSE AXIS IS NORMAL TO A FLAT PLATE

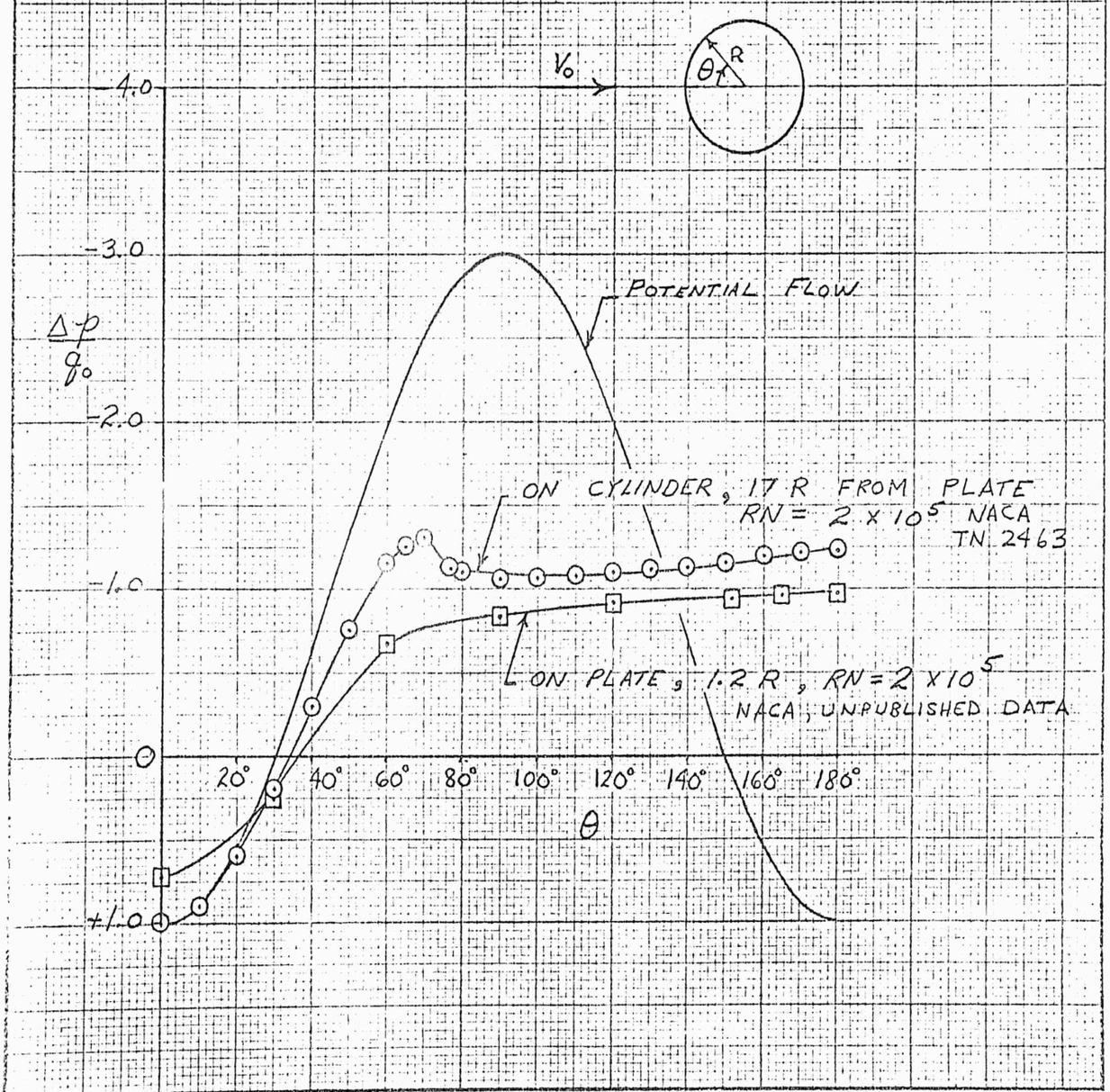

E-1-10A
REV 2/49

PREPARED JBS 7-31-61 PAGE

CHECKED REPORT NO.

REVISED MODEL

FIG F4

COMPARISON OF CALCULATED LIFT WITH EXPERIMENTAL VALUES

CONSTANT POWER

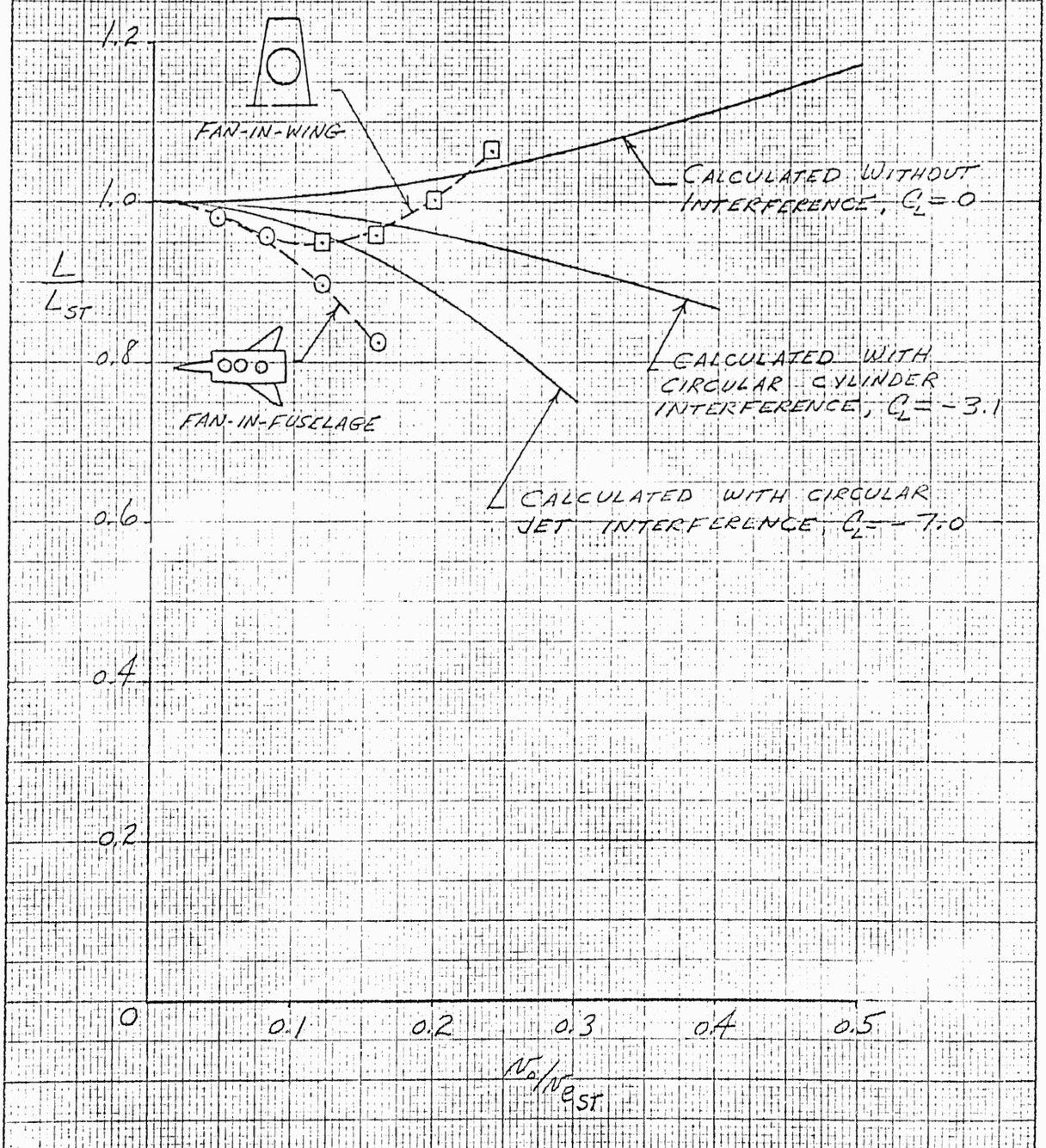

E-1-10A
REV. 2/49

PREPARED JBS 7-31-61 PAGE

CHECKED REPORT NO.

REVISED MODEL

FIG F5

COMPARISON OF CALCULATED PITCHING MOMENT -- WITH EXPERIMENTAL VALUES

CONSTANT POWER

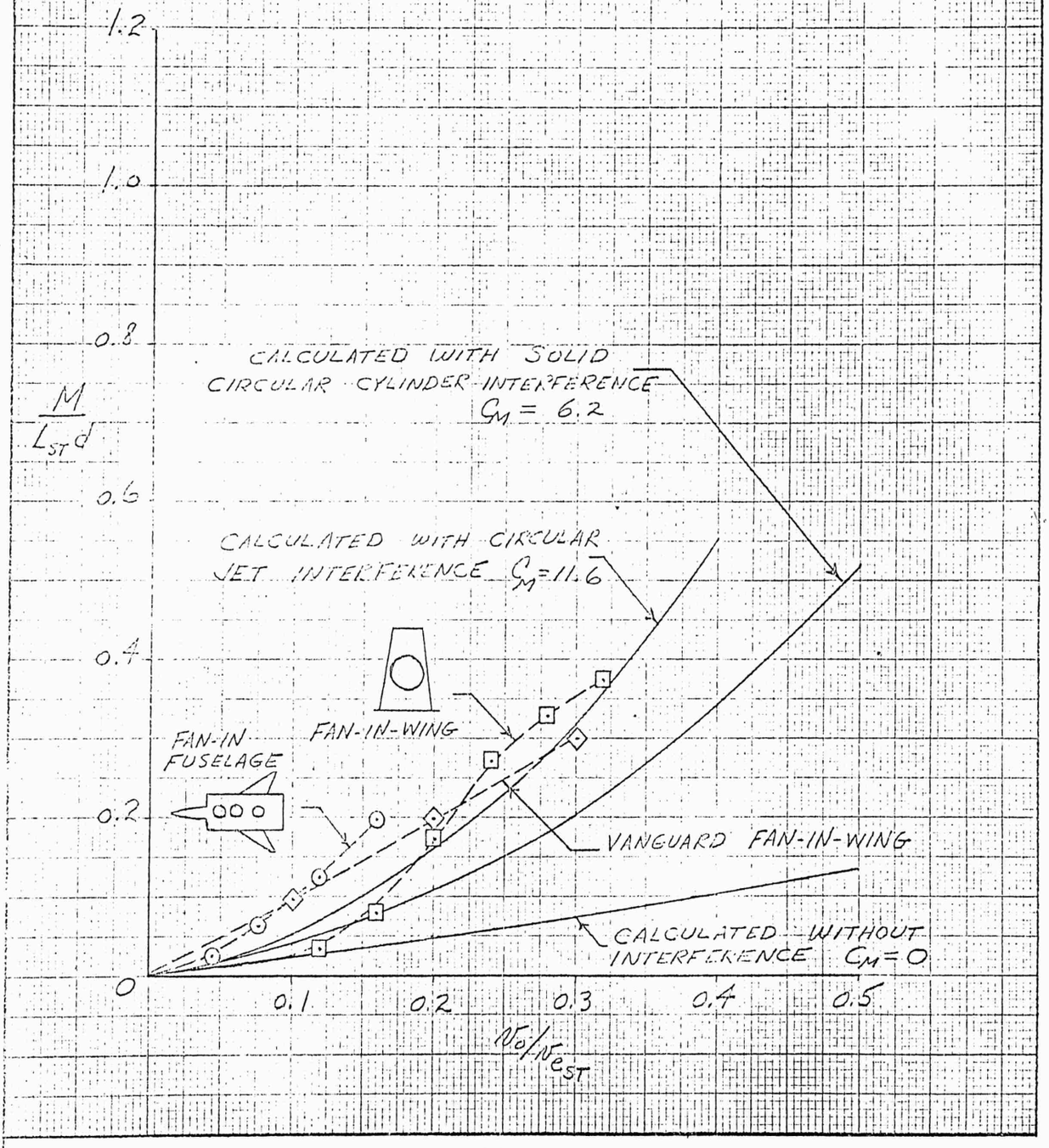

E-1-10A
REV. 2/60

SECTION G

DESIGN OF DEFLECTION VANES

The design of a grid of turning vanes constitutes a part of the general VTO problem. In particular, it is understood that it is entirely undesirable to expose a propeller or fan to a flow at an angle with the axis even for a short period. A system of baffles or turning vanes may, therefore, be required in any practical solution of the VTO problem. We shall not, in the present paper, specify when or where such a baffle system is or may be required but merely give the design information required for the proper solution. The proper use of deflection vanes is taken up in Section I.

The basic conformal transformation for cascades has been known for some time. (See Ref. G1.) We shall in the following give the direct routine method for the solution of any given case based on methods given in Ref. G1.

In Figure G1 is shown a set of turning vanes. Inlet velocity is w_1 at an angle shown as α_1 and an outlet velocity w_2 at an angle α_2. In general, it is desirable to provide at least a small acceleration of the flow through the vanes, which means that w_2 is to be a little greater than w_1 or the angle α_1 is to be a little larger than α_2. This also means that there is a small overpressure on the upstream side of the grid. In fact

$$p_1 - p_2 = \tfrac{1}{2}\rho\left(w_2^2 - w_1^2\right)$$

This may also be written

$$p_1 - p_2 = \tfrac{1}{2}\rho\left(w_{2t}^2 - w_{1t}^2\right) \qquad (1)$$

where w_{2t} is the tangential component of w_2 and w_{1t} is the tangential component of w_1. (See Figure G2.) The resulting pressure force as can be seen is <u>normal</u> to the grid. The force <u>along</u> the grid axis is further

$$\rho w_n\left(w_{2t} - w_{1t}\right) \qquad (2)$$

where w_n is the velocity perpendicular to the grid axis and common to inlet and outlet.

The right-hand section of expression (1) can be written:

$$\tfrac{1}{2}\rho\left(w_{2t} - w_{1t}\right)\left(w_{2t} + w_{1t}\right)$$

The geometric addition of the forces (1) and (2) therefore is:

$$\rho(w_{2t} - w_{1t})\left[W_n + \frac{w_{2t} + w_{1t}}{2}\right]$$

From Figure G2 it may, however, be seen that the bracket expresses the mean value of the velocities w_1 and w_2. Let the vector

$$W_m = \frac{W_1 + W_2}{2}$$

Then the force on the grid for a single element of width t and unit length is

$$F = \rho t \left(w_{2t} - w_{1t}\right) W_m \qquad (3)$$

This force is seen to be perpendicular to the mean or average velocity w_m as shown in Figure G2.

It is interesting to note that the circulation Γ can be read off Figure G1 as

$$\Gamma = \left(w_{2t} - w_{1t}\right) t \qquad (4)$$

This is true since the elements cancel everywhere except at plus or minus infinity. Note that the force F in Figure G2 points downward. Hence a counter clockwise circulation Γ.

Thus, finally $P = \rho \Gamma W_m$

$$P = \rho \Gamma W_m \text{ and } P \perp W_m \qquad (5)$$

with $$w_m = \frac{w_1 + w_2}{2}$$

It is at this point interesting to make the remark that this result is true regardless of the shape of the grid elements. Since the force is perpendicular to the mean velocity the center of gravity of the vortex system is located behind the semichord of the elements in Figure G1. However, the exact location is not of importance as is the case for a single wing or wing section.

It is desirable to know the value of the lift coefficient C_L since experience shows that excessive values are not allowable. We may write:

$$P = C_L \frac{1}{2} \rho w_m^2 l \qquad (6)$$

where l is the chord of the element (Figure G1). In contrast to the expression (5) which is an exact expression regardless of the shape of the element, the value of C_L as defined by Equation (6) is strictly accurate only for small deflections and infinitely thin elements.

In Figure G2 it is seen that the value w_m is very much smaller than the velocities w_1 and w_2. In actual practise the value of w_m would be made slightly greater than w_1 and smaller than w_2 to provide continuous acceleration through the channel. The expression (6) where C_L is based on w_m^2 would, therefore, give the wrong impression of the realistic value of C_L. Since nevertheless we shall,

for convenience, adopt the use of Equation (6) we shall remember that the real value of C_L is very much lower for large angles of deflection. In fact, the velocity in the representative point may be defined as

$$W_R = \frac{|W_1| + |W_2|}{2}$$

and one may write with the realistic value of C_L

$$P = C_{L_R} \frac{1}{2} \rho \left[\frac{|W_1| + |W_2|}{2} \right]^2 \ell \qquad (7)$$

where $|w_1|$ and $|w_2|$ represents the numerical values of the vectors w_1 and w_2.

Consequently, the "realistic" value of the lift coefficient is in terms of the fictional value

$$C_{L_R} = C_L \left[\frac{W_1 + W_2}{|W_1| + |W_2|} \right]^2 \qquad (8)$$

The ratio of the real C_L to the fictional value is thus given by the square of ratio of the geometric sum of the vectors w_1 and w_2 to the square of the arithmetic sum of same: Since the angles α_1 and α_2 in the cases of importance in VTO design are of approximately the same value, we shall employ the mean or average value α_m. We have then approximately

$$C_{L_R} = C_L \cos^2\left(\frac{\pi}{2} - \alpha_m\right)$$

where thus $\left(\frac{\pi}{2} - \alpha_m\right)$ is one half of the total deflection angle. In the two cases shown in the following the deflection angles are 27° and 55° and the "real" values of C_L are therefore lower than the given artificial values by factors $\cos^2 13.5^\circ$ and $\cos^2 27.5^\circ$ or 0.94 and 0.79, respectively. In the second case shown there is an indicated value of $C_L = 1.04$, the "realistic" value with uniformily contracting channels is therefore only

$$C_L = 1.04 \cdot 0.79 = 0.82$$

Reverting to the artificially defined value of C_L (Equation (6)) and using Equation (5) one has the relation for C_L (without correction)

$$C_L = 2 \frac{\tau}{\ell} \cdot \frac{W_{2t} - W_{1t}}{W_m}$$

EXAMPLES

As experimental checking is proposed, we shall show two examples obtained by routine method from Reference G1. Figure G3 shows a grid for a total deflection of 27°. The angles with the normal are chosen to be 10° on the inlet side and 17° on the outlet side. The spacing t is taken as 30 m/m and the projection of the chord $\ell = 40$ m/m. We are performing the routine calculation for circular

arc profiles. The values of w_m, w_{2t}, and w_{1t} may now be immediately taken from a graph similar to that of Figure G2 and we have for C_L

$$C_L = \frac{t}{\ell} \cdot \frac{2(w_{2t}-w_{1t})}{w_m} = 0.72$$

The only other value required is the radius of curvature of the circular arc section. This is obtained by using Figure G4 which is based directly on a routine method given in Reference G1.

One has only need for two quantities. One is the mean deflection angle

$$\beta_m = \frac{\sigma_1 + \sigma_2}{2} = \frac{-10^\circ + 17^\circ}{2} = 3.5^\circ$$

The second is a factor μ which contains all the complications of the theory but which may be given in a single chart, Figure G5, taken from Reference G1. With $\beta_m = 3.5^\circ$ and $\frac{t}{\ell} = 0.75$ one gets directly from this graph $\mu = 0.675$. This value is now used to find the angle "exaggeration" up stream and down stream by the following scheme (see Figure G4)

$$\beta_a - \beta_m = \frac{1}{\mu}(\sigma_2 - \beta_m) = \frac{1}{0.675}(17^\circ - 3.5^\circ) = 20^\circ$$

$$\beta_m - \beta_e = \frac{1}{\mu}(\beta_m - \sigma_1) = \frac{1}{0.675}(3.5^\circ + 10^\circ) = 20^\circ$$

Thus

$$\beta_e = -16.5^\circ \quad \text{and} \quad \beta_a = 23.5^\circ$$

The mean radius of curvature is, therefore, (see Figure G3)

$$R_m = \frac{\ell}{2} \frac{1}{\sin 20^\circ} = 58.5 \text{ m/m}$$

This is the value for the radius of curvature of a skeleton circular arc element. In reality the channel will be designed for a gradual increase in the velocity, thus being slightly thicker in the middle section. The total deflection designed for 27° will be somewhat smaller as a result of the effect of a boundary layer on the upper rear surface. The projected value of $C_L = 0.72$ (to be corrected by a factor of 0.94 as above) will be somewhat decreased in an actual experiment.

Finally, a second example has been worked through also based on the routine method of Reference G1. The total deflection is here 55° (see Figure G6). The projected chord length is again 40 m/m and the spacing is chosen as 20 m/m. Repeating the same calculations the results obtained are shown in this figure. The resulting radius of curvature is 33.6 m/m. Experiments will be proposed to confirm the accuracy of the calculations and to obtain knowledge of the optimum efficiency possible by refinement in the design procedure.

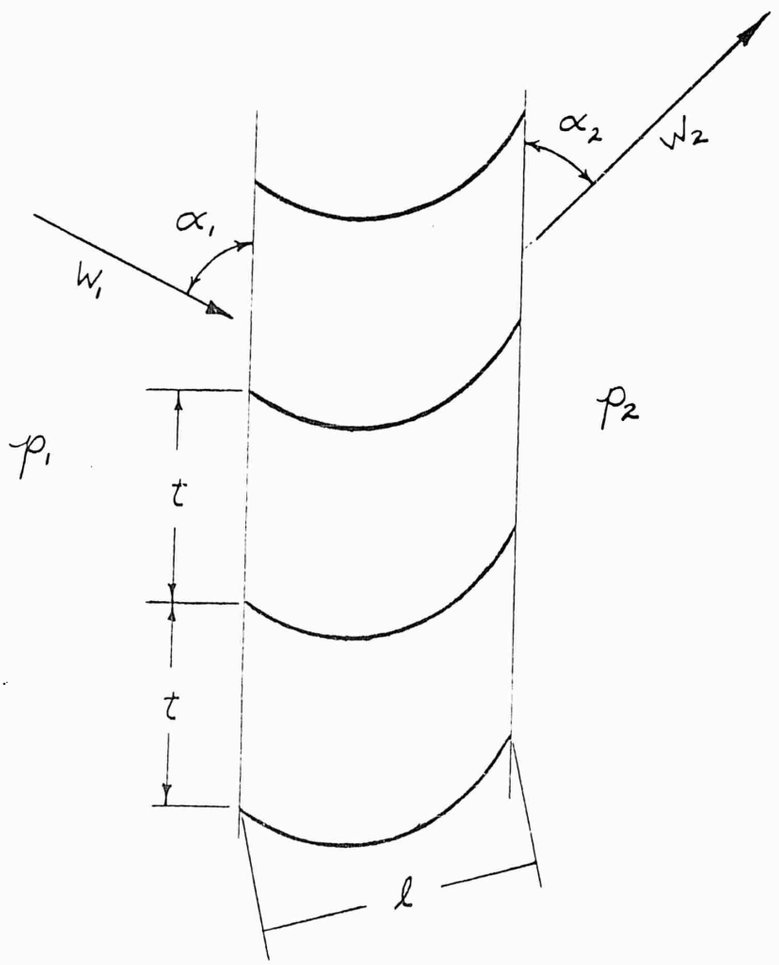

FIG. G1

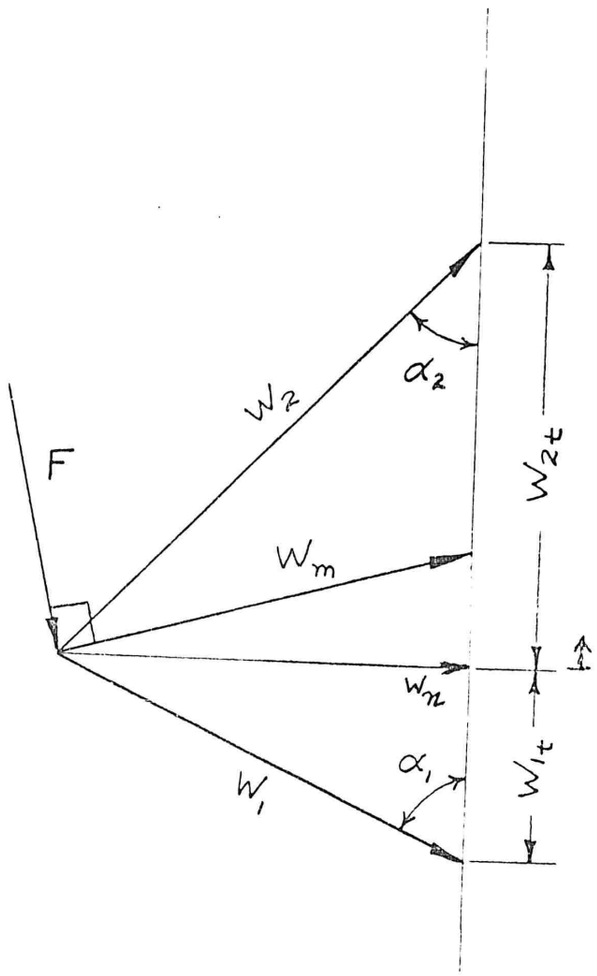

FIG. 62

FIG. 63

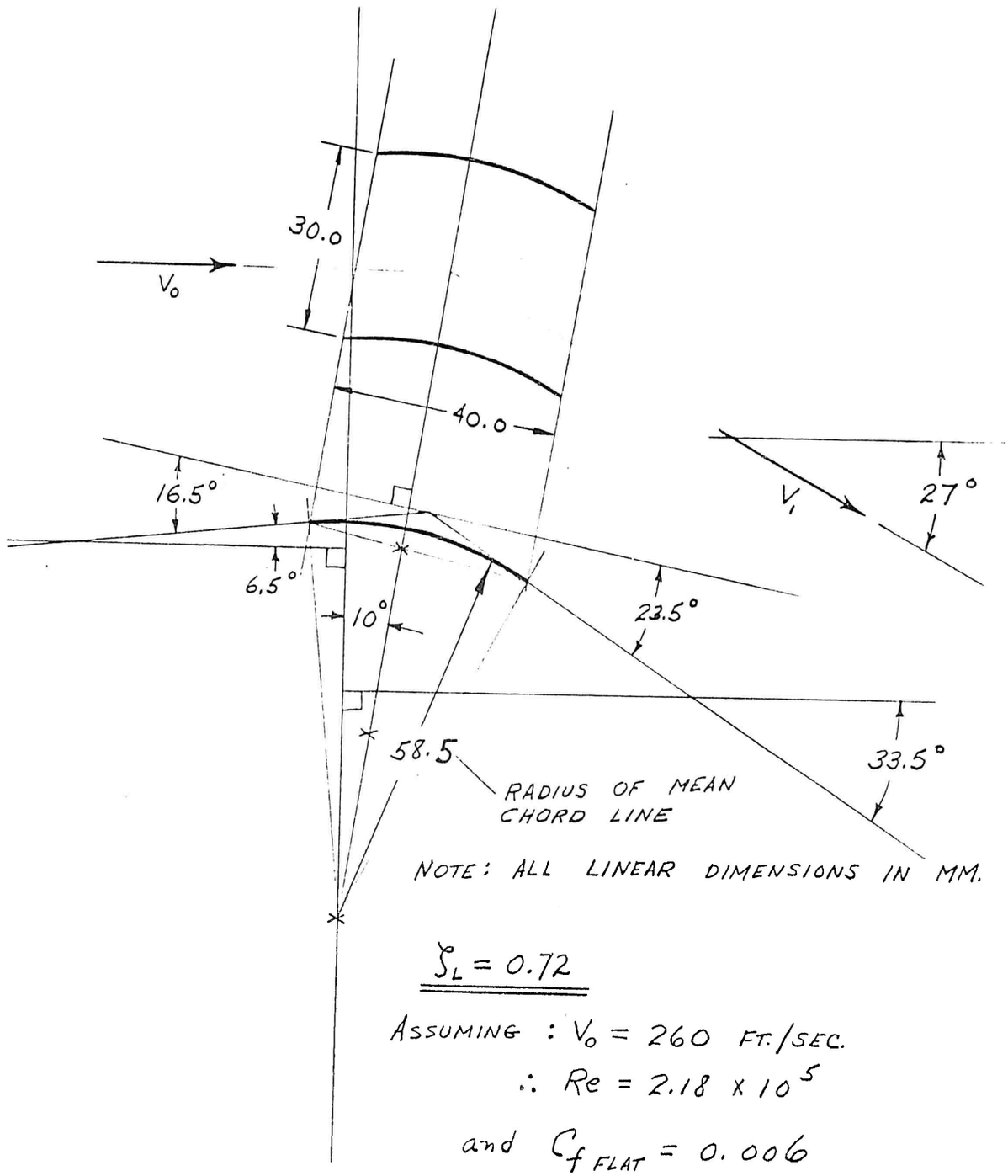

$\zeta_L = 0.72$

ASSUMING : $V_0 = 260$ FT./SEC.

$\therefore Re = 2.18 \times 10^5$

and $C_{f\ \text{FLAT PLATE}} = 0.006$

$$\eta = 1 - C_f \frac{c}{t} = 0.992$$

FIG. 64

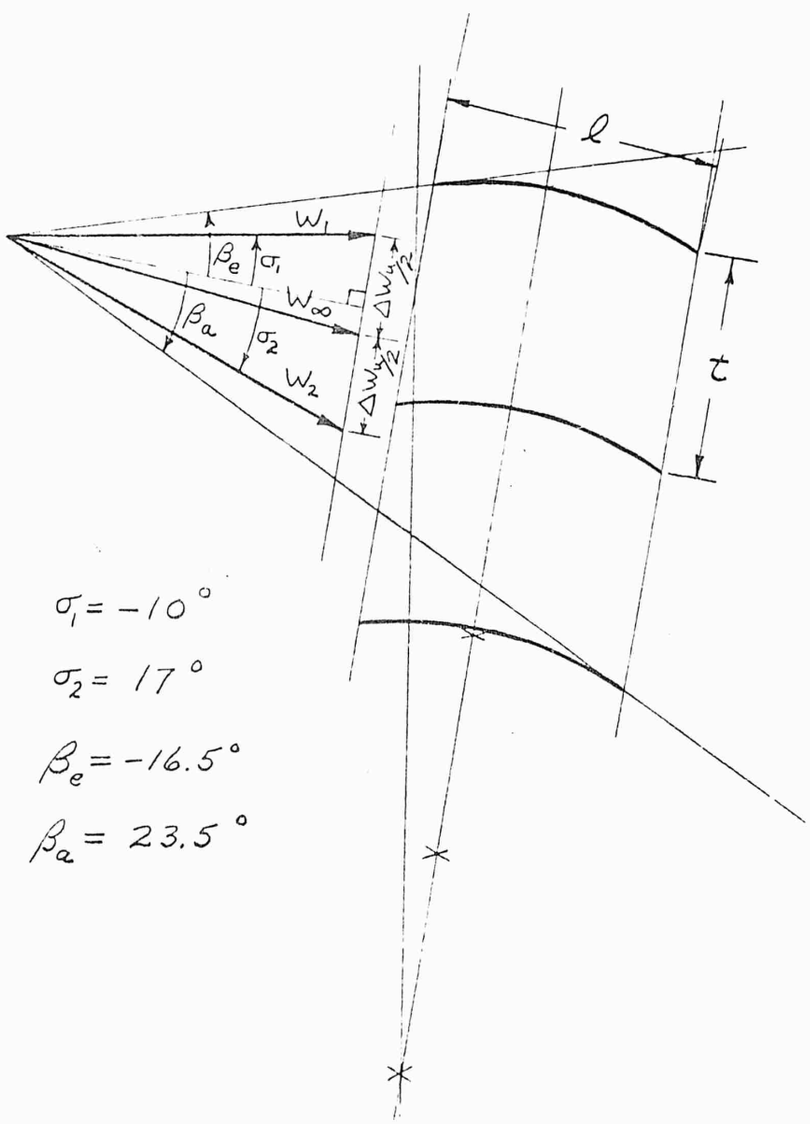

$\sigma_1 = -10^\circ$

$\sigma_2 = 17^\circ$

$\beta_e = -16.5^\circ$

$\beta_a = 23.5^\circ$

PREPARED JRS 1-12-60 PAGE

CHECKED REPORT NO

REVISED MODEL

REPUBLIC AVIATION

FIG G5

INVERSE OF RELATIVE ANGLE EXAGGERATION μ AS A FUNCTION OF MEAN DEFLECTION ANGLE β_m AND PITCH/CHORD RATIO t/ℓ

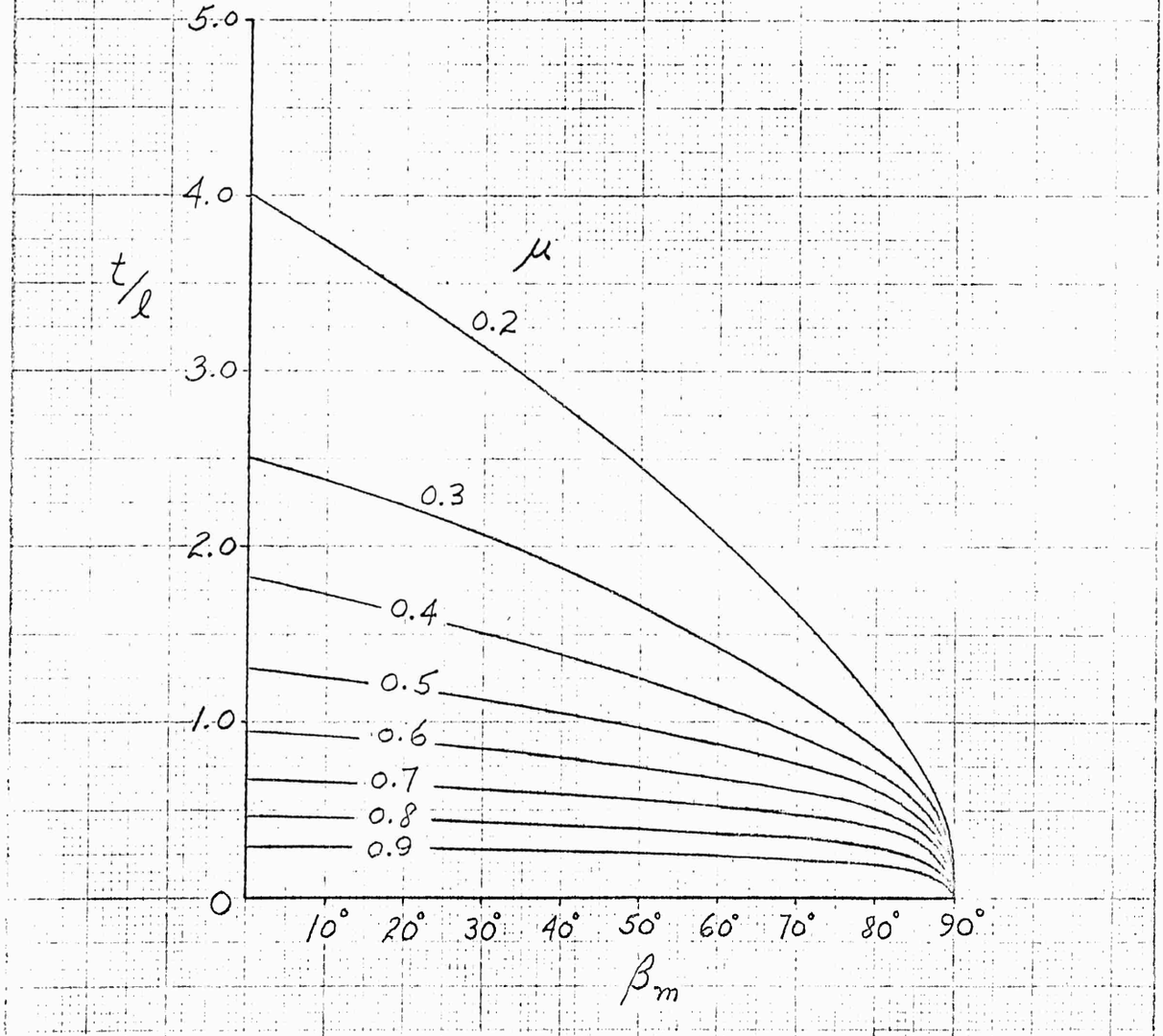

Fig. G6

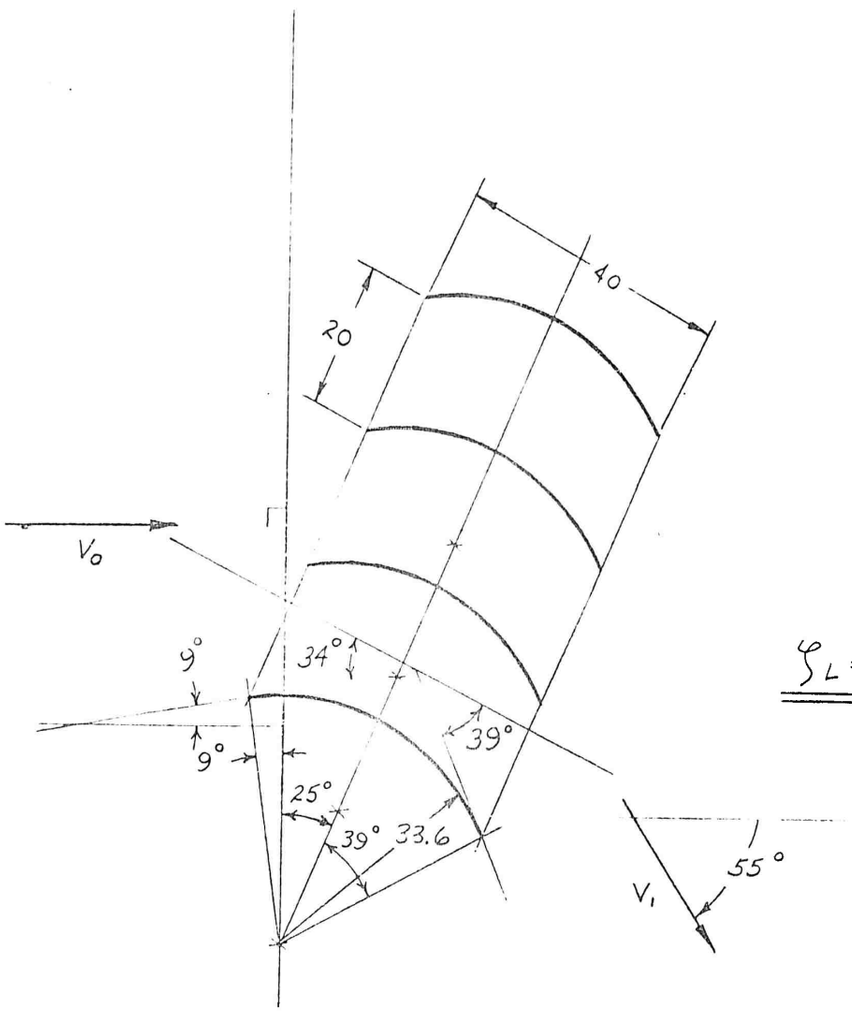

$\varphi_L = 1.04$

SCALE : 1 : 1

(LINEAR DIMENSIONS IN MM.)

SECTION H

Report No.61/7

Experimental

Investigation of a cascade of circular arc sections with and without a downstream channel

[Project No. 6-C 3338 - 548722 of Republic Aviation Corporation, Farmingdale, New York, U.S.A., Jan. 18, 1961]

Summary:

A cascade of circular arc sections, which shall serve as a deflection grid in a 55°-bend, was investigated by the wake traversing method. Measurements were taken with and without a channel downstream of the cascade.

It was found that, though the measured discharge angle fitted very well with theory, the losses were rather high. They still increased when a channel was installed behind the cascade. The reason is that separation occurred at the lower surfaces (pressure sides) of the blades. When using a downstream channel, the inlet air angle of the cascade decreased and separation increased.

List of contents:

Institute of Fluid Mechanics of the Technical University Braunschweig

The Director:

H. Schlichting

(Prof.Dr.H.Schlichting)

The Author:

A. Klein

(Dipl.-Ing.A.Klein)

1) Introduction

Deflection vanes are commonly used in bent channels to avoid wall separation and thus to reduce total head losses. For reasons of convenience, often blades of circular arc sections are used. This report presents measurements with a cascade consisting of such blades which is to be used in a 55°-bend. The geometry of the cascade had been determined theoretically. With the aid of the wake traversing method the total head losses were measured, the discharge angle and the static pressure drop across the cascade were checked, and this both with and without a channel behind the cascade.

2) Symbols (see figure H2)

b	blade span (= 300 mm)
c	blade chord (= 40 mm)
d	distance between blades (= 20 mm)
r	radius of camber line of the circular arc sections
x	axis in chordwise direction
y	axis perpendicular to chordwise direction
p_o	total head
p	static pressure
q	dynamic head
w	flow velocity
$R = \frac{\varrho \cdot w \cdot c}{\mu}$	Reynolds number
c_D	drag coefficient of blade
c_f	drag coefficient of flat plate
$\zeta = \frac{p_{o1}-p_{o2}}{q_1}$	loss coefficient of cascade
β	angle between flow direction and a perpendicular to the cascade axis
γ	stagger angle, angle between cascade axis and a perpendicular to the chord
ϱ	density of the air
μ	dynamic viscosity of the air
$\eta = 1-\zeta$	efficiency of the cascade

Subscripts

1	upstream of blade row
2	downstream of blade row
loc	local value

3) Method of test

The investigation was carried out with the small cascade tunnel of the Institute of Fluid Mechanics of the Technical University Braunschweig (director: Professor Dr. H. Schlichting). A view of this facility is given in Fig.H1. The inlet air angle could be varied by turning the big disk to which the cascade was fixed.

The geometry of the cascade had been determined theoretically with the aid of potential flow theory. It is shown in Fig.H2. The blades had circular arc shape and consisted of metal with a thickness of 1,5 mm, the radius of the camber line being r=33,6mm. The leading edges were rounded and the trailing edges sharpened thoroughly to get good airfoil sections. The blades were set with a stagger angle of $\gamma = 2{,}5^{\circ}$. The total deflection of the cascade was to be 55°, thus the inlet air angle was $\beta_1 = 25^{\circ}$, whereas the discharge angle was expected to be $\beta_2 = 30^{\circ}$. Both the inlet and discharge directions formed an angle of 9° with the tangents to the camber line at the leading and trailing edges (see Figure H2). The chord length was c = 40 mm, the distance between the blades d = 20 mm, thus the solidity d/c = 0,5. The cascade consisted of 20 vanes. The blade span was b = 300 mm. Test was performed with an entering velocity of $w_1 = 55$ m/s corresponding to a Reynolds number of $R_1 = 145\,000$.

The probe used was a conical one of small dimensions. It allowed simultaneous measurement of total head, static pressure and flow direction. A photograph of the cascade and the probe is shown in Fig.H3.

First of all the cascade was investigated alone. It was set with the design inlet angle of $\beta_1 = 25^{\circ}$. The total head loss and the discharge angle were measured behind the central blade at a

probe's distance of one chord downstream of the trailing edge at midspan position. They were taken as the mean values over one spacing of the blades.

After this a channel of 345 mm height and a length of its center line of 1,4 m (see Figure H2) was installed downstream of the cascade such as to have a bend with a total deflection of 55°. Measurements were taken at a distance from the trailing edge of $x/l = 6,0$ in the middle of the channel over three spacings. They revealed the amazing fact, that the losses were twice as high as without the channel. The measurements were repeated at $x/l = 1,0$ to have a better possibility of comparing with the data without channel. Total head loss was only reduced slightly. The channel was removed again, and a new test was run at a lower Reynolds number of $R_1 = 75\,000$, since it was presumed that the Reynolds number had been near its critical value with the tests before, and thus a slight change in flow pattern caused by the channel might have led to laminar separation of the upper surfaces (suction sides). No particular rise of the losses was found, however. Bad directional setting of the channel could not be the reason for the high losses either, since it had been done carefully and since the cascade's discharge angle fitted very well with the channel's direction.

An answer to the question could only be found by measuring at different inlet angles, i.e. by determining the cascade's polar curve. Thus additional tests were run with the isolated cascade at $\beta_1 = 15°$, $20°$, $30°$ and $35°$.

4) Discussion of results

The discharge angle fitted very well with theory, it was found to be $\beta_2 = 29,5°$, i.e. only half a degree less than was to be expected according to potential flow theory.

The total head losses are presented in Table H1. The distribution of the local loss coefficient

$$\zeta_{loc} = \frac{(p_{o1}-p_{o2})_{loc}}{q_1} \qquad (1)$$

with channel, as measured six chords behind the grid, is shown in FigH4 over three spacings. The wake of the central blade as measured one chord downstream of the cascade is shown in FigH5.

As can be seen, the losses are $\zeta = 0,185$ when using the downstream channel, but only $\zeta = 0,092$ without it. In the first case, losses reduce slightly to $\zeta = 0,166$ when measuring only one chord behind the blade's trailing edge instead of six chords. In the second case, losses increase slightly from $\zeta = 0,092$ to $\zeta = 0,103$ when lowering Reynolds number from $R_1 = 145\,000$ to $R_1 = 75\,000$. Because of the latter result, separation at the upper surface cannot be an explanation for the considerable difference between the losses of the cascade without and with the channel.

Variation of the inlet air angle showed that the reason for the high loss is a lower surface (pressure side) stall. This can be seen very well from FigH5, which shows the wakes at different inlet angles β_1. The pressure sides of the wakes get larger with decreasing inlet angle, the losses thus increase.

A better understanding of the underlying flow mechanism yields the polar curve of FigH6. The total head loss with channel corresponds to the loss of a cascade without channel that has a $7,3^\circ$ smaller inlet angle, namely $\beta_1 = 17,7^\circ$. Obviously installing a channel behind the cascade causes rather a severe change of its inlet angle. Thus the idea that a channel downstream of a cascade does not change the flow conditions in front of the cascade, if only the channel slopes back with its discharge angle does not appear to be correct. Maybe it is with blades of much larger chord. But in the present case one must adopt another concept, namely, first of all, imagine a bent channel without any grid. The streamlines then will be curved in some particular way. When inserting a cascade, this will experience a different inlet air angle than if it were isolated, according to the already existing curvature of the streamlines. Thus the change of the grid's inlet angle, when using a downstream channel, seems to be quite reasonable. This fact may or may not change the loss across the cascade, depending on its geometry. In the present

case it led to a big change, since the inlet conditions of the grid were bad already at the design angle of $\beta_1 = 25^0$. Namely, the polar curve (Fig.H6) shows that the blades' lower surfaces were stalled already then. The reason for this is the fact that the flow direction forms an angle of 9^0 with the tangent to the camber line at the leading edge (see Fig.H2), thus the stagnation point being located at the blade's upper surface. Even a small decrease of inlet angle will lead to a considerable increase in total head loss then.

Fig.H6 shows also that the cascade works rather far away from its optimum configuration which exists with an inlet angle of $\beta_1 = 32^0$ instead of $\beta_1 = 25^0$. The loss coefficient then is only $\zeta = 0{,}045$ instead of $\zeta = 0{,}092$. It does not appear to be very favourable, however, to have the isolated grid work at its optimum inlet angle. Namely, as was shown by the experiments, the set-up with the channel then would work at a smaller inlet angle, i.e. in a region of higher losses. Minimum loss with the channel configuration will probably be attained at inlet angles of the isolated grid that are 5^0 to 7^0 higher than its optimum angle, i.e. at about $\beta_1 = 38^0$.

Fig.H7 shows the efficiency of the cascade plotted versus the inlet angle. It is defined by

$$\eta = 1 - c_D \cdot \frac{c}{d} \quad . \tag{2}$$

In the case of a cascade with zero stagger (see Ref. H1)

$$\eta = 1 - \zeta \quad , \tag{3}$$

where

$$\zeta = \frac{p_{o1} - p_{o2}}{q_1} \quad . \tag{4}$$

The graph of Fig.H7 was calculated with equ.(3) since the stagger of only $\gamma = 2{,}5^0$ can be neglected.

Fig.H7 shows also the efficiency of a cascade of flat plates with zero deflection and when separation is not taken into account. It was found by introducing

$$c_D = c_f = 0{,}0066 \quad ,$$

the value for turbulent flow at a Reynolds number of $R_1 = 150\,000$. The flat plate efficiency is

$$\eta_{\substack{\text{flat}\\\text{plate}}} = 0{,}987 \quad ,$$

whereas the cascade's optimum efficiency is $\underline{\eta = 0{,}955}$, and that one at the design inlet angle is only

$$\underline{\eta = 0{,}903}$$

without a channel behind the cascade.

Suggestions for improvement

It is of no use, however, to increase the cascade's inlet angle since the total deflection would be greater than 55° in that case. Improvement can only be obtained by changing the cascade's geometry. The trailing edge geometry should be kept the same because the discharge angle fitted well with theory. But the leading edge geometry should be altered such that the flow direction and the tangent to the camber line do not form an angle of $+9^\circ$ as they do with the present configuration, but an angle of -5° to -7°. The set-up with the channel will work then just at the cascade's optimum.

5) Conclusions

The loss coefficient of a cascade of circular arc airfoils was investigated experimentally with and without a channel downstream of the cascade. The turning angle was checked. It was found that the discharge angle compared very well with potential flow theory. But the losses were rather high since the cascade did not work at its optimum configuration. The set-up with the channel yielded even higher losses since the inlet air angle of the cascade was shifted by the channel in an unfavourable way.

The geometry of the cascade should be altered by leaving the trailing edge configuration, but diminishing the camber such as

to have an angle of -5° to -7° between the flow direction and the tangent to the camber line at the leading edge, instead of $+9^{\circ}$ as with the present vanes.

List of figures and tables

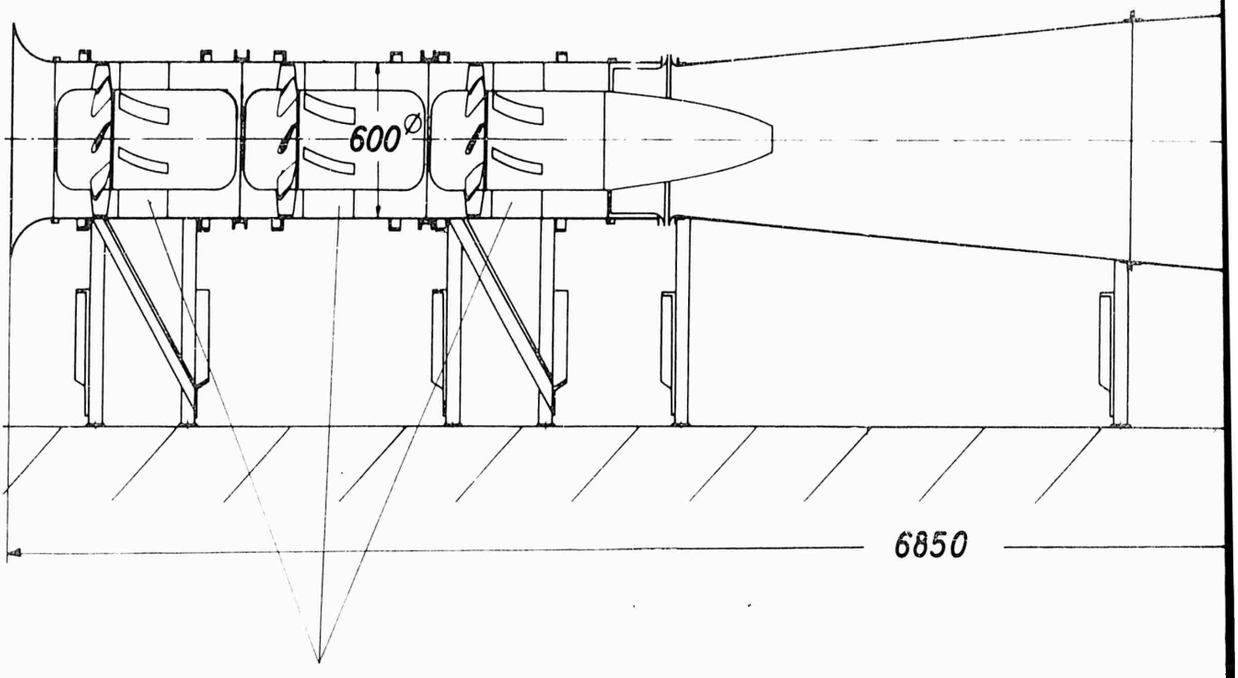

3 Fans

Dif

1

Institut für Strömungsmechanik T.H. Braunschweig	Small cascade tunnel	Blatt Nr. 9
		Fig. 1

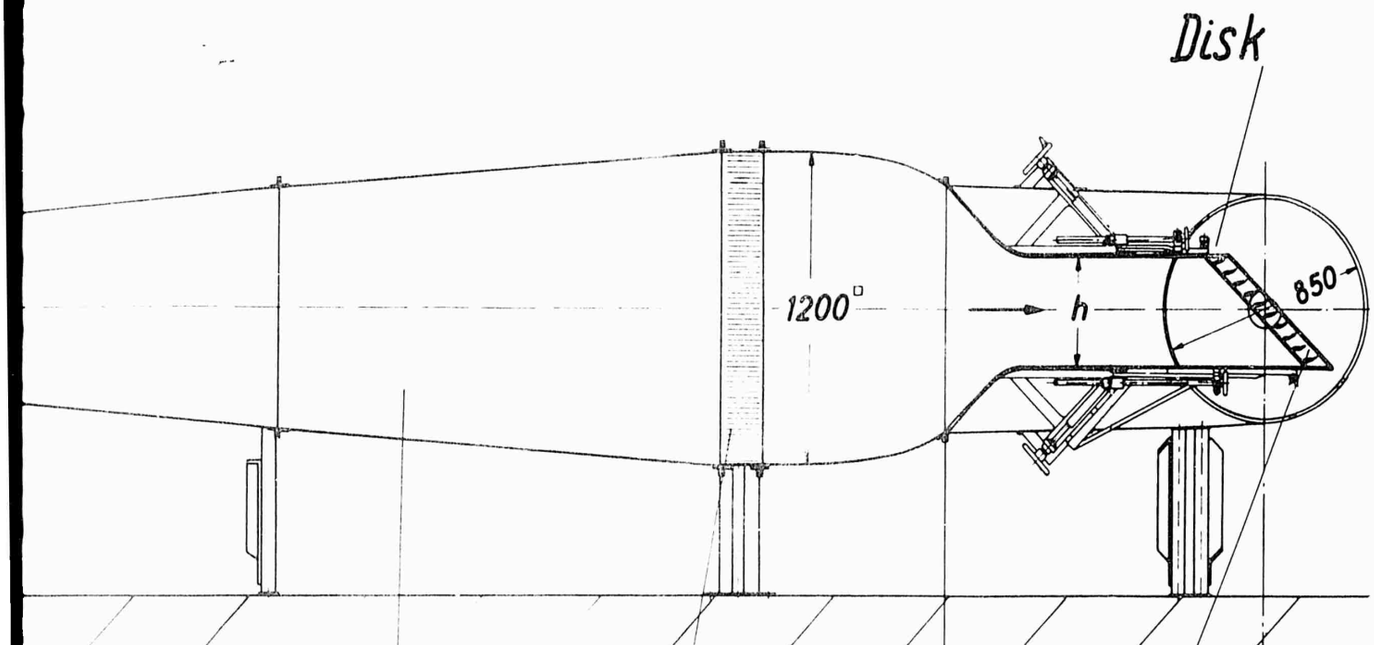

Diffuser Honeycomb Cascade

2

Bearbeitet: Klein	Datum: 15.3.61	Skizzenblatt Nr.:	Bericht Nr.: 61/7

Institut für Strömungsmechanik T.E. Braunschweig	Notations with the cascade and geometrical relations	Blatt Nr. 10
		Fig. H2

a) Geometry of cascade:

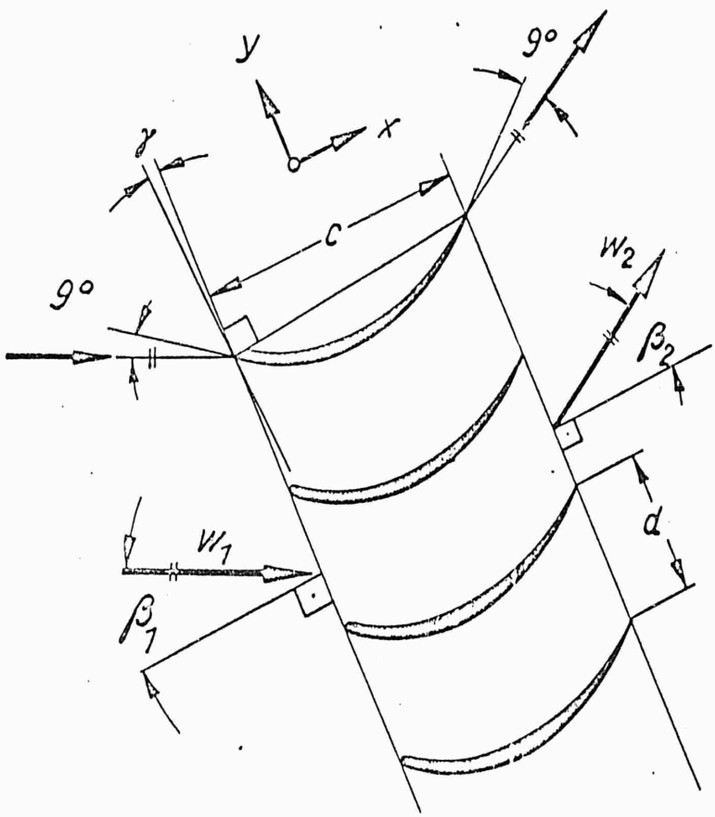

Profile of Blades:

Circular arc section with a thickness of 1,5 mm and a radius of r = 33,6 mm

$c = 40\ mm$
$d = 20\ mm$
$d/c = 0{,}5$
$\beta_1 = 25°$
$\beta_2 = 30°$
$\gamma = 2{,}5°$
$w_1 = 55\ m/s$
$R_1 = 145000$

b) Cascade with channel:

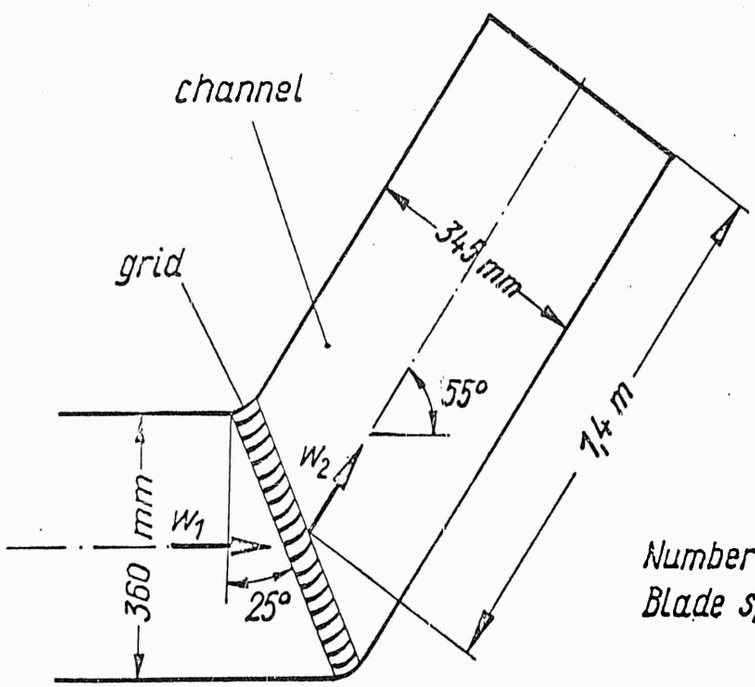

Number of Blades: 20
Blade span: b = 300 mm

Institut für Strömungsmechanik T. H. Braunschweig	Cascade and probe (photograph)	Blatt Nr. 11
		Fig. 3

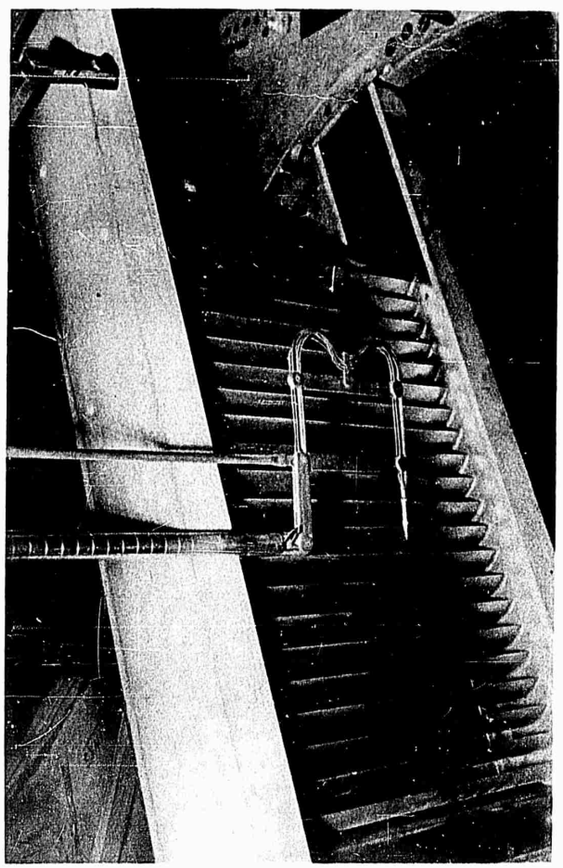

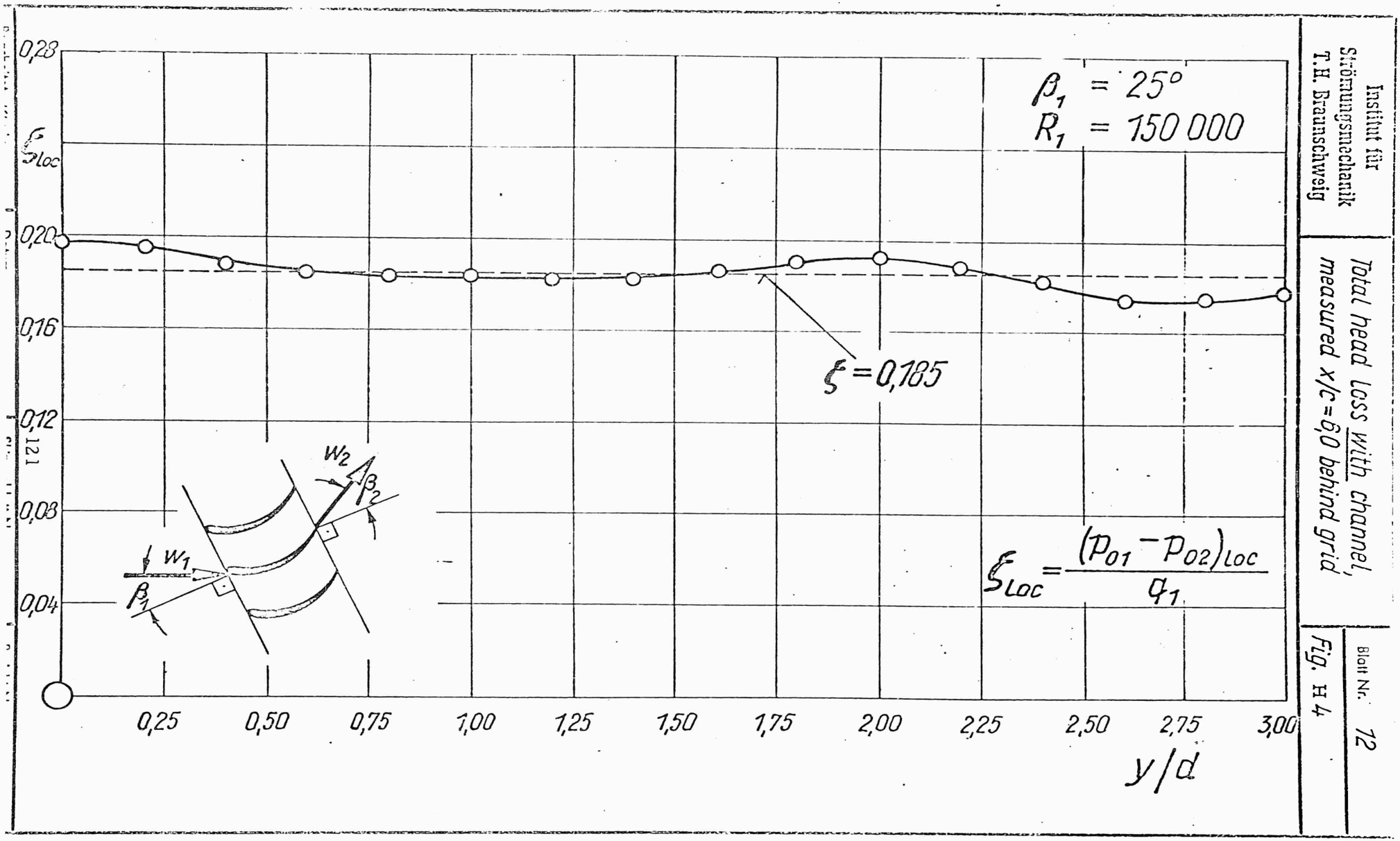

Institut für Strömungsmechanik T.H. Braunschweig

Total head loss with channel, measured x/c=6,0 behind grid

Blatt Nr. 72

Fig. H 4

Institut für Strömungsmechanik T.H. Braunschweig

Wake of central blade, measured x/c = 1,0 behind grid

Blatt Nr. 13

Fig. H 5

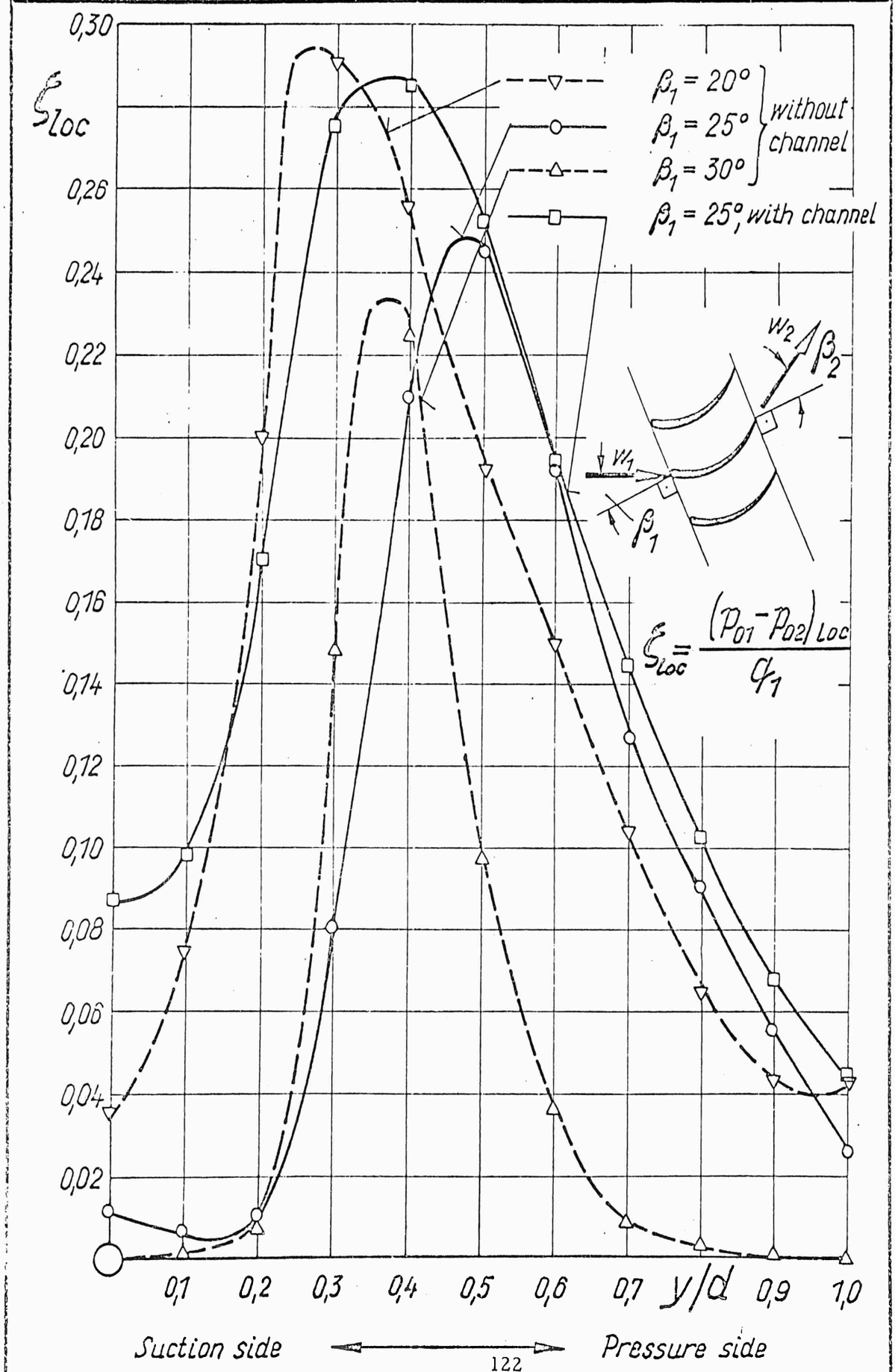

Institut für Strömungsmechanik T.H. Braunschweig	Polar curve of cascade without channel	Blatt Nr. 14
		Fig. H6

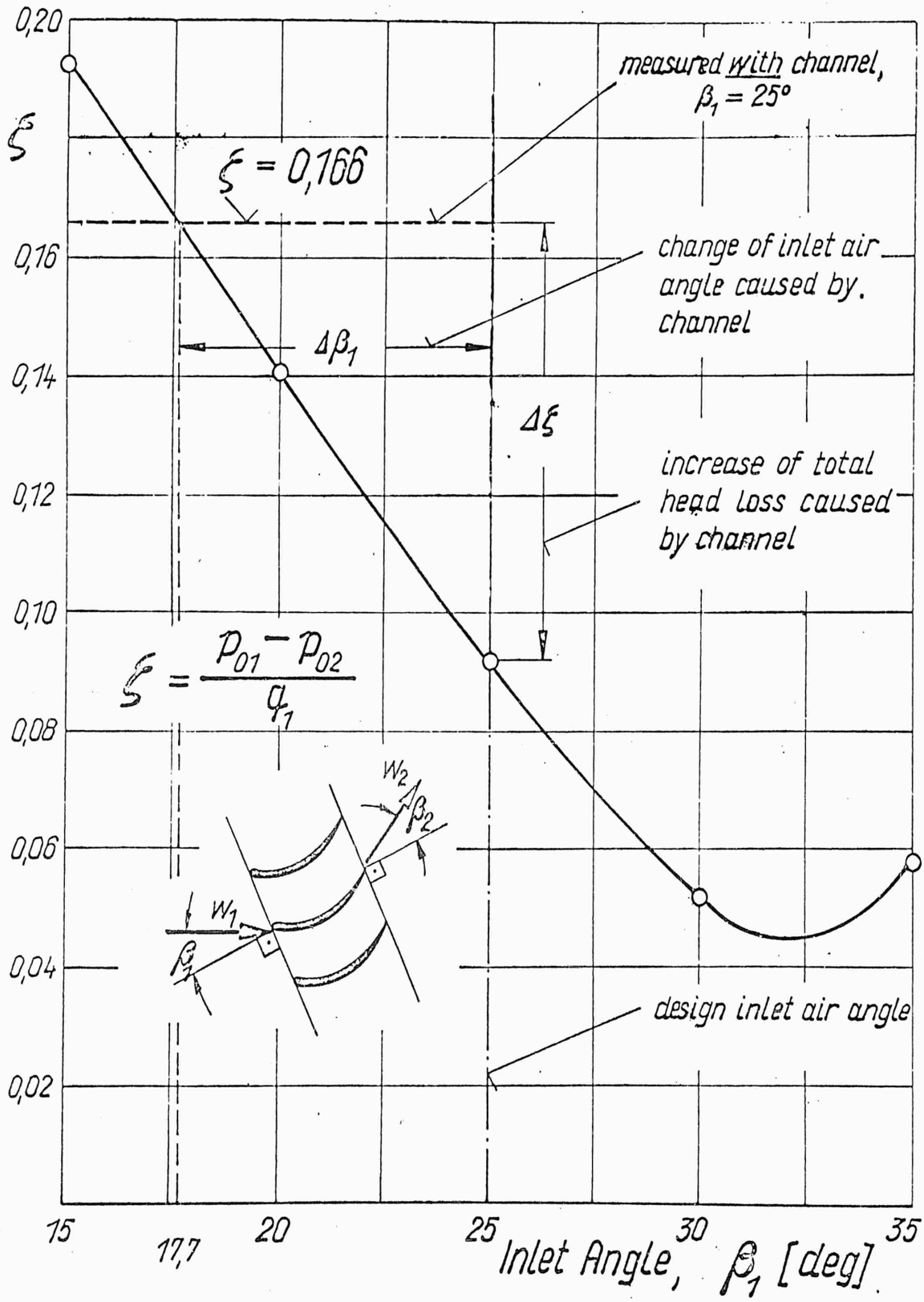

Institut für Strömungsmechanik T.H. Braunschweig	Efficiency of the cascade versus inlet air angle	Blatt Nr. 15
		Fig. H 7

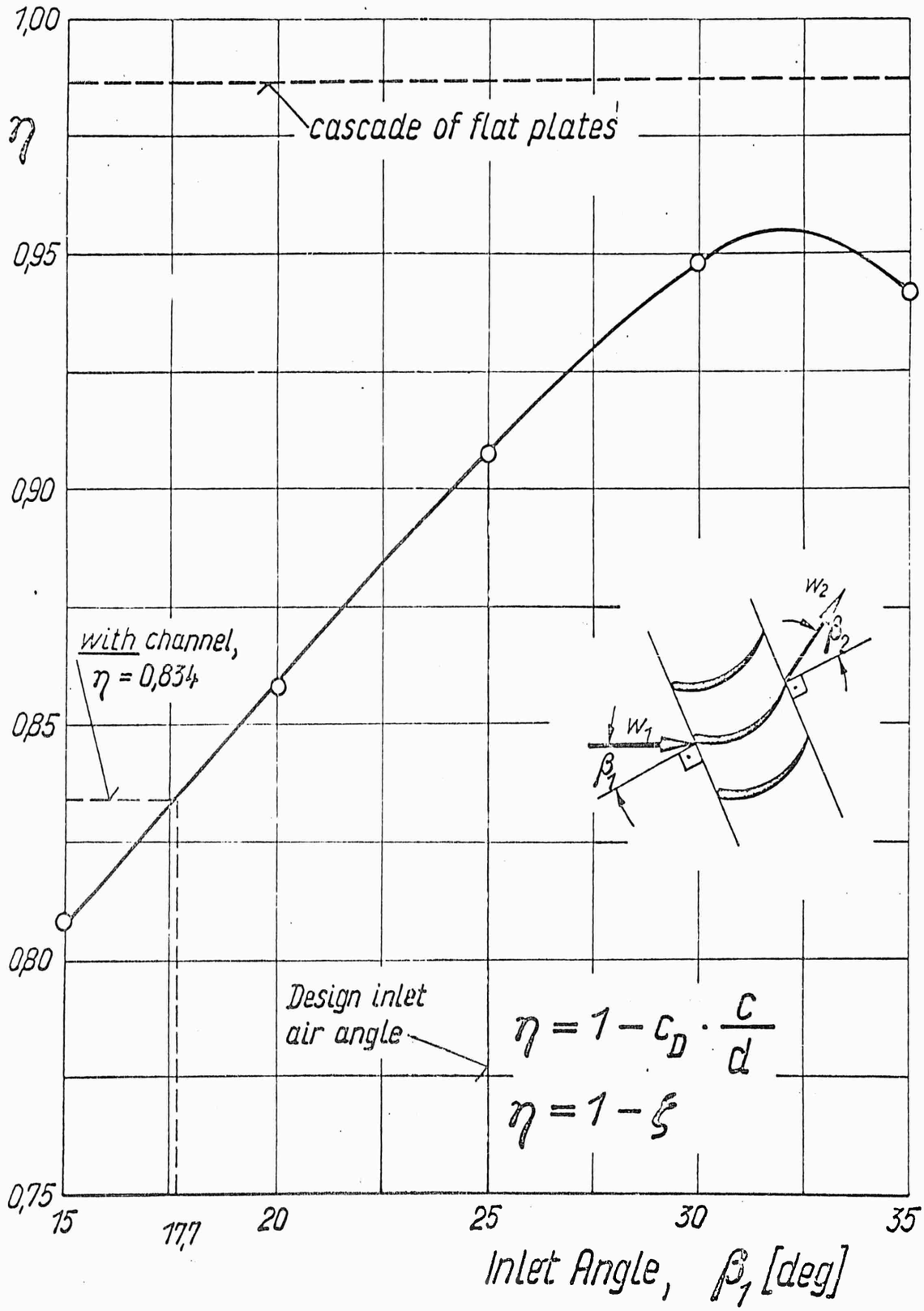

β_1 [deg]	without channel x/c = 1,0		with channel R_1 = 150 000	
	R_1	ζ	x/c	ζ
15	145 000	0,192	—	—
20	145 000	0,142	—	—
25	145 000	0,092	1,0	0,166
	75 000	0,103	6,0	0,185 *)
30	145 000	0,052	—	—
35	145 000	0,058	—	—

*) This value is the mean loss coefficient over three spacings, while all the others were obtained over one spacing only

$$R_1 = \frac{\varrho \cdot w_1 \cdot c}{\mu} \; ; \qquad \zeta = \frac{p_{01} - p_{02}}{q_1}$$

x/c: Distance of probe behind trailing edge in chordwise direction

SECTION I

COMMENTS ON CASCADE TEST RESULTS

The tests made by the "Institut für Strömungsmechanik" at Braunschweig, Germany are of great value to determine the optimum cascade for use in VTO. It is to be stated categorically that a propeller or fan, under no circumstances, should be exposed to a non-axial stream. Not only are the mechanical stresses excessive but also the efficiency of the propeller is drastically reduced under the very condition for which the highest efficiency is required. Propellers in ducts have been tested adequately for any and all purposes. Nevertheless, there is, of course, still need for ordinary model testing as basis for actual design and construction of VTOL airplanes, in particular to insure compatability of the propeller and duct.

With propeller-duct and ordinary airplane testing quite fully explored it was considered desirable to obtain design information on cascades as the only field not adequately explored. It was for this reason that the present test series was conducted.

The experimental cascade had been designed from exact theory (Section G of this volume). The test data revealed the interesting fact that the duct walls should have been eliminated. In other words, the cascade should have been tested as a free stream deflector or, if in a duct, the duct walls should have been streamlined. Fortunately, because of the extensive data, including wake surveys, it is quite simple to obtain the desired information on the efficiency of properly designed baffles. The actual result may be obtained as follows:

The channel on the inlet side which was present in all the tests forced a straightening of the flow (parallel to the walls) so that the flow enters the cascade near zero degrees instead of the theoretically prescribed 9° (see Figure H2 in Institute report). As the flow is prevented from entering at the proper angle it stalls on the pressure side. In fact, the highest efficiency is reached when the inlet angle β_1 = approximately 32° (see Figure H7) which gives an angle of attack of the air with the leading edge of the blades of only 2°. Notice the drastic reduction in the loss on the pressure side (Figure H5) at $\beta = 30^{\circ}$. The efficiency reached about 95% in spite of the fact that one has now a diverging channel. The cross section of the duct on the outlet side is proportional to $\cos 25^{\circ}$ and on the inlet side to $\cos 30^{\circ}$ or the ratio is $\frac{.866}{.94}$ which corresponds to more than 7% divergence instead of the originally intended convergence of 7% with the outlet angle at $\beta_2 = 30^{\circ}$ and the inlet at $\beta_1 = 25^{\circ}$ (in reverse order).

It is proper to expect the test conforming with the theoretically prescribed inlet and outlet angles to give proper condition for the suction side (Figure H5 curve for $\beta_1 = 25^\circ$ without outlet channel). Further, it is proper to use the curve for $\beta_1 = 30^\circ$ for the pressure side since this side is not too much affected by the divergence of the channel. We obtain thus, from Figure H5 by drawing an internal contour curve, a rather accurate measure as to the loss in the ideal case. This loss seems to be between 1/2 and 2/3 of that of the best case observed. As the lowest loss measured (in the diverging channel with $\beta_1 = 30^\circ$) was 4.5% the ideal loss is thus estimated as

$$\zeta = 2.25 - 3.\%$$

This compares with a skin friction loss of 1.3% as the absolute minimum.

We may, therefore, state in final conclusion that carefully designed baffles may reach an efficiency of 97 to 98%. Thus such elements may be used freely for any purpose of directing the flow in a VTO airplane. The incurred loss is much less than that caused by a non-axial inflow into a propeller.

It is of interest to note that Dr. Schlichting had given the value of 98% as the expected value for the efficiency in the initial discussion of the contract negotiations on the cascade tests at Göttingen.

REFERENCES

A1. "Theoretical Investigation of Ducted Propeller Aerodynamics" - Vols. I & II by Dr. Th. Theodorsen - August 10th, 1960 - U. S. Army Transportation Research Command - Contract No. DA 44-177-TC-606.

A2. "On the Vortex Theory of Screw Propellers" - by Goldstein - Proceedings of the Royal Society (London) A, 23.

A3. "Theory of Propellers" - by Dr. Th. Theodorsen - McGraw Hill Book Company - 1948.

D1. "Evaluation of Integrals for the Flow Field of Cylindrical Vortex Sheets" - by H. V. Waldinger - TM 60-512.

F1. "Experimental Investigation of the Pressure Distribution About a Yawed Circular Cylinder in the Critical Reynolds Number Range" - by W. J. Bursnall & L. K. Loftin, Jr. - NACA TN 2463 - September, 1951.

F2. "Theoretical Investigation of Ducted Propeller Aerodynamics" - by Dr. Th. Theodorsen - Vol. I - August 10th, 1960 - U. S. Army Transportation Research Command - Contract No. DA 44-177-TC-606.

F3. NASA Conference on V/STOL Aircraft - A Compilation of the Papers Presented - Langley Research Center - November, 1960.

G1. "Die Strömung Um Die Schaufeln Von Turbomaschinen" - by F. Weinig - Leipzig/Verlag Von Johann Ambrosius Barth, 1935.

H1. "Ueber die Theoretische Berechnung der Strömungsverluste Eines Ebenen Schaufelgitters" - by H. Schlichting & N. Scholz - Ing. Arch. Vol. XIX, 1951, P. 42-65.

DISTRIBUTION LIST

"Theoretical Investigation of Ducted Propeller Aerodynamics"
(VOL. III and IV)
Final Report
Prepared under Contract DA 44-177-TC-674

Commandant
U. S. Army Command & General Staff College
ATTN: Archives
Fort Leavenworth, Kansas (1)

Commandant
Army War College
ATTN: Library
Carlisle Barracks, Pennsylvania (1)

Commandant
U. S. Army Aviation School
ATTN: Combat Developments Office
Fort Rucker, Alabama (1)

President
U. S. Army Aviation Board
ATTN: ATBG-DG
Fort Rucker, Alabama (1)

Commanding General
United States Army Aviation Center
ATTN: Transportation Officer
Fort Rucker, Alabama (1)

Headquarters
U. S. Army Aviation Test Office
ATTN: FTZAT
Edwards Air Force Base, California (1)

Commander
Naval Air Test Center
ATTN: U. S. Army Liaison Officer (1)
ATTN: Technical Library (1)
Patuxent River, Maryland

Commanding General
U. S. Army Ordnance Missile Command
ATTN: ORDXM-T
Redstone Arsenal, Alabama (1)

Deputy President
The Ordnance Board
ATTN: Library
Aberdeen Proving Ground, Maryland (1)

Chief of Transportation
ATTN: TCDRD (2)
Department of the Army
Washington 25, D. C.

Commanding General
U. S. Army Transportation Materiel Command
ATTN: Deputy for Aviation (2)
ATTN: TCMC-APU (4)
P. O. Box 209, Main Station
St. Louis 66, Missouri

Commanding Officer
U. S. Army Transportation Research Command Liaison Office
Wright-Patterson Air Force Base, Ohio (1)

Commandant
U. S. Army Transportation School
ATTN: Adjutant
Fort Eustis, Virginia (2)

Commander
Aeronautical Systems Division
ATTN: WWRMPT
Air Force Systems Command
Wright-Patterson Air Force Base, Ohio (2)

Commanding Officer
U. S. Army Transportation Research Command
ATTN: Executive for Programs (1)
ATTN: DCO for Aviation (1)
ATTN: Aviation Directorate (4)
ATTN: Military Liaison & Advisory Office (4)
ATTN: Long Range Technical Forecast Office (1)
ATTN: Research Reference Center (10)
Fort Eustis, Virginia

Commanding General
Air Research and Development Command
ATTN: RDR-LA (1)
Andrews Air Force Base
Washington 25, D. C.

Director
Air University Library
ATTN: AUL-8680
Maxwell Air Force Base, Alabama (1)

Library
Technical Reports Section
U. S. Naval Postgraduate School
Monterey, California (1)

Commanding Officer and Director
David Taylor Model Basin
Aerodynamics Laboratory
Washington 7, D. C. (1)

Chief, Bureau of Naval Weapons
ATTN: RA-4 (1)
ATTN: RRSY-13 (1)
ATTN: RRSY-5 (1)
Department of the Navy
Washington 25, D. C.

Chief of Naval Research
Code 461, Maj. L. C. Robertson
Washington 25, D. C. (1)

* U. S. Army Standardization Group, U. K.
Box 65, U. S. Navy 100
FPO New York, New York (1)

Director
Operations Research Office
ATTN: Library
The Johns Hopkins University
6935 Arlington Road
Bethesda, Maryland (1)

National Aviation Facilities Experimental Center
ATTN: Library
Atlantic City, New Jersey (1)

National Aeronautics and Space Administration
ATTN: Bertram M. Mulcahy
Assistant Director of Technical Information
1520 H Street, N. W.
Washington 25, D. C. (1)

Librarian
Langley Research Center
National Aeronautics & Space Administration
Langley Field, Virginia (1)

Ames Research Center
National Aeronautics and Space Agency
ATTN: Library
Moffett Field, California (1)

National Aeronautics and Space Administration
Lewis Research Center
ATTN: Library
21000 Brookpark Road
Cleveland 35, Ohio (1)

* Commander
Armed Services Technical Information Agency
ATTN: TIPCR
Arlington Hall Station
Arlington 12, Virginia (10)

Chief of Research and Development
ATTN: Air Mobility Division
Department of the Army
Washington 25, D. C. (1)

* Senior Standardization Representative
U. S. Army Standardization Group, Canada
c/o Director of Equipment Policy
Canadian Army Headquarters
Ottawa, Canada (1)

* Canadian Army Liaison Officer
Liaison Group, Room 208
U. S. Army Transportation School
Fort Eustis, Virginia (3)

* British Joint Services Mission (Army Staff)
ATTN: Lt. Col. R. J. Wade, RE
DAQMG (Mov & Tn)
3100 Massachusetts Avenue, N. W.
Washington 8, D. C. (3)

John J. Glennon, Librarian
Institute of the Aerospace Sciences
2 E. 64th Street
New York 21, New York (1)

Chief
U. S. Army Research and Development Liaison Group (9851 DU)
ATTN: USATRECOM Liaison Officer
APO 757, New York, New York (1)

The Boeing Company
ATTN: Aero-Space Division
P. O. Box 3707
Seattle 24, Washington (1)

Bell Helicopter Company
Division of Bell Aerospace Corporation
ATTN: Mr. Robert Lynn
P. O. Box 482
Fort Worth 1, Texas (1)

Bell Aerosystems Company
Division of Bell Aerospace Corporation
ATTN: Library
Buffalo 5, New York (1)

CONVAIR
A Division of General Dynamics Corporation
ATTN: Library
San Diego 12, California (1)

Cornell Aeronautical Laboratory, Inc.
ATTN: Library
4455 Genesee Street
Buffalo 21, New York (1)

Doak Aircraft Corporation
ATTN: Library
22309 South Western Avenue
Torrance, California (1)

Douglas Aircraft Corporation
El Segundo Division
827 Lapham Street
El Segundo, California (1)

Georgia Technical Research Institute
Georgia Institute of Technology
ATTN: Library
Atlanta, Georgia (1)

Grumman Aircraft Engineering Corporation
ATTN: Library
Bethpage, Long Island, New York (1)

Hiller Aircraft Corporation
ATTN: Library
Palo Alto, California (1)

Kaman Aircraft Corporation
ATTN: Library
Bloomfield, Connecticut (1)

Kellett Aircraft Corp.
ATTN: Library
P. O. Box 35
Willow Grove, Pennsylvania (1)

Lockheed Aircraft Corporation
Georgia Division
ATTN: Library
Marietta, Georgia (1)

McDonnell Aircraft Corporation
ATTN: Library
St. Louis, Missouri (1)

Massachusetts Institute of Technology
ATTN: Mr. Rene Miller
Aeronautical Engineering Department (1)
Cambridge, Massachusetts

Piasecki Aircraft Corporation
ATTN: Library
Philadelphia, Pennsylvania (1)

Princeton University
ATTN: Library
Princeton, New Jersey (1)

Ryan Aeronautical Company
ATTN: Library
San Diego, California (1)

United Aircraft Corporation
Sikorsky Aircraft Division
ATTN: Library
Stratford, Connecticut (1)

University of Wichita
ATTN: Library
Wichita, Kansas (1)

Vertol Division
Boeing Airplane Company
ATTN: Mr. W. Z. Stepniewski
Morton, Pennsylvania (1)

AD_____ Accession No. _____
Republic Aviation Corporation,
Farmingdale, L.I., New York

THEORETICAL INVESTIGATION OF DUCTED PROPELLER AERODYNAMICS - VOL. III.
Th. Theodorsen, G. Nomicos

Final Report, September 1961, xxi, 138 pp, illus. - (Contract No. DA 44-177-TC-674), TASK No. 9R 38-11-009-12,
VOL. III-TCREC 61-119;VOL. IV-TCREC 60-120

Problems of the ducted fan and its application in VTOL aircraft are investigated in this report.
In Volume III, general considerations are presented for the design of vertical

(over)

UNCLASSIFIED
1. Shrouded Propellers
2. Vertical Take-off Planes
I. Theodorsen, Theodore
II. Nomicos, G.
III. Army Transportation Res. Command, Ft. Eustis, Va.
IV. Contract No. DA 44-177-TC-674

AD_____ Accession No. _____
Republic Aviation Corporation,
Farmingdale, L.I., New York

THEORETICAL INVESTIGATION OF DUCTED PROPELLER AERODYNAMICS - VOL. III.
Th. Theodorsen, G. Nomicos

Final Report, September 1961, xxi, 138 pp, illus. - (Contract No. DA 44-177-TC-674), TASK No. 9R 38-11-009-12,
VOL. III-TCREC 61-119;VOL. IV-TCREC 60-120

Problems of the ducted fan and its application in VTOL aircraft are investigated in this report.
In Volume III, general considerations are presented for the design of vertical

(over)

UNCLASSIFIED
1. Shrouded Propellers
2. Vertical Take-off Planes
I. Theodorsen, Theodore
II. Nomicos, G.
III. Army Transportation Res. Command, Ft. Eustis, Va.
IV. Contract No. DA 44-177-TC-674

AD_____ Accession No. _____
Republic Aviation Corporation
Farmingdale, L.I., New York

THEORETICAL INVESTIGATION OF DUCTED PROPELLER AERODYNAMICS - VOL. III.
Th. Theodorsen, G. Nomicos

Final Report, September 1961, xxi, 138 pp, illus. - (Contract No. DA 44-177-TC-674), TASK No. 9R 38-11-009-12,
VOL. III-TCREC 61-119;VOL. IV-TCREC 60-120

Problems of the ducted fan and its application in VTOL aircraft are investigated in this report.
In Volume III, general considerations are presented for the design of vertical

(over)

UNCLASSIFIED
1. Shrouded Propellers
2. Vertical Take-off Planes
I. Theodorsen, Theodore
II. Nomicos, G.
III. Army Transportation Res. Command, Ft. Eustis, Va.
IV. Contract No. DA 44-177-TC-674

AD_____ Accession No. _____
Republic Aviation Corporation
Farmingdale, L.I., New York

THEORETICAL INVESTIGATION OF DUCTED PROPELLER AERODYNAMICS - VOL. III.
Th. Theodorsen, G. Nomicos

Final Report, September 1961, xxi, 138 pp, illus. - (Contract No. DA 44-177-TC-674), TASK No. 9R 38-11-009-12,
VOL. III-TCREC 61-119;VOL. IV-TCREC 60-120

Problems of the ducted fan and its application in VTOL aircraft are investigated in this report.
In Volume III, general considerations are presented for the design of vertical

(over)

UNCLASSIFIED
1. Shrouded Propellers
2. Vertical Take-off Planes
I. Theodorsen, Theodore
II. Nomicos, G.
III. Army Transportation Res. Command, Ft. Eustis, Va.
IV. Contract No. DA 44-177-TC-674

take-off aircraft. The ideal loading of single rotation propellers in a circular duct is examined. The flow field has been derived for a non-uniform sink distribution in a circular disk and for a cylindrical non-uniform vortex sheet. The velocity field and forces on a flat plate due to a cylindrical jet with an elliptical cross-section have also been derived. Some experimental data are given in tabular and graphic form on the interference effect of a jet on the VTOL aircraft. Design requirements of deflection vanes are discussed with the results of an experimental investigation on a cascade of circular arc sections.	take-off aircraft. The ideal loading of single rotation propellers in a circular duct is examined. The flow field has been derived for a non-uniform sink distribution in a circular disk and for a cylindrical non-uniform vortex sheet. The velocity field and forces on a flat plate due to a cylindrical jet with an elliptical cross-section have also been derived. Some experimental data are given in tabular and graphic form on the interference effect of a jet on the VTOL aircraft. Design requirements of deflection vanes are discussed with the results of an experimental investigation on a cascade of circular arc sections.
take-off aircraft. The ideal loading of single rotation propellers in a circular duct is examined. The flow field has been derived for a non-uniform sink distribution in a circular disk and for a cylindrical non-uniform vortex sheet. The velocity field and forces on a flat plate due to a cylindrical jet with an elliptical cross-section have also been derived. Some experimental data are given in tabular and graphic form on the interference effect of a jet on the VTOL aircraft. Design requirements of deflection vanes are discussed with the results of an experimental investigation on a cascade of circular arc sections.	take-off aircraft. The ideal loading of single rotation propellers in a circular duct is examined. The flow field has been derived for a non-uniform sink distribution in a circular disk and for a cylindrical non-uniform vortex sheet. The velocity field and forces on a flat plate due to a cylindrical jet with an elliptical cross-section have also been derived. Some experimental data are given in tabular and graphic form on the interference effect of a jet on the VTOL aircraft. Design requirements of deflection vanes are discussed with the results of an experimental investigation on a cascade of circular arc sections.

AD_____ Accession No. _____
Republic Aviation Corporation,
Farmingdale, L.I., New York

THEORETICAL INVESTIGATION OF DUCTED PROPELLER AERODYNAMICS - VOL. III.
Th. Theodorsen, G. Nomicos

Final Report, September 1961, xxi, 138 pp, illus. - (Contract No. DA 44-177-TC-674), TASK No. 9R 38-11-009-12,
VOL. III-TCREC 61-119;VOL. IV-TCREC 60-120

Problems of the ducted fan and its application in VTOL aircraft are investigated in this report.
In Volume III, general considerations are presented for the design of vertical
(over)

UNCLASSIFIED
1. Shrouded Propellers
2. Vertical Take-off Planes
I. Theodorsen, Theodore
II. Nomicos, G.
III. Army Transportation Res. Command, Ft. Eustis, Va.
IV. Contract No. DA 44-177-TC-674

AD_____ Accession No. _____
Republic Aviation Corporation,
Farmingdale, L.I., New York

THEORETICAL INVESTIGATION OF DUCTED PROPELLER AERODYNAMICS - VOL. III.
Th. Theodorsen, G. Nomicos

Final Report, September 1961, xxi, 138 pp, illus. - (Contract No. DA 44-177-TC-674), TASK No. 9R 38-11-009-12,
VOL. III-TCREC 61-119;VOL. IV-TCREC 60-120

Problems of the ducted fan and its application in VTOL aircraft are investigated in this report.
In Volume III, general considerations are presented for the design of vertical
(over)

UNCLASSIFIED
1. Shrouded Propellers
2. Vertical Take-off Planes
I. Theodorsen, Theodore
II. Nomicos, G.
III. Army Transportation Res. Command, Ft. Eustis, Va.
IV. Contract No. DA 44-177-TC-674

AD_____ Accession No. _____
Republic Aviation Corporation
Farmingdale, L.I., New York

THEORETICAL INVESTIGATION OF DUCTED PROPELLER AERODYNAMICS - VOL. III.
Th. Theodorsen, G. Nomicos

Final Report, September 1961, xxi, 138 pp, illus. - (Contract No. DA 44-177-TC-674), TASK No. 9R 38-11-009-12,
VOL. III-TCREC 61-119;VOL. IV-TCREC 60-120

Problems of the ducted fan and its application in VTOL aircraft are investigated in this report.
In Volume III, general considerations are presented for the design of vertical
(over)

UNCLASSIFIED
1. Shrouded Propellers
2. Vertical Take-off Planes
I. Theodorsen, Theodore
II. Nomicos, G.
III. Army Transportation Res. Command, Ft. Eustis, Va.
IV. Contract No. DA 44-177-TC-674

AD_____ Accession No. _____
Republic Aviation Corporation
Farmingdale, L.I., New York

THEORETICAL INVESTIGATION OF DUCTED PROPELLER AERODYNAMICS - VOL. III.
Th. Theodorsen, G. Nomicos

Final Report, September 1961, xxi, 138 pp, illus. - (Contract No. DA 44-177-TC-674), TASK No. 9R 38-11-009-12,
VOL. III-TCREC 61-119;VOL. IV-TCREC 60-120

Problems of the ducted fan and its application in VTOL aircraft are investigated in this report.
In Volume III, general considerations are presented for the design of vertical
(over)

UNCLASSIFIED
1. Shrouded Propellers
2. Vertical Take-off Planes
I. Theodorsen, Theodore
II. Nomicos, G.
III. Army Transportation Res. Command, Ft. Eustis, Va.
IV. Contract No. DA 44-177-TC-674

take-off aircraft. The ideal loading of single rotation propellers in a circular duct is examined. The flow field has been derived for a non-uniform sink distribution in a circular disk and for a cylindrical non-uniform vortex sheet. The velocity field and forces on a flat plate due to a cylindrical jet with an elliptical cross-section have also been derived. Some experimental data are given in tabular and graphic form on the interference effect of a jet on the VTOL aircraft. Design requirements of deflection vanes are discussed with the results of an experimental investigation on a cascade of circular arc sections.	take-off aircraft. The ideal loading of single rotation propellers in a circular duct is examined. The flow field has been derived for a non-uniform sink distribution in a circular disk and for a cylindrical non-uniform vortex sheet. The velocity field and forces on a flat plate due to a cylindrical jet with an elliptical cross-section have also been derived. Some experimental data are given in tabular and graphic form on the interference effect of a jet on the VTOL aircraft. Design requirements of deflection vanes are discussed with the results of an experimental investigation on a cascade of circular arc sections.
take-off aircraft. The ideal loading of single rotation propellers in a circular duct is examined. The flow field has been derived for a non-uniform sink distribution in a circular disk and for a cylindrical non-uniform vortex sheet. The velocity field and forces on a flat plate due to a cylindrical jet with an elliptical cross-section have also been derived. Some experimental data are given in tabular and graphic form on the interference effect of a jet on the VTOL aircraft. Design requirements of deflection vanes are discussed with the results of an experimental investigation on a cascade of circular arc sections.	take-off aircraft. The ideal loading of single rotation propellers in a circular duct is examined. The flow field has been derived for a non-uniform sink distribution in a circular disk and for a cylindrical non-uniform vortex sheet. The velocity field and forces on a flat plate due to a cylindrical jet with an elliptical cross-section have also been derived. Some experimental data are given in tabular and graphic form on the interference effect of a jet on the VTOL aircraft. Design requirements of deflection vanes are discussed with the results of an experimental investigation on a cascade of circular arc sections.